Aus dem Institut für Virologie

Direktor: Prof. Dr. Stephan Becker

des Fachbereichs Medizin der Philipps-Universität Marburg

in Zusammenarbeit mit dem Paul-Ehrlich-Institut Langen

Innate Immunity to Ebola Virus

Inaugural-Dissertation zur Erlangung des Doktorgrades der gesamten Naturwissenschaften (Dr. rer. nat.)

dem Fachbereich Medizin der Philipps-Universität Marburg vorgelegt von

Johanna Wildemann

Geboren in Stuttgart

Marburg, 2022

Diese Doktorarbeit wurde in der Nachwuchsgruppe 3 „Zelluläre Aspekte von Pathogen-Wirt-Interaktionen“ unter der Leitung von Dr. Renate König am Paul-Ehrlich-Institut in Langen durchgeführt und dem Promotionsausschuss der Universität Marburg vorgelegt.

Angenommen vom Fachbereich Medizin der Philipps-Universität Marburg am:
14.10.2022

Gedruckt mit Genehmigung des Fachbereichs Medizin

Dekanin: Frau Prof. Dr. D. Hilfiker-Kleiner
Referent: Herr Prof. Dr. S. Becker/Frau Dr. R. König
1. Korreferent: Herr Prof. Dr. L. Schulte

Table of Contents

List of abbreviations

°C	Degree Celsius
4cis	Tetracistronic minigenome
A	Adenosine
ADAR	Adenosine deaminase acting on RNA
A-to-I	Adenosine to Inosine
ATP	Adenosine triphosphate
AUT	Austria
BDBV	Bundibugyo virus
BEL	Belgium
BOMV	Bombali virus
bp	Base pairs
BSA	Bovine serum albumine
BSL	Biosafety level
C	Cytosine
C_2H_6O	Ethanol
CARD	Caspase activation and recruitment domain
Cas9	CRISPR-associated protein 9
CD	Cluster of differentiation
cDNA	Complementary DNA
CH_3OH	Methanol
cm	Centimeter
CO_2	Carbon dioxide
CRISPR	Clustered regularly interspaced short palindromic repeats
CTD	C-terminal regulatory domain
DAPI	4’,6-Diamidino-2-phenylindol
DC	Dendritic cell
DIs	Defective interfering particles
DMEM	Dulbecco’s Modified Eagle’s Medium

DMSO	Dimethyl sulfoxide
DNA	Desoxyribonucleic acid
dNTPs	Desoxynucleoside triphosphates
ds	Double-stranded
EBOV	Ebola virus
E. coli	*Escherichia coli*
EDTA	Ethylenediaminetetraacetic acid
eIF2α	Eukaryotic initiation factor 2α
ELISA	Enzyme-linked immunosorbent assay
EMA	European Medicines Agency
FACS	Fluorescence activated cell sorting
FBS	Fetal bovine serum
FDA	Food and Drug Administration
g	Gram
G	Guanine
GB	Great-Brittain
GER	Germany
GM-CSF	Granulocyte-macrophage colony-stimulating factor
GP	Glycoprotein
gRNA	Guide RNA
H	Hour/hours
HEPES	(4-(2-hydroxyethyl)-1-piperazineethanesulfonic acid
HF	hemorrhagic fever
HF-buffer	High fidelity buffer
hpi	Hours post infection
hpt	Hours post transfection
HRP	Horseradish-peroxidase
HUJV	Huángjiāo virus
I	Inosine
IAV	Influenza A virus

IFN	Interferon
IFNAR	IFN-α receptor
IID	IFN-inhibitory domain
IκB	Inhibitor of nuclear factor κB
IKKε	IκB kinase epsilon
IL	Interleukin
IRF	IFN regulatory factor
ISG	IFN-stimulated gene
JAK	Janus kinase
kb	kilobases
KO	Knock-out
KPNA	karyopherin-α
L	*Filoviridae* viral polymerase
LB	Luria Broth
LLOV	Lloviu virus
LPG2	Laboratory of genetics and physiology 2
m1	Mutant 1
m2	Mutant 2
MARV	Marburg virus
MAVS	mitochondrial antiviral-signaling molecule
Mc	monoclonal
MDA5	Melanoma differentiation associated gene 5
MDDC	Monocyte-derived DC
MDM	Monocyte-derived macrophage
MeV	Measles virus
µg	Microgram
$MgCl_2$	Magnesium chloride
min	Minute/minutes
mL	Milliliter
µL	Microliter

MLAV	Měnglà virus
µM	Micromolar
MOPS	3-(N-morpholino)propanesulfonic acid
mRNA	Messenger RNA
NF-κB	Nuclear factor 'kappa-light-chain-enhancer' of activated B-cells
ng	Nanogram
NLR	NOD-like receptor
nluc	Nanoluciferase
nm	Nanometer
NOD	Nucleotide-binding oligomerization domain
NP	Nucleoprotein
NSV	Negative-sense RNA virus
OAS	Oligoadenylate synthetase
Opti-MEM	Optimized minimal essential medium
ORF	Open reading frame
PACT	Protein activator of the IFN-induced PKR
PAMP	Pathogen-associated molecular pattern
PBMC	Peripheral blood mononuclear cell
PBS	Phosphate-buffered saline
pc	polyclonal
PEG	Poly(ethylene)glycol
PFA	Paraformaldehyde
PKR	Protein kinase R
PMA	Phorbol-12-myristyl-13-acetate
PNK	Polynucleotidkinase
Poly I:C	Polyinosinic:polycytidylic acid
pp/p	Di-/Triphosphates
PRR	Pattern recognition receptor
PVDF	Polyvinylidenfluorid
RAVV	Ravn virus

RESTV	Reston virus
RIG-I	Retinoic acid inducible gene I
RIPA	Radioimmunoprecipitation
RLR	RIG-I-like receptor
RLU	Relative light unit
RNA	Ribonucleic acid
RNAi	RNA interference
RNPs	Ribonucleoproteins
RPL13a	Ribosomal Protein L13a
rpm	Rounds per minute
RPMI	Roswell Park Memorial Institute
RPS27a	Ubiquitin-40S ribosomal protein S27a
(RT-q)PCR	(Reverse Transcription quantitative) Polymerase Chain Reaction
s	Second/seconds
SARS-CoV-2	Severe acute respiratory syndrome Coronavirus 2
SD	Standard-deviation
SDS-PAGE	Sodium dodecylsulfate polyacrylamide gel electrophoresis
SeV	Sendai virus
SINE	Short interspersed nuclear elements
siRNA	small interfering RNA
SOC	Super optimal broth with catabolite repression
ss	Singlestranded
(s)sGP	(small) soluble GP
STAT	signal transducers and activators of transcription
STING	Stimulator of interferon genes protein
SUDV	Sudan virus
SUMO	Small ubiquitin-related modifier
TAE	Tris-acetate-EDTA
TAFV	Taï Forest virus
TAM	Tyro3, Axl, and Mer

TBK1	Tank binding kinase 1
TBST	Tris-buffered saline with 0.1% (v/v) Tween®-20
TE	Tris EDTA
Temp.	Temperature
TIM	T cell/transmembrane, immunoglobulin, and mucin
TLR	Toll-like receptor
trVLP	transcription- and replication competent VLP
U	Uracil
USA	United States of America
UV	Ultraviolet
V	Volt
VLP	Virus-like particle
VP	Viral protein
VSV	Vesicular stomatitis virus
WHO	World Health Organization
XILV	Xīlǎng virus

Amino acids one letter code

A	Alanine
C	Cystein
D	Aspartic acid
E	Glutamic acid
F	Phenylalanine
G	Glycine
H	Histidine
I	Isoleucine
K	Lysine
L	Leucine
M	Methionine
N	Asparagine
P	Proline
Q	Glutamine
R	Arginine
S	Serine
T	Threonine
V	Valine
W	Tryptophan
Y	Tyrosine

List of figures

List of tables

1 Introduction

1.1 Taxonomy and epidemiology of *Filoviridae*

Ebola virus (EBOV) is the most well-known representative of the family *Filoviridae* among eleven families within the order of Mononegavirales. Mononegavirales comprise viruses with linear, single-stranded, non-segmented, negative-sense RNA. The family *Filoviridae* currently consists of six genera with twelve viruses (Kuhn et al., 2019). The genus *Ebolavirus* includes six species for six viruses: EBOV (WHO/International Study Team, 1978b), Sudan virus (SUDV) (WHO/International Study Team, 1978a), Taï Forest virus (TAFV) (Le Guenno et al., 1995), Bundibugyo virus (BDBV) (Towner et al., 2008), Reston virus (RESTV) (Jahrling et al., 1990), and Bombali virus (BOMV) (Goldstein et al., 2018). The genus *Marburgvirus* consists of Marburg virus (MARV) and Ravn virus (RAVV) (Bausch et al., 2006). More recently discovered genera are *Cuevavirus* (Lloviu virus - LLOV) (Negredo et al., 2011), *Dianlovirus* (Měnglà virus - MLAV) (Yang et al., 2019), *Striavirus* (Xīlǎng virus - XILV), and *Thamnovirus* (Huángjiāo virus - HUJV) (Shi et al., 2018; Amarasinghe et al., 2019) (Table 1).

Several filoviruses are able to cause severe infections in humans, including potentially fatal hemorrhagic fever (HF) (Basler, 2017) (Table 1). The first documented human infection caused by a filovirus occurred in 1967 in Marburg (Germany) (Martini, 1969). Laboratory workers were infected during the preparation of monkey tissue for vaccine production. The - to this date unknown - disease also occurred in other laboratories, which received monkeys from the same breeding, imported from Uganda. In total, 31 people got infected of which seven died. The pathogenic agent was identified by electron microscopy and named MARV (Slenczka and Klenk, 2007). Since 1967, there have been several smaller MARV outbreaks and two major outbreaks in Africa or in non-African countries due to import of infected animals from African countries. Up to date, a total amount of almost 600 MARV cases have been registered by the World Health Organization (WHO), with a fatality rate of around 80% (WHO, 2022b). In 1987, the second *Marburgvirus* RAVV was discovered in Kenya (Johnson et al., 1996). Only three

human RAVV infections have been confirmed, of which two persons died (Burk et al., 2016). In 1976, the first recorded *Ebolavirus* outbreaks occurred simultaneously around Yambuku, Zaire (today Democratic Republic of Congo) (WHO/International Study Team, 1978b) and in South Sudan (WHO/International Study Team, 1978a). The causative agents for both outbreaks were identified as two distinct new members of the filoviruses, namely EBOV and SUDV, respectively (Cox et al., 1983). During the 1976 outbreaks a total number of 602 infections were counted, of which around 72% were fatal (WHO, 2022a). In 1989, the presumable human non-pathogenic RESTV was discovered in the United States of America (USA) in cynomolgus macaques imported from the Philippines (Jahrling et al., 1990). In 1994, TAFV was isolated from a patient in the Taï forest reserve in Cote d'Ivoire. Up to date, this has been the sole registered human infection with TAFV and it was not lethal (WHO, 2022a). In 2007, an outbreak with a novel filovirus occurred in Uganda, the causative agent was named BDBV. Of 149 infected people, 37 died (WHO, 2022a). From 2014 to 2016, the largest filovirus outbreak up to date was caused by EBOV and happened in Guinea, Liberia, and Sierra Leone. The epidemic counted 28,616 infections of which 11,310 people died. Since 2014, there have been almost yearly smaller outbreaks. Overall, since the first discovery of EBOV in 1976, more than 33,000 people have been infected with ebolaviruses, of which 44% died (WHO, 2022a). Additionally, several other filoviruses were identified on the basis of isolated sequences. LLOV sequences were isolated in 2002 from bats in caves in Spain (Negredo et al., 2011). BOMV genomes were discovered from bat samples taken in 2016 in Sierra Leone (Goldstein et al., 2018). XILV and HUJV sequences were discovered in captured fish in the East China Sea (Shi et al., 2018). MLAV was discovered in bats in China (Yang et al., 2019) (Table 1).

This thesis, unless stated otherwise, focuses on EBOV.

Table 1: Filovirus taxonomy, including human pathogenicity and initial discovery.

Genus	*Virus name*	*Abbreviation*	*Human pathogen*	*Initial discovery*
Ebolavirus	Ebola virus	EBOV	Yes	1976
	Sudan virus	SUDV	Yes	1976
	Reston virus	RESTV	No	1989
	Taï Forest virus	TAFV	Yes	1994
	Bundibugyo virus	BDBV	Yes	2007
	Bombali virus	BOMV	?	2016
Marburgvirus	Marburg virus	MARV	Yes	1967
	Ravn virus	RAVV	Yes	1987
Cuevavirus	LLoviu virus	LLOV	?	2002
Striavirus	Xīlǎng virus	XILV	?	2016[a]
Thamnovirus	Huángjiāo virus	HUJV	?	2016[a]
Dianlovirus	Měnglà virus	MLAV	?	2019[a]

a) Year of publication

1.2 Ebola virus particles

1.2.1 Morphology

The filamentous shape of these viruses originally led to the name *Filoviridae* (latin: *filum* = thread) and infectious EBOV particles are around 1000 nm in length (Geisbert and Jahrling, 1995). As all filoviruses, EBOV is enveloped and possesses a linear, negative sense, single-stranded, and non-segmented RNA genome. The genome is covered by nucleoproteins (NP) which are associated to the polymerase (L). The polymerase further binds viral protein (VP) 35 and VP30. VP24 surrounds the nucleocapsid. The VP40 matrix is surrounded by the envelope and binds the surface glycoprotein (GP) (Beniac et al., 2012; Bharat et al., 2012) (Figure 1).

1.2.2 Genome organization of Ebola virus

The EBOV genome is 19 kb long and encodes seven viral structural proteins and additional non-structural proteins. The seven viral genes are consecutively arranged and proteins are encoded by the respective open reading frames (ORFs). Genes for the following proteins are situated on the negative genome from 3' to 5': NP, VP35, VP40, GP, VP30, VP24, L (Sanchez et al., 1993) (Figure 1). Additionally, soluble GP (sGP), and small soluble GP (ssGP) are encoded by the same gene as GP and are translationally processed (Sanchez et al., 1996; Mehedi et al., 2011). The ORFs are framed by non-translated intergenic regions, with a long intergenic region between VP30 and VP24. Highly conserved transcription start and stop patterns can be found before and after each gene. Additionally, extragenic regions containing cis-acting elements can be found at the 3' and 5' ends of the genome, called leader and trailer. They are highly conserved and complementary motifs within these regions lead to formation of stem-loop structures (Sanchez et al., 1993). These structures are essential for transcription initiation, replication, and encapsidation of the genomic RNA (Sztuba-Solinska et al., 2016).

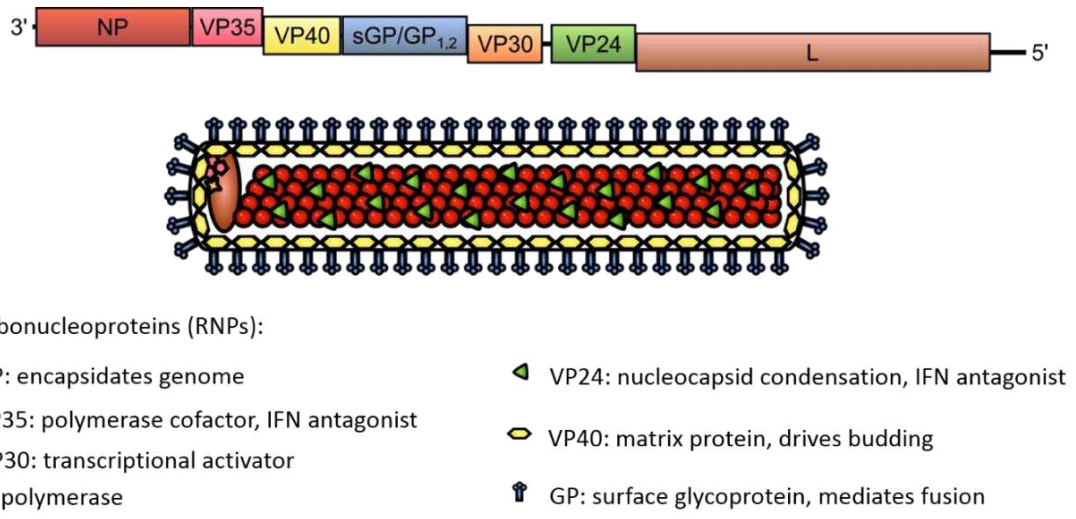

Figure 1: Genome organization of EBOV and particle structure. The filamentous shaped EBOV particles contain the negative genome, which is encapsidated by the nucleoprotein (NP) and viral protein (VP) 24. At one end of the encapsidated genome, the polymerase (L) is associated to VP35 and VP30. NP, L, VP35, and VP30 are the ribonucleoproteins (RNPs). The VP40 matrix surrounds the transcription and replication apparatus. The surface glycoproteins (GPs) are located on the matrix to mediate fusion with the target cell. Figure kindly provided by Thomas Hoenen (and adapted from (Hoenen et al., 2019) with the license number: 5260651490377).

1.2.3 Life cycle and protein functions of Ebola virus

The entry and uncoating process starts with the viral attachment to the cell membrane by interaction of the viral surface GP with one of many possible attachment factors, leading to infection of many different cell types (see 1.3.2). For example, C-type lectins can function as attachment factors as well as cellular phosphatidyl serine receptors, e.g. T cell/transmembrane, immunoglobulin, and mucin (TIM) or Tyro3, Axl, and Mer (TAM) family members that interact with phosphatidyl serines on the viral envelope (Chan et al., 2001; Alvarez et al., 2002; Simmons et al., 2003; Gramberg et al., 2005; Shimojima et al., 2006; Schornberg et al., 2009; Kondratowicz et al., 2011; Jemielity et al., 2013). Mainly macropinocytosis leads to uptake of the virus, although other routes of uptake, such as clathrin-mediated endocytosis, have been described (Nanbo et al., 2010; Saeed et al., 2010; Aleksandrowicz et al., 2011; Bhattacharyya et al., 2011; Hunt et al., 2011). Upon uptake, the virion-containing endosomes acidify and proteolysis of EBOV GP is conducted by cellular cathepsin B or L (Chandran et al., 2005; Sanchez, 2007). Nevertheless, it was shown that cathepsin-mediated cleavage of GP is not essential for EBOV replication (Marzi et al., 2012). The proteolysis of GP exposes a GP interaction site for the cellular transmembrane glycoprotein Niemann-Pick C1, which leads to the fusion of viral and endosomal membranes upon binding (Carette et al., 2011; Côté et al., 2011). Membrane fusion leads to release of the nucleocapsid into the cytoplasm, where transcription and replication of the viral genome starts.

The transcription and replication process takes place in cytoplasmic viral inclusion bodies (Hoenen et al., 2012). The ribonucleoproteins (RNPs) polymerase L, its co-factor VP35, the transcription factor VP30, and NP are packaged in the viral particles and facilitate primary transcription of the viral genome into polyadenylated, monocistronic mRNAs with a 5'-cap (Mühlberger et al., 1996; Weik et al., 2002). Host cellular proteins translate the mRNAs into newly synthesized viral proteins, which in turn promote secondary transcription and replication of the viral genome. For replication of the viral genome, the polymerase synthesizes full-length viral antigenomes, which are encapsidated with NP. These antigenomes serve as templates for the synthesis of new

viral RNA, which is also encapsidated (Mühlberger et al., 1998; Mühlberger et al., 1999; Mühlberger, 2007). EBOV NP, VP35, and VP24 are essential to mediate the nucleocapsid transport to the site of budding (Takamatsu et al., 2018). Nucleocapsids are condensed by VP24 and viral particles are assembled at the plasma membrane (Han et al., 2003; Licata et al., 2004; Hoenen et al., 2006), where VP40 serves as a matrix protein that drives budding of the particles from the cell surface (Harty et al., 2000; Scianimanico et al., 2000; Timmins et al., 2001). The additional proteins sGP and ssGP, have a not yet clearly determined function. They are truncated versions of GP and produced by co-transcriptional mRNA editing (Mühlberger, 2007; Zhu et al., 2019). However, immune subversion by sGP has been suggested a possible function (Bradley et al., 2018). Besides their essential roles in the viral lifecycle, several viral proteins fulfill another major function by modulating the host's innate immune pathways. Particularly VP35 and VP24 are well characterized in their roles as innate sensing antagonists (Basler, 2015), which will be discussed in detail later (see 1.4.3).

1.3 Pathogenesis, clinical appearance, and therapy

Bats are the proposed reservoir for EBOV (Leendertz et al., 2016; Schuh et al., 2017; Emanuel et al., 2018). Humans, non-human primates, as well as several other mammals are highly susceptible to EBOV infection and can suffer from severe pathogenicity (Weingartl et al., 2013; Atherstone et al., 2021). Spillover to humans can occur through direct physical contact to infected animals such as bats and apes or through contact with contaminated animal products, e.g. by the preparation of bush meat for consumption. Human to human transmission of EBOV occurs via close contact or body fluids (Judson et al., 2015; Vetter et al., 2016). Diagnostic rapid viral antigen detection kits as well as PCR-tests are available and have been proven to be effective to detect EBOV infections (Sanchez et al., 1999; CDC, 2022).

Initially, unspecific symptoms typically start after an incubation period of 3 to 12 (in rare cases 2 to 21) days and include fever, headache and muscle pain. Gastrointestinal

symptoms such as abdominal pain, nausea, vomiting, and diarrhea can follow, as well as a maculopapular rash. Around 65% of the patients develop hemorrhagic manifestations, including gastrointestinal bleedings, but also occasional bleedings from injection sites or mucosal membranes. Renal and respiratory failure can follow (Kortepeter et al., 2011; Jacob et al., 2020). Usually, fatal courses are caused by multi-organ failure and occur 6 to 16 days after symptom onset (Baize et al., 1999; Bwaka et al., 1999).

Viral persistence in EBOV disease survivors was verified from several immune-privileged sites such as eye (Varkey et al., 2015), central nervous system (Jacobs et al., 2016), and urogenital system (Christie et al., 2015; Dokubo et al., 2018). Recently, one case of reactivation of EBOV was associated to the 2014-16 outbreak nearly five years later (Keita et al., 2021). However, rare data exists on the persistence of EBOV in the body.

Even though there has been a lot of research on the mechanisms of EBOV infections over the past years, it is not yet fully understood which factors determine disease severity.

1.3.1 Prevention and therapy

Best prevention of infection is the physical isolation of confirmed cases and suspected cases. Since 2019, three EBOV vaccines, which were evaluated in several outbreaks in Africa during the past years, have been authorized by several drug admission agencies (e.g. by the US Food and Drug Administration (FDA) and the European Medicines Agency (EMA)) (WHO, 2022a). Ervebo is a replication-competent, attenuated, recombinant vesicular stomatitis virus (VSV) aiming to elicit an immune response against EBOV GP. The combination vaccine Zabdeno/Mvabea includes the first dose of Zabdeno with a replication-defective, recombinant adenovirus 26 encoding the EBOV GP and the second dose Mvabea with a replication-incompetent, recombinant modified vaccinia virus Ankara expressing GP of EBOV, SUDV, MARV, and TAFV (Jacob et al., 2020; Woolsey and Geisbert, 2021). Given the high case fatality rate of EBOV, vaccines were mainly tested during outbreaks in the framework of ring vaccination trials, without a placebo group. Therefore, pre-exposure vaccine efficiency is still under determination. However,

individuals who were vaccinated early after contact to (suspect) cases, showed significantly lower risk of infection.

After infection, direct medical countermeasures include supportive care such as compensation of fluid loss by administration of crystalloid solutions. Symptom-specific treatments include anti-emetic and anti-diarrhoeal medicine. Furthermore, two monoclonal antibody products have recently been approved by the FDA and the EMA as antiviral strategies. Both have only mild adverse events and showed improvement of survival rates compared to control groups (Jacob et al., 2020; WHO, 2022a).

1.3.2 Target cells, viral dissemination, and interference with the innate immunity

EBOV can infect a large number of cells. First target cells including the circulating immune cells macrophages and dendritic cells (DCs) spread the virus through the body (Geisbert et al., 2003; Bray and Geisbert, 2005), affecting monocytes, hepatocytes, Kupffer cells, fibroblasts, epithelial cells, endothelial cells, and cells of the adrenal gland tissue (Geisbert et al., 2003). On the one hand, early infection seems to induce a strong inflammatory response mediated by macrophages and other immune cells (Gupta et al., 2001; Ströher et al., 2001; Olejnik et al., 2017a). On the other hand, EBOV infection leads to a substantial abolishment of secreted interferon (IFN) in macrophages and DCs as well as abolishment of inflammatory cytokines in DCs (Bosio et al., 2003; Mahanty et al., 2003; Lubaki et al., 2013). The loss of IFN-signaling leads to a suppression of conventional maturation of DCs and impaired function as antigen-presenting cells (Liu, 2001; Bosio et al., 2003). However, monocytes and macrophages elicit strong activation of pro-inflammatory pathways, leading to recruitment and activation of further immune cells, which eventually results in an uncontrolled amplification of inflammation – a cytokine storm (Feldmann et al., 1996; Ksiazek et al., 1999; Gupta et al., 2001; Ströher et al., 2001). The contrast between the cytokine storm initiated in macrophages and the fail of adaptive immune activation by DCs are probably the main causes of pathogenesis. The exact details of virus – innate sensing interactions will be discussed in the next chapter.

1.4 Interaction of Ebola virus with the innate immune system

The innate immune system is the first challenge a virus encounters after infection of a host cell. A whole network of cellular pathways and signaling cascades has been discovered that interact in autocrine and paracrine manners to protect the body from viral infections by activating further defense mechanisms and inhibiting viral growth (Takeuchi and Akira, 2009). The interactions between viruses and the innate immune response have been extensively studied for many different viruses, including EBOV (Ramanan et al., 2011; Olejnik et al., 2017b). In this regard, a major research focus has been on how viruses counteract, avoid, or deregulate this first line of host defense (García-Sastre, 2017). At the same time, many cellular strategies to recognize and battle intruders have evolved (Kumar et al., 2011; Schneider et al., 2014). The relationship between EBOV and IFNs and pro-inflammatory responses has received much attention over the past years owing to a search of early biomarkers for fatal disease progression (McElroy et al., 2014). Nevertheless, disease outcome can only be linked to very limited clinical data and predictions are difficult to be made based on specific biomarkers.

1.4.1 Overview of the innate immune system

This chapter will provide an overview of proteins that are known to sense RNA with a focus on the cytosolic retinoic acid inducible gene-I (RIG-I)-like receptor family (RLRs) (Bartok and Hartmann, 2020; Liu and Gack, 2020), due to their relevance in the context of innate sensing of EBOV. The early innate immune system consists of signaling proteins that are activated in cascades upon stimulation of pattern recognition receptors (PRRs). These receptors are able to recognize pathogen-associated molecular patterns (PAMPs), which are conserved pathogen features, such as specific RNA structures. Activation of receptors and downstream signaling leads to the production of signaling molecules, which include cytokines and chemokines such as IFNs and interferon-stimulated genes (ISGs) as well as inflammasome-dependent responses. These signaling molecules attract further immune cells and trigger the adaptive immune response. Different groups of

PRRs are expressed in various locations of the cell and can sense different PAMPs (Saito and Gale, 2007; Wilkins and Gale, 2010).

1.4.2 Innate sensing of viral RNA in the cytosol

The group of RLRs includes three receptors – namely RIG-I, melanoma differentiation associated gene 5 (MDA5), and laboratory of genetics and physiology 2 (LGP2). RLRs are expressed in a wide variety of immune cells as well as non-immune cells. Both, RIG-I and MDA5 use the same downstream signaling pathway and are main sensors for RNA viruses that replicate in the cytosol. They share a common domain structure, a C-terminal regulatory domain (CTD) and a central DExD/H box helicase flanked by a tandem caspase activation and recruitment domain (CARD) that facilitates downstream signaling. LGP2 lacks the CARDs being unable to activate further signaling, but it was hypothesized that LGP2 regulates RIG-I and MDA5 (Bruns et al., 2013). Generally speaking, RIG-I is mainly activated by RNA motifs of negative-sense RNA viruses (NSVs), whereas MDA5 rather recognizes structures of positive-sense RNA viruses (Liu and Gack, 2020). In particular, RIG-I can sense shorter double-stranded (ds) RNA sequences of up to 20 base pairs (bp) harboring 5'-di- or triphosphates (5'-pp/5'-ppp) (Hornung et al., 2006; Pichlmair et al., 2006; Kato et al., 2008; Schmidt et al., 2009; Baum et al., 2010; Marq et al., 2011; Goubau et al., 2014) or blunt ends (Schlee and Hartmann, 2016). Common structures in NSVs, such as (sub)genomic panhandle structures were shown to be recognized by RIG-I despite mismatches and bulge loops within ds regions (Schlee et al., 2009; Liu et al., 2015). In contrast, MDA5 is suggested to bind long viral dsRNAs of more than 300 bp in higher order structures (Kato et al., 2008; Deddouche et al., 2014; Runge et al., 2014). Recently, it was shown that MDA5 is also able to recognize endogenous RNA in the form of transposable *Alu* elements belonging to the short interspersed nuclear elements (SINEs), which form dsRNA motifs (Ahmad et al., 2018).

Upon binding of viral RNA to the CTD and helicase of RIG-I or MDA5, a conformational change leads to the exposure of the CARD domain, providing an interaction site for the CARD domain of mitochondrial antiviral-signaling molecule (MAVS) (Kawai et al., 2005; Xu et al., 2005). MAVS subsequently forms aggregates to which various adaptor proteins

are recruited, which in turn activate kinases such as Tank binding kinase 1 (TBK1) and IκB kinase epsilon (IKKε), which directly phosphorylate the IFN regulatory factor 3 and 7 (IRF-3/-7). IRF-3 and IRF-7 are immediate transcription factors for the expression of type I and type III IFNs, including IFN-α and IFN-β, as well as numerous ISGs (Seth et al., 2005). Two direct target genes of IRF-3 are for example ISG54 and ISG56, whose expression can be used as a readout of viral innate sensing activity (Nakaya et al., 2001; Grandvaux et al., 2002).

In a positive feedback-loop, many different cytokines can activate the production of more IFNs and ISGs in an autocrine and paracrine manner via the cytokine receptors and the JAK-STAT pathway. The JAK-STAT pathway is induced by binding of IFN to the IFNAR (IFN-α receptor), to which Janus kinases (JAKs) are attached. Through the activation of the IFNAR by IFN, intracellular JAKs auto-phosphorylate, which induces the phosphorylation of signal transducers and activators of transcription (STATs) (Darnell et al., 1994; Schneider et al., 2014; Morris et al., 2018). Phosphorylated STATs are subsequently transported into the nucleus by the cargo carrier karyopherin-α (KPNA) nuclear transporters to activate transcription processes (McBride and Reich, 2003).

Two additional cytosolic host factors need to be introduced here: Protein kinase R (PKR) and protein activator of the interferon-induced protein kinase R (PACT). First, PKR is a dsRNA-dependent protein kinase and can be activated by secondary structures of 5’-ppp RNA or by very long dsRNA (Nanduri et al., 1998; Nallagatla et al., 2007). Activated PKR targets the mRNA processing leading to inhibition of host and viral cap-dependent translation as well as cell growth (Dar et al., 2005; Liu et al., 2020). Interestingly, activated PKR is able to modulate RLR signaling, although the mechanism is not fully understood yet (Chen and Hur, 2021). Second, PACT is a direct dsRNA-independent activator of PKR, being able to stimulate PKR upon a variety of stress stimuli (Patel and Sen, 1998). Importantly, PACT is a PKR-independent activator of RIG-I, maintaining a strong RIG-I dependent antiviral response (Kok et al., 2011).

1.4.3 Ebola virus interferon-antagonism strategies

EBOV has developed several mechanisms to counteract IFN activation and to manipulate host signaling proteins, for instance by using deregulating strategies to suppress cytosolic signaling and to downregulate ISG induced cellular pathways. First experimental evidences demonstrated that virus- or dsRNA-induced signaling was inhibited by EBOV in endothelial cells. EBOV infection itself did not induce the expression of specific ISGs, indicating that specifically IFN signaling was targeted, as pro-inflammatory cytokine secretion was not impaired (Harcourt et al., 1998, 1999). To understand IFN antagonistic strategies of EBOV proteins, researchers have been using model systems, such as the highly immunogenic NSV Sendai virus (SeV) or synthetic dsRNA (e.g. poly I:C) to induce innate signaling in cells. Antagonizing actions of EBOV proteins can be evaluated by measuring the inhibition of the IFN response (Olejnik et al., 2017b). The next chapters describe in detail the functions of the best studied EBOV IFN-antagonistic proteins, VP35 and VP24.

1.4.3.1 VP35

EBOV VP35 has been studied extensively since its first description as an IFN-antagonistic viral protein (Basler et al., 2000). By now, multiple studies have shown that VP35 suppresses cytosolic signaling through a variety of mechanisms. VP35 is able to directly regulate phosphorylation and SUMOylation events in the IFN-activation cascade, to sequester RIG-I-activating dsRNA, to interfere with cellular key host inducers of the IFN response, and to interfere with host translational shutdown measures (Table 2).

More specifically, VP35 has been demonstrated to prevent the phosphorylation of IRF-3 and IRF-7 by acting as a decoy substrate for the kinases TBK1 and IKKε. Phosphorylation of VP35 instead of IRF-3 and IRF-7 by TBK1 and IKKε, inhibits downstream activation and translocation of IRF-3 or IRF-7 into the nucleus (Prins et al., 2009).

Additionally, VP35 is able to increase SUMOylation of IRF-7 as well as IRF-3 and thereby inhibits IFN production. Mechanistically, VP35 promotes SUMOylation by interacting with a complex comprised of SUMO E3 protein ligase PIAS1, the SUMO-conjugating enzyme UBC9, and IRF-7, leading to dampened IRF-7-dependent transcriptional responses (Kubota et al., 2008; Chang et al., 2009).

Besides that, VP35 is able to bind dsRNA. The association of dsRNA to VP35 masks it from RIG-I sensing, thereby preventing RLR-mediated IFN responses (Hartman et al., 2004; Cárdenas et al., 2006; Edwards et al., 2016). Structurally, several amino acids of VP35 were identified as crucial for dsRNA-binding and subsequent inhibition of sensing. To understand this function mechanistically and to identify specific motifs in VP35 responsible for dsRNA-binding, several parts of VP35 were mutated and IFN-antagonistic activity was evaluated. Interestingly, a C-terminal basic stretch could be identified to be the IFN-antagonistic motif of VP35, which shows a strong amino acid homology to the IFN-antagonistic NS1 protein of influenza A virus (IAV) (Hartman et al., 2004). Mutations of positions R312, and to a lesser extent R305 and K309 could restore ISG induction e.g. upon SeV infection (Hartman et al., 2004; Cárdenas et al., 2006; Leung et al., 2010). Mechanistically, VP35 mutants R312A and K309A could not bind poly I:C dsRNA in a pulldown-assay anymore (Cárdenas et al., 2006). In accordance with this, cell infection models with recombinant EBOV harbouring a VP35 R312A mutation led to upregulated IFN-α as well as ISG54 and ISG56 compared to wt VP35 EBOV (Kuzmin et al., 2017). Additionally, several other key amino acids have been described to have IFN-antagonistic functions, e.g. mutations in position K319 or R322 also abrogate dsRNA-binding activity of VP35 and are consequently less IFN-antagonistic than wt VP35 (Leung et al., 2010; Zhang et al., 2017). Furthermore, position F239 was found to be essential in masking 5'-ppp and thereby inhibiting RLR signaling (Leung et al., 2010). In accordance, loss of dsRNA-binding with a mutation of the mentioned amino acids could also be confirmed by molecular dynamics simulations (Zhang et al., 2017). Consistent with these findings, the carboxy-terminal half of VP35 comprising the amino acid residues 220-340 (Reid et al., 2005) was therefore named IFN-inhibitory domain (IID) (Leung et al., 2010) (Figure 2). The strong dsRNA-binding ability of VP35 raised the question which kinds of

dsRNA are bound by VP35 during infection to prevent RLR activation. Deep sequencing studies discovered that VP35 was able to selectively bind highly immunostimulatory SeV dsRNA (Dilley et al., 2017). Furthermore, it was shown previously that VP35 is able to sequester EBOV-derived, *in vitro*-transcribed dsRNA from RIG-I (Cárdenas et al., 2006). Nevertheless, binding of VP35 to EBOV self-RNA during infection has not been shown yet.

Interestingly, the IID is also crucial for VP35 interaction with the host protein PACT. PACT is usually an important activator of PKR as well as RIG-I (Kok et al., 2011). Even though VP35 binding to PACT leads to RNA-independent inhibition of PACT-mediated RIG-I activation, mutations in the VP35 IID restored PACT – RIG-I interactions (Luthra et al., 2013). On a related note, VP35 is able to inhibit ISG-induced cellular pathways by interfering with PKR activation, presumably via interaction with PACT or by sequestration of dsRNA (Schümann et al., 2009). However, this has not yet been understood in detail. Usually, PKR is phosphorylated after dsRNA binding, leading to negative regulation of cellular translation, which is also reversed by VP35. Surprisingly, this antagonism was not abolished by introduction of the R312A mutation alone, but rather two alanine substitutions in the IID were shown to be necessary (Feng et al., 2007; Schümann et al., 2009), suggesting that dsRNA-sequestration is not sufficient to antagonize PKR-mediated pathways.

Figure 2: Schematic overview of the EBOV VP35 gene. The 340 amino acid long gene contains an approximately 120 amino acid long domain that can interact in an IFN-antagonistic manner with the innate sensing pathways – the IFN-inhibitory domain (IID). Especially the first basic patch (FBP) and the central basic patch (CBP) contain amino acids that are essential for IFN-antagonism, including F239, R305, K309, R312, K319, R322, K339.

When analyzing infection studies with recombinant viruses harboring mutations in the VP35 IID, the importance for virus propagation and immune system suppression becomes evident. Several studies determined growth capabilities of recombinant virus carrying mutations in the IID. Indeed, growth was attenuated in cell culture, probably due to higher levels of IFN induction and the establishment of an antiviral state in virus-producing cells (Hartman et al., 2006; Leung et al., 2009; Prins et al., 2010a). Additional studies analyzed EBOV infection of the antigen-presenting cells monocyte-derived DCs (MDDCs) and subsequent MDDC-mediated activation of the adaptive immune response. Surprisingly, it was shown that the dsRNA-binding property of VP35 and the subsequent inhibition of RLR-induced IFN production inhibited the maturation of MDDCs (Yen et al., 2014), underlining the importance of the IID for viral infection and propagation in host cells. In accordance, further studies demonstrated that in DCs these IFN-antagonistic strategies were responsible for an aberrant maturation of the cell, which impaired an adequate activation of especially $CD8^+$ and $CD4^+$ T-cells of the adaptive immune response (Bosio et al., 2003; Mahanty et al., 2003; Lubaki et al., 2013). It is believed that the downregulation of the IFN response supports virus spreading throughout most tissues and organs of the body. However, IFNAR-mediated signaling was not impaired by VP35 (Basler et al., 2003), suggesting that VP35 antagonizes mainly very early sensing events (Figure 3).

In animals models, infection with a VP35-mutated recombinant virus led to IFN-pathway activation as shown by a strong expression of IFN-related genes (Hartman et al., 2008b). Remarkably, just the single mutation of R312 in the VP35 IID and resulting loss of IFN-antagonism impaired virulence significantly in animal models (Hartman et al., 2008a; Prins et al., 2010b). Consistent with this, challenging cynomolgus macaques with a mutated VP35 harboring F239A, K319A, R322A mutations led to a robust immune reaction with mild symptoms, but was able to protect the animals during following wt EBOV challenge (Woolsey et al., 2019). These observations underline that the dsRNA-binding function of VP35 is essential for proper replication of the virus.

1.4.3.2 VP24

Besides the many different strategies of VP35 to avoid IFN activation, VP24 is another important IFN-antagonist. To avoid the establishment of an antiviral state, VP24 interferes with the IFNAR-mediated JAK-STAT pathway. VP24 competes with STATs for KPNA transporter binding and thereby blocks the nuclear import of activated STAT1 (Reid et al., 2006; Reid et al., 2007; Xu et al., 2014; Schwarz et al., 2017) (Table 2). As KPNAs are cargo carriers for different transcription factors and proteins, it is not yet known whether only STAT nuclear import is diminished or if also other pathways are affected by this block (McBride and Reich, 2003) (Figure 3).

Table 2: Antagonistic strategies of EBOV VP35 and VP24 to avoid innate sensing.

Antagonistic strategy	Viral benefit	Viral protein
Sequestering of RIG-I activating dsRNA	Inhibition of RLR-signaling	VP35
Decoy substrate for TBK1 and IKKε	Inhibition of IRF-3 and IRF-7 activation	VP35
Inhibition of PACT-mediated RIG-I activation	Suppression of IFN-β promoter activity	VP35
Inhibition of PKR-activation	Upregulation of protein translation	VP35
Negative influence on IRF-3 and IRF-7 activation by promoting SUMOylation	Inhibition of IRF-3 and IRF-7 activation	VP35
Competition with STATs for KPNA binding	Inhibition of IFN-induced signaling	VP24

1.4.4 Sensing of Ebola virus

EBOV antagonistic functions profoundly impact host innate and adaptive immune responses by globally downregulating important innate immune pathways, particularly RLR signaling. Up to now, it has not been fully understood which PAMPs of EBOV could lead to IFN response. However, the importance of RIG-I during EBOV infection was shown by a study in which RIG-I activation prior to EBOV infection was sufficient to

control viral replication (Spiropoulou et al., 2009). In general, RIG-I is able to sense genomic and subgenomic RNA of negative sense RNA viruses with short dsRNA motifs such as panhandle structures and 5’-ppp (Liu and Gack, 2020). Indeed, production of dsRNA motifs in EBOV genomic RNA as well as mRNA were experimentally proven (Mühlberger et al., 1996; Bach et al., 2021). The highly conserved transcription start sequences and the reinitiation sequences were able to form secondary structures. In line with this, EBOV RNA from particles was sensed by RIG-I, but not by MDA5, suggesting that 5'-ppp with dsRNA motifs are major EBOV PAMPs (Weber et al., 2013). These findings were further supported by decreased sensing of phosphatase-treated EBOV RNA (Habjan et al., 2008).

Besides viral genome features, PAMPs can also derive from defective interfering RNA (DI-RNAs). DI-RNAs are defective viral genome parts and have dsRNA features due to self-interaction of complementary RNA regions and can contain 5’-ppp, which makes them an ideal RLR agonist as well as PKR activator (Takeuchi et al., 2008; Baum et al., 2010; Boonyaratanakornkit et al., 2011). They can be accidently produced by recombination of the genome or defective replication and lead to strong innate sensing (Vignuzzi and López, 2019). For other Mononegavirales such as measles virus (MeV) or SeV, DI-RNAs were determined as the major PAMPs (Strahle et al., 2006; Pfaller et al., 2014). For EBOV, few publications state DI-RNA production during viral replication (Calain et al., 1999). One study identified high amounts of DI-RNA during passaging EBOV in a cell line (Calain et al., 1999), and it was suggested that this may explain persistence of viral genomes for a very long time after acute EBOV infection (Calain et al., 2016). However, a connection between possible EBOV DI-RNA and innate immunity has never been shown.

1.4.5 Role of ADAR1 as a cellular modulator of viral RNA

Besides sensing activity, several cytosolic host factors are able to modify viral as well as cellular RNA, modulating the innate immune response. A prominent example is a family of enzymes known as adenosine deaminases acting on RNA (ADARs). The family consists of three different enzymes with ADAR1 being the most prominent representative.

ADAR1 is an essential RNA-modifying cellular protein that serves to sense dsRNA with the consequence of suppressing innate immune responses. ADAR1 features three distinct mechanisms. First, ADAR1 contains dsRNA-binding domains that are able to bind and sequester cellular or viral RNA to prevent RLR sensing and activation (Vogel et al., 2020). Second, the catalytically active adenosine deaminase domain edits RNA by deamination from adenosine to inosine (A-to-I-editing). As inosine (I) pairs with cytosine (C) instead of uracil (U), ADAR1 editing can alter mRNA decoding, resulting in an amino acid change within the encoded protein (Licht et al., 2019). A third mechanism is the destabilization of RNA within dsRNA motifs, inhibiting sensing of (self-)RNA (Bass and Weintraub, 1988; Bass et al., 1989; Wagner et al., 1989; Serra et al., 2004) as I:U base pairs are less stable than A:U base pairs. These alterations in the RNA secondary structure impairs recognition of RNA by innate immune receptors such as RLRs and is one important features to discriminate between self- and non-self RNA (Mannion et al., 2014; Liddicoat et al., 2015; Pestal et al., 2015) (Figure 3). As well as the RLR pathway, PKR plays an important role during the regulation of innate sensing of not only viruses but also self-RNA and interplays with ADAR1 (Toth et al., 2009; Okonski and Samuel, 2013; Chung et al., 2018). A-to-I editing sites in the human transcriptome are present in noncoding RNAs, pre-mRNAs, and mRNAs with editing sites being mostly *Alu* elements with dsRNA motifs (Levanon et al., 2004; Ramaswami et al., 2012). Remarkably, the total amount of edited adenosines in *Alu* elements has been shown to be below 1% (Bazak et al., 2014; Tan et al., 2017), but nevertheless this seems to be enough to diminish sensing of self-RNA. ADAR1 is expressed in two isoforms (Patterson and Samuel, 1995; Liu et al., 1997). The IFN-inducible ADAR1^{p150} is located mainly in the cytosol, but is able to shuttle between cytosol and nucleus (Eckmann et al., 2001), whereas the constitutively expressed isoform p110 is situated in the nucleus (Liu et al., 1997; George and Samuel, 1999; Kawakubo and Samuel, 2000).

Even though ADAR1 editing is supposed to be highly selective and restricted to self-RNA, it was shown that RNA of several viruses including but not restricted to MeV (Pfaller et al., 2018), SeV (Yang et al., 2014), IAV (Chassey et al., 2013) and recently hepatitis B virus (Wang et al., 2021) and SARS-CoV-2 (Di Giorgio et al., 2020) is targeted by ADAR1.

Especially DI-RNAs of viruses were shown to be a subject for ADAR1-editing (Pfaller et al., 2015). Editing of viral DI-RNAs or genomes can lead to ADAR1-dependent negative regulation of the innate sensing IFN-pathway and establishes ADAR1 as a proviral factor for several viruses (Toth et al., 2009; Li et al., 2012; Pfaller et al., 2014). However, ADAR1 can also act in an antiviral manner by introducing hypermutations into the viral genome (Cattaneo et al., 1988; Bass et al., 1989).

Several recent publications support the hypothesis of EBOV RNA editing by ADAR1. Potential ADAR1-edited genome parts were identified in samples from EBOV disease survivors (Dudas et al., 2017; Whitmer et al., 2018). Another publication suggests potential ADAR1 activity on Marburg virus genomic RNA, a close relative of EBOV, by deep sequencing (Shabman et al., 2014). Furthermore, in an *in silico* approach using algorithms for genome alignment, possible filovirus A-to-I editing sites were identified (Brody et al., 2017). Another recent publication describes the detection of A-to-G (guanine) editing in EBOV genomes upon passaging in bat cells, the natural reservoir of EBOV and to a lower extent in human 293T cells, suggesting ADAR1 activity (Whitfield et al., 2020). Additionally, it was recently shown that the 3'-untranslated regions of EBOV mRNA are ADAR1-edited leading to increased viral translation (Khadka et al., 2021). However, the underlining potential interaction of ADAR1 with EBOV RNA and the consequence for innate sensing of EBOV RNA has not yet been fully determined.

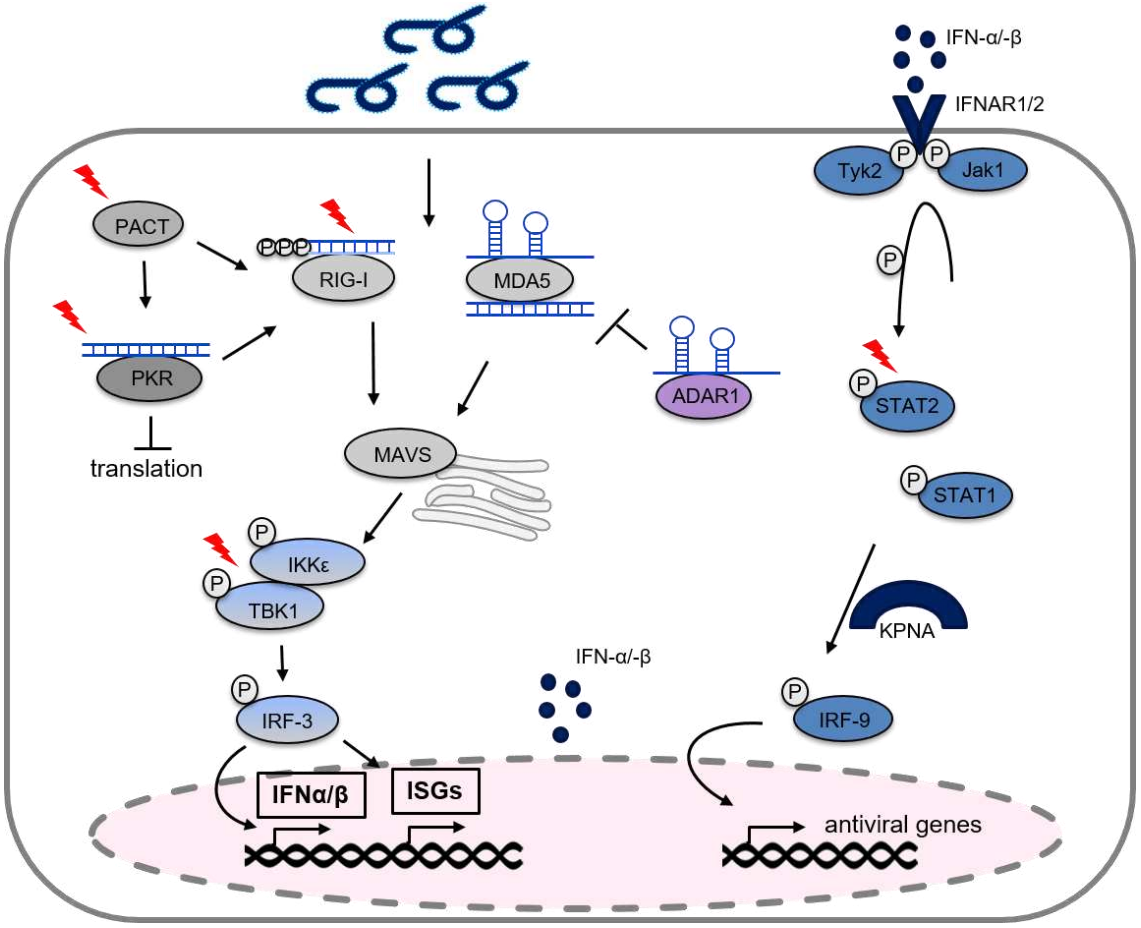

Figure 3: Schematic representation of relevant sensing pathways including inhibitory interactions of EBOV with pathway members. The cytosolic sensors RIG-I and MDA5 can sense different RNA features and subsequently activate the IFN-pathway via MAVS and IRF-3 phosphorylation. PACT is activated by a variety of stimuli and can enhance RIG-I and PKR activation, of which latter one can also be activated by dsRNA features and introduces translational shutdown and can further activate RIG-I. ADAR1 also recognizes dsRNA features and modifies RNA, which abrogates RLR mediated sensing. IFNs can signal in an autocrine and paracrine manner to produce a positive feedback loop via the IFNAR receptors and the JAK-STAT pathway, during which KPNAs transport phosphorylated STATs into the nucleus. Red flashes indicate main antagonistic actions of EBOV.

1.5 Studying virus – host interactions with a reverse genetics system under biosafety level 1/2 conditions

Due to the high pathogenicity as well as the extremely fatal proceeding of viral HF, EBOV is categorized as a biosafety level (BSL) 4 agent. Exceptionally high safety standards apply to working with this category of viruses, which is why many laboratories cannot work with the wt virus. The transcription and replication of a negative viral RNA requires

a RNA-dependent RNA-polymerase and specific RNPs. Consequently, eukaryotic cells cannot produce infectious particles from naked NSV RNA. Therefore, the negative-sense viral RNA does not apply to strict safety measurements and can be handled under BSL-1/2 conditions, as the naked RNA is not infectious (Conzelmann, 2004). Reverse genetics systems make use of this feature by the transcription and replication from complementary DNA (cDNA). In contrast to forward genetics, reverse genetics defines the alteration of a virus genotype and the subsequent analysis of the phenotype. Reverse genetics systems are not only a helpful tool to research extremely dangerous and infectious viruses but also to analyze virtually all steps of the viral life cycle. By introducing targeted changes into the viral genome, it is possible to study direct consequences of the manipulation on e.g. interaction with the immune system, virus entry, transcription, replication, morphogenesis, and budding. There are basically two systems, the minigenome system and the transcription and replication competent virus-like particle system (trVLP system), that allow research under BSL-1/2 conditions and which are used and further developed for very specific research questions (Hoenen et al., 2011). Especially in the research of virus – host interactions reverse genetics systems have been extremely helpful.

1.5.1 Minigenome system

The first minigenome system for EBOV was established in 1999 (Mühlberger et al., 1999). In general, in minigenome systems a reporter gene is flanked by leader and trailer sequences of the EBOV genome, which contain signals for the RNPs (Figure 4A). To facilitate transcription and replication of the minigenome, EBOV RNPs L, VP35, VP30, and NP need to be provided in *trans*. Therefore, they are either cloned on single plasmids and transfected into the producer cell, or they are brought into cells by helper virus infections. Additionally, a T7 DNA-dependent RNA-polymerase is necessary and is usually provided on a plasmid. Thus, the plasmid-based expressed proteins transcribe and replicate the minigenome which is before converted from cDNA into RNA by the T7-polymerase. NP encapsidates the negative RNA minigenome and the nucleocapsid is transcribed by the plasmid-derived RNPs into mRNA and translated into the reporter

protein. The introduction of a reporter such as luciferase offers the opportunity for an easy and fast readout of infectivity. With the minigenome system it is possible to study aspects regarding secondary transcription, meaning the transcription of mRNA by available RNPs, as well as the genome replication.

1.5.2 Transcription and replication competent virus-like particle system

The transcription and replication competent virus-like particle (trVLP) system is sometimes also referred to infectious VLP (iVLP) system. This system functions similar to the minigenome system, but additionally to the reporter gene, all viral genes besides the RNPs, are encoded on one plasmid. In the case of EBOV, a luciferase-reporter (luc), VP40, GP, and VP24 are encoded on a so called tetracistronic minigenome (4cis) (Figure 4A). Comparable to the minigenome assay, the RNPs NP, VP35, L, and VP30 are encoded on separate plasmids and are transfected into cells together with a T7-polymerase and the tetracistronic minigenome. Particles produced in these systems can be used to infect a new generation of cells. In order to infect cells more effectively, it is possible to pre-transfect an EBOV receptor encoding plasmid, such as Tim-1 (Kondratowicz et al., 2011) (Figure 4B). Depending on the research purpose, RNP pre-transfected cells (Watanabe et al., 2004) or naïve cells can be infected with trVLPs (Hoenen et al., 2006). The produced trVLPs are identical to wt EBOV particles, which is a big advantage for viral life cycle research. Even though all viral proteins are potentially packaged in the VLPs, secondary transcription and ongoing replication is only possible in RNP pre-transfected cells. In naïve cells, the life cycle stops after primary transcription by the packaged RNPs. As the virus is not able to further propagate without actively transfected RNPs, the trVLP system is very save to work with under BSL-1/2 conditions (Hoenen et al., 2014).

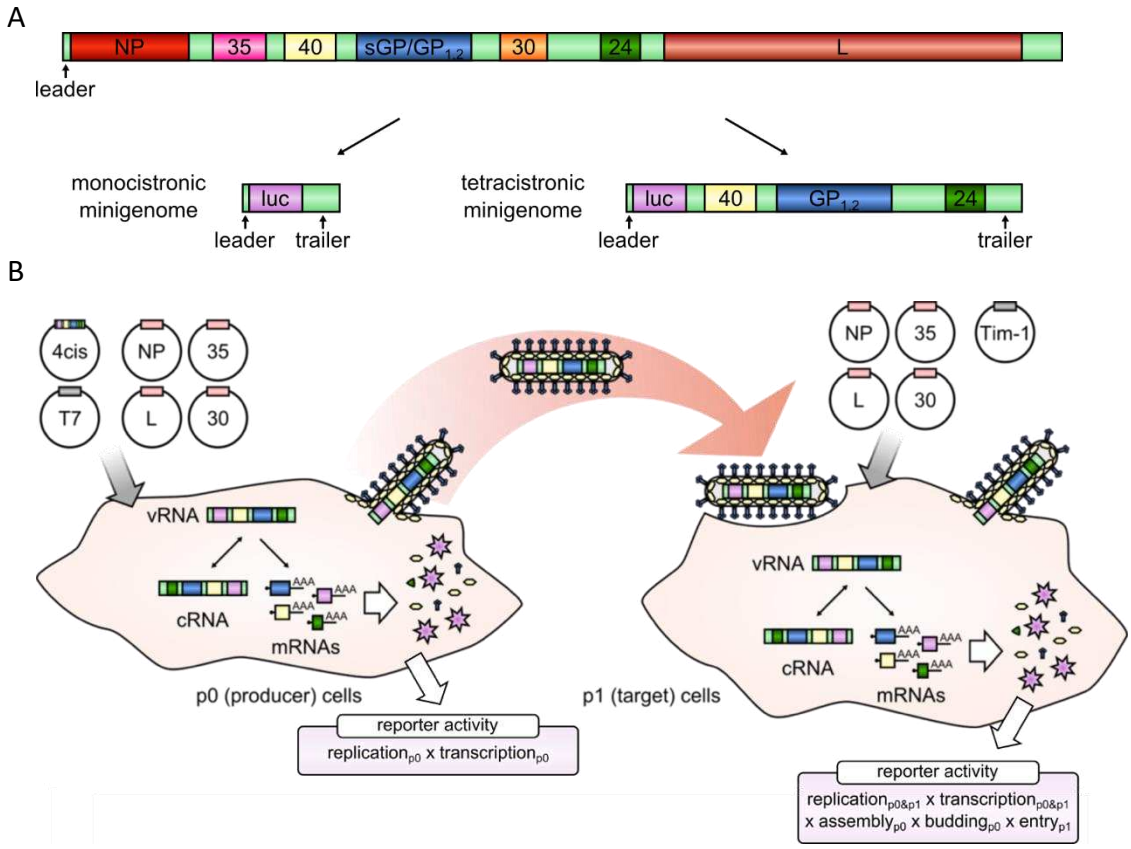

Figure 4: Schematic representation of the minigenome and the trVLP assay. A) Comparison of full-length EBOV genome with shortened monocistronic (1cis) or tetracistronic minigenome (4cis) used in trVLP system. B) trVLP production: p0 cells are transfected with 4cis (encoding a luciferase (luc), VP40, GP, VP24), T7-polymerase, and viral RNPs (NP, VP35, L, VP30). Starting with T7-driven transcription, 4cis is replicated via a cRNA intermediate and transcribed into mRNAs. Subsequently, viral proteins are translated from these mRNAs and are able to assemble into trVLPs. Next, p1 cells are pre-transfected with viral proteins NP, VP35, L, VP30, and Tim-1 (attachment factor) and infected with trVLP-containing supernatant. Infectivity can be determined by luciferase-readout of a luciferase-reporter, which is encoded on 4cis. Figure kindly provided by Thomas Hoenen (and adapted from (Biedenkopf and Hoenen, 2017) with the license number: 5260650035345).

1.6 Aim of this thesis

Initial EBOV replication occurs in DCs and macrophages, the sentinel cells of our immune system. However, infected DCs fail to orchestrate an effective immune response. Virulence is partly associated to EBOV protein VP35, an IFN-antagonist which effectively counteracts the activation of RNA receptors from the RLR pathway family. Nevertheless, by introducing specific mutations in the EBOV VP35 IID strong IFN responses can be detected. Therefore, the early immune response to EBOV seems to be crucial for disease outcome. Cytoplasmic sensing of EBOV has been extensively studied and yet the role of RLRs as proximal sensors as well as possible co-factors involved in sensing have not been determined in detail. Therefore, the thesis aimed to identify and analyze cellular immune sensors and co-factors involved in the early innate sensing pathway and to determine PAMPs of EBOV.

The first goal of the thesis was to optimize a RNA interference (RNAi) screening approach in order to identify immune sensors and co-factors involved in EBOV sensing using an established RNAi library (König et al., 2010; Soonthornvacharin et al., 2017). The siRNAs are expected to target crucial known and unknown proteins regulating the innate immune response. In general, upon siRNA knock-down, cells will be infected with trVLPs. The planned readout was ISG54 induction measured by RT-qPCR. Upon silencing of positive regulators of sensing, it was expected to see less ISG54 signal in comparison to the negative control RNAi treatment and upon silencing of negative regulators, innate sensing was expected to increase. In order to prepare for the RNAi screen, a siRNA transfection assay was optimized. Furthermore, the trVLP assay was established in our laboratory and a new VP35 mutant was cloned to decrease IFN-antagonistic activity in our assays. The mutant was evaluated regarding the IFN-antagonistic capacity as well as regarding the function as a polymerase co-factor.

The second goal was to determine host sensors that could recognize immunostimulatory EBOV RNA. Therefore, RNA was isolated from concentrated trVLPs and quantified by RT-qPCR. RNA was transfected into immunocompetent cell lines pre-treated with siRNAs

for various PRRs and analyzed regarding the ISG54 induction capacity. Furthermore, an immunofluorescence assay was applied to identify possible immunostimulatory dsRNA features of EBOV wt RNA (isolated at the BSL-4 facilities of the Friedrich-Loeffler-Institut).

In the final aim of this thesis, the effect of the RNA-modifying enzyme ADAR1 on innate sensing of EBOV RNA was assessed. Therefore, ADAR1 knock-out cells as well as knock-out cells expressing ADAR1^{p150}, ADAR1^{p110} or an enzyme-inactive mutant ADAR1^{p150in} were generated followed by trVLP production in these cells. Isolated EBOV trVLP RNA was transfected into immunocompetent cells to determine the potential of the respective EBOV RNAs to induce an innate immune response measured by RT-qPCR, as well as Western Blot analysis.

In conclusion, this thesis aims to analyze innate sensors and regulators of the innate signaling pathway, which might be relevant not only for EBOV infection but also for other pathogen infections. Furthermore, the goal was to analyze sensing of EBOV RNA and to investigate a link to altered innate sensing depending on the host factor ADAR1. Providing a better understanding of virus – host interactions and signaling pathways in viral infections is essential in order to develop novel therapeutic and prophylactic antiviral interventions.

2 Materials

2.1 Equipment and consumables

2.1.1 General laboratory equipment

General laboratory equipment	Name	Source
Agarose gel electrophoresis apparatus	Mini-Sub Cell® GT System/ Sub-Cell® GT System	Bio-Rad Laboratories GmbH, Munich (GER)
Automated cell counter	Cellometer Auto T4, Nexcelom Bioscience	VWR, Radnor (US)
Biological safety cabinet	SterilGARD® III Advance	The Baker Company, Sanford (US)
Cell separator	AutoMACS Pro	Miltenyi Biotec, Bergisch-Gladbach (GER)
Centrifuges	Centrifuge 5810 R, Centrifuge 5424 R	Eppendorf, Hamburg (GER)
CO_2 incubator	HERAcell 240	Thermo Fisher Scientific Inc., Waltham (US)
Counting chamber	Neubauer chamber	LO Laboroptik, Lancing (GB)
Electrophoresis system	Novex® Mini-Cell, X Cell Sure Lock, Life Technologies	Thermo Fisher Scientific Inc., Waltham (US)
Flow Cytometer	MACSQuant Analyzer 10	Miltenyi Biotec, Bergisch-Gladbach (GER)
Freezing Container	Nalgene® Mr. Frosty™	Thermo Fisher Scientific Inc., Waltham (US)
Gel blotting module	Novex® XCell II™, Life Technologies	Thermo Fisher Scientific Inc., Waltham (US)
Heater with stirring function	RCT basic	IKA®, Staufen im Breisgau (GER)

High content confocal imaging system	Operetta	PerkinElmer, Waltham (US)
Liquid nitrogen storage compound		Messer, Bad Soden im Taunus (GER)
Luciferase and fluorescence reader	Pherastar FS	BMG Labtech, Ortenberg (GER)
Microscopes	Axiovert 40 C, Eclipse TS 100 Leica SP8	Carl Zeiss Vision, Aalen (GER) Nikon, Chiyoda (JPN) Leica, Wetzlar (GER)
Microvolume spectrophotometer	NanoDrop	Thermo Fisher Scientific Inc., Waltham (US)
Multichannel electronic pipettors	E-Clip pipette	Thermo Fisher Scientific Inc., Waltham (US)
Pipettes	Eppendorf Research® Plus	Eppendorf AG, Hamburg (GER)
Pipettor	Accu-jet pro	Brand, Wertheim (GER)
Platform shaker	Duomax 1030	Heidolph Instruments, Schwabach (GER)
Power supply for gel electrophoresis	PowerPac HC	Bio-Rad Laboratories GmbH, Munich (GER)
Rotor for Ultracentrifugation	SW 32 Ti Swinging-Bucket Rotor	Beckman Coulter, Brea (US)
Scale	XB 160M	Precisa Gravimetrics AG, Dietikon (CHE)
Table top centrifuge	Mini-Centrifuge	Carl Roth GmbH + Co. KG, Karlsruhe (GER)
Thermal cycler for polymerase chain reaction (PCR)	Mastercycler® Nexus	Eppendorf AG, Hamburg (GER)
Thermal cycler for reverse transcription quantitative PCR (RT-qPCR)	CFX384™ Real-Time System	Bio-Rad Laboratories GmbH, Munich (GER)
Thermomixer	Thermomixer comfort	Eppendorf AG, Hamburg (GER)

Ultracentrifuge	Optima L-80 XP	Beckman Coulter, Brea (US)
UV transilluminator		Intas, Göttingen (GER)
UV-Vis spectrophotometer	GeneQuant™ 1300, biochrom™	Harvard Bioscience Inc., Holliston (US)
Vortex mixer	Vortex-Genie 2®	Scientific Industries Inc., Bohemia (US)
Waterbath	SUB Aqua 12 Plus	Grant Instruments, Cambridge (UK)
Western Blot development machine	Curix 60	Agfa, Mortsel (BEL)

2.1.2 Consumables

General consumables	**Cat.No.**	**Source**
Autoradiography film	10607665	Thermo Fisher Scientific Inc., Waltham (US)
Cellometer Disposable Counting Chambers	CHT4-PD100-002	Nexcelom Bioscience, VWR, Radnor (US)
Cell culture flasks (75 cm^2)	658170	Greiner AG, Kremsmünster (AUT)
Cryogenic storage tubes (1.8 mL)	72.379.992	Sarstedt, Nümbrecht (GER)
Cuvettes	XK23	Carl Roth GmbH + Co. KG, Karlsruhe (GER)
Filter paper (Whatman)	11350474	Thermo Fisher Scientific Inc., Waltham (US)
Filter units for syringes (0.4 µM, 0.7 µM)	542040, 542070	Greiner AG, Kremsmünster (AUT)
Microcentrifuge tubes (1.5 mL, 2 mL)	72.706.400, 72.695.400	Sarstedt, Nümbrecht (GER)
Microplate, transparent, 96-well, 6-well (F-bottom)	167008	Thermo Fisher Scientific Inc., Waltham (US)

Microplate, transparent, 96-well (V-bottom)	249935	Thermo Fisher Scientific Inc., Waltham (US)
Microplate, transparent bottom, black, 384-well (F-bottom)	781097	Greiner AG, Kremsmünster (AUT)
Microplate, white, 96-well (F-bottom)	655073	Greiner AG, Kremsmünster (AUT)
Parafilm	10018130	Bemis™ Curwood™, Thermo Fisher Scientific Inc., Waltham (US)
PCR plates, hard-shell, 384-well	HSP3805	Bio-Rad Laboratories GmbH, Munich (GER)
PCR tubes (200 µL)	710970	Biozym, Hessisch Oldendorf (GER)
Petridishes (10 cm)	664160	Greiner AG, Kremsmünster (AUT)
Pipette tips, with filter (20 µL, 100 µL, 200 µL, 300 µL, 1000 µL)	70.1116.210, 70.760.212, 70.3050.255	Biosphere® plus, VWR, Radnor (US)
Pipette tips, with filter for electronic pipettors (12.5 µL, 125 µL)	15942021, 15286293	Thermo Fisher Scientific Inc., Waltham (US)
Pipettes, with filter (5 mL, 10 mL, 25 mL)	606180, 607180, 760180	Cellstar®, Greiner AG, Kremsmünster (AUT)
Polypropylene tubes (15 mL, 50 mL)	188261, 227261	Cellstar®, Greiner AG, Kremsmünster (AUT)
PVDF membrane	15269894	Thermo Fisher Scientific Inc., Waltham (US)
Syringes	4616200V	Omnifix® Braun, Melsungen (GER)
Ultracentrifugation tubes	344058	Beckman Coulter, Brea (US)

2.2 Reagents

Reagent	Cat. No.	Source
Agarose	840004	Biozym, Hessisch Oldendorf (GER)
Ampicillin	K029	Carl Roth GmbH + Co. KG, Karlsruhe (GER)
Antioxidant	11529166	Thermo Fisher Scientific Inc., Waltham (US)
Bovine Serum Albumine (BSA)	8076.4	Carl Roth GmbH + Co. KG, Karlsruhe (GER)
Bradford reagent	5000006	Bio-Rad Laboratories GmbH, Munich (GER)
CD14 MicroBeads	130-050-201	Miltenyi Biotec, Bergisch-Gladbach (GER)
DAPI	10374168	Thermo Fisher Scientific Inc., Waltham (US)
DMSO	A994.2	Carl Roth GmbH + Co. KG, Karlsruhe (GER)
Ethanol abs. (C_2H_6O)	5054	Carl Roth GmbH + Co. KG, Karlsruhe (GER)
Ethanol vergällt (C_2H_6O)		Media kitchen, Paul-Ehrlich-Institut
Glycerol	3783.1	Carl Roth GmbH + Co. KG, Karlsruhe (GER)
Histopaque®-1077	10771	Sigma-Aldrich; Merck KGaA (GER)
Lipofectamine™ 2000	11668-019	Thermo Fisher Scientific Inc., Waltham (US)
Metafectene®	T020	Biontex, München (GER)
β-mercaptoethanol	M6250	Sigma-Aldrich; Merck KGaA (GER)
Methanol (CH_3OH)	T909	Carl Roth GmbH + Co. KG, Karlsruhe (GER)
Paraformaldehyde (PFA)	P6148	Sigma-Aldrich; Merck KGaA (GER)

Passive lysis buffer (5x)	E1941	Promega, Fitchburg (US)
Phorbol-12-myristyl-13-acetate (PMA)	P1585	Sigma-Aldrich; Merck KGaA (GER)
Poly(ethylene)glycol-8000 (PEG)	P2139	Sigma-Aldrich; Merck KGaA (GER)
Poly-l-lysine	25988-63-0	Sigma-Aldrich; Merck KGaA (GER)
Powdered milk	T145	Carl Roth GmbH + Co. KG, Karlsruhe (GER)
Protein gels, (10-well, 15-well)	12020166, 12030166	Thermo Fisher Scientific Inc., Waltham (US)
Protein sample buffer (4x)	NP0007	Thermo Fisher Scientific Inc., Waltham (US)
Puromycin	P9620	Sigma-Aldrich; Merck KGaA (GER)
RNAimax	13778-030	Thermo Fisher Scientific Inc., Waltham (US)
Rnasin® Ribonuclease Inhibitor	N2511	Promega, Fitchburg (US)
Sample reducing agent (10x)	NP0004	Thermo Fisher Scientific Inc., Waltham (US)
Sodium dodecyl sulfate (SDS)	151-21-3	Thermo Fisher Scientific Inc., Waltham (US)
Saccharose (Sucrose)	S9378	Sigma-Aldrich; Merck KGaA (GER)
Transfer buffer (20x)	NP0006-1	Thermo Fisher Scientific Inc., Waltham (US)
TransIT®-LT1	MIR2304	Mirus, Madison (US)
Triton X-100	3051.2	Carl Roth GmbH + Co. KG, Karlsruhe (GER)
Tween®-20	912712	Carl Roth GmbH + Co. KG, Karlsruhe (GER)

2.2.1 Kits

Kit	Cat. No.	Source
ATPlite Luminescence Assay System	6016943	PerkinElmer, Waltham (US)
DNase I kit	E1010	Zymo Research, Freiburg (GER)
DNeasy Blood & Tissues kit	69504	Qiagen, Hilden (GER)
ECL Prime solution detection reagent	28980926	GE Healthcare, Chicago (US)
GeneJET Plasmid Miniprep kit	K0502	Thermo Fisher Scientific Inc., Waltham (US)
iProof™ high-fidelity DNA polymerase kit	172-5331	Bio-Rad Laboratories GmbH, Munich (GER)
Maxima H Minus First Strand cDNA Synthesis Kit	K1681	Thermo Fisher Scientific Inc., Waltham (US)
Maxima SYBR Green qPCR Master Mix (2X) kit	K0251	Thermo Fisher Scientific Inc., Waltham (US)
Nano-Glo® Luciferase Assay	N1110	Promega, Fitchburg (US)
NucleoBond® Xtra Midi kit	740410.100	Macherey-Nagel, Düren (GER)
NucleoSpin® Gel and PCR Clean-up kit	740609.250	Macherey-Nagel, Düren (GER)
NucleoSpin® RNA Plus kit	740984.250	Macherey-Nagel, Düren (GER)
PCR Mycoplasma Test Kit II	A8994	AppliChem, Darmstadt (GER)
pGEM®-T Easy Vector Systems	A1360	Promega, Fitchburg (US)
QuantiTect® SYBR® Green RT-PCR kit	204245	Qiagen, Hilden (GER)

Quick-RNA viral kit	R1034	Zymo Research, Freiburg (GER)
TURBO DNA-free™ Kit	10792877	Thermo Fisher Scientific Inc., Waltham (US)
VeriKine Human Interferon Beta ELISA Kit	41410-1	PBL Assay Science, Piscataway (US)

2.3 Cells, viruses, bacteria

2.3.1 Cells

Cell line	Origin	ATCC no.	Properties	Reference/Source
A549	Human lung epithelial carcinoma	CCL-185	Adherent/ suspension	(Giard et al., 1973)
HEK 293T/17	human embryonic kidney; expressing SV40 large T antigen; specific clone selected for high transfectability	CRL-11268	adherent	(Pear et al., 1993)
HepG2	Human liver epithelial hepatocellular carcinoma	HB-8065	adherent	(Aden et al., 1979)
THP-1	Human acute monocytic leukemia	TIB-202	suspension	(Tsuchiya et al., 1982)

2.3.2 Viruses and virus-related material

Virus(-material)	Provided by/Origin
EBOV RNA (Mayinga-isolate with 4 silent mutations)	Thomas Hoenen, Friedrich-Loeffler-Institut, Greifswald (GER)

Measles virus (C-defective) RNA	Christian Pfaller, Paul-Ehrlich-Institut, Langen (GER)
Sendai virus Cantell strain	Georg Kochs, Medical Center-University of Freiburg (GER) (Cantell and Hirvonen, 1981)

2.3.3 Bacterial strains

Bacterial strain	Genotype	Source
DH5α	F- ϕ80lacZΔM15 Δ(lacZYA-argF) U169 recA1 endA1 hsdR17 (rk-, mk+) phoA supE44 λ- thi-1 gyrA96 relA1	Thermo Fisher Scientific Inc., Waltham (US)
E. coli GM33	F- λ-IN(rrnD-rrnE)1 cysG-(trpS, dam)-aro B3sup-85 supD-dcm-flaA1	Kind gift of Stefan Finke, Friedrich-Loeffler-Institut (Marinus, 1973)
Stbl3	F-mcrB mrrhsdS20(rB-, mB-) recA13 supE44 ara-14 galK2 lacY1 proA2 rpsL20(StrR) xyl-5 λ-leumtl-1	Thermo Fisher Scientific Inc., Waltham (US)
XL1 blue	recA1 endA1 gyrA96 thi-1 hsdR17 supE44 relA1 lac [F´ proAB lacIqZΔM15 Tn10 (Tetr)]	Agilent Technologies, Santa Clara (US)

2.4 Buffers and solutions

2.4.1 Buffers

Name	Formulation or source
Fluorescence activated cell sorting (FACS) buffer	Media kitchen, Paul-Ehrlich-Institut
Freezing medium for adherent cells	10% (v/v) DMSO, 20% (v/v) FBS in DMEM/ RPMI-1640

Freezing medium for suspension cells	10% (v/v) RPMI-1640, 20% (v/v) FBS in DMEM/ RPMI-1640
Lysogeny broth (LB) medium	Media kitchen, Paul-Ehrlich-Institut
LB agar plates (10 cm) with ampicillin	Media kitchen, Paul-Ehrlich-Institut
MACS buffer	Media kitchen, Paul-Ehrlich-Institut
3-(N-morpholino)propanesulfonic acid (MOPS) running buffer	1 M MOPS, 1 M Tris, 69.3 mM SDS, 20.5 mM EDTA Titriplex II
Phosphate Buffered Saline (PBS)	Media kitchen, Paul-Ehrlich-Institut
Radioimmunoprecipitation (RIPA) lysis buffer	100 mM NaCl, 20 mM Tris (pH 7.5), 10 mM EDTA (pH 7.5), 1% (*w/v*) sodium deoxycholate, 1% (*v/v*) Triton X-100), protease inhibitor cocktail (Complete Protease Inhibitor Cocktail, Roche)
Super optimal broth with catabolite repression (SOC) medium	Media kitchen, Paul-Ehrlich-Institut
Stripping buffer	2% (w/v) SDS, 62.5 mM Tris-HCl [pH 6.8], add 100 mM 2-mercaptoethanol before use
TAE buffer	Media kitchen, Paul-Ehrlich-Institut
Transfer buffer for blotting	42.5 mL 20x transfer buffer, 80 mL Methanol, 2.125 mL antioxidant, 725 mL H_2O
Tris-buffered saline with 0.1% (v/v) Tween®-20 (TBST) buffer, pH 7.4	50 mM Tris-HCl, 150 mM NaCl, 0.1% Tween 20, Media kitchen, Paul-Ehrlich-Institut
TE buffer	Media kitchen, Paul-Ehrlich-Institut

2.4.2 Solutions

Solution	Cat. No.	Source
Ammonium chloride		Media kitchen, Paul-Ehrlich-Institut
Opti-Mem® I (1x)	31985-062	Gibco®, Thermo Fisher Scientific Inc., Waltham (US)
Trypsin-EDTA (0.05% trypsin)		Media kitchen, Paul-Ehrlich-Institut

2.4.3 Cell growth media, supplementals, and stimuli

Media/supplemental	Cat. No.	Source
DMEM – high glucose	D6546-500ML	Sigma-Aldrich; Merck KGaA (GER)
Fetal bovine serum (FBS)	F7524	Sigma-Aldrich; Merck KGaA (GER)
GM-CSF	Tradename: Leukine® (sargramostim)	Genzyme, Sanofi, Paris (FRA)
HEPES		Media kitchen, Paul-Ehrlich-Institut
IFN-α2	11100-1	PBL Interferon
IL-4	200-04	Peprotech GmbH, Cranbury (US)
L-glutamine solution	G7513-100ML	Sigma-Aldrich; Merck KGaA (GER)
RPMI-1640	R0883-500ML	Sigma-Aldrich; Merck KGaA (GER)
Sodium pyruvate		Media kitchen, Paul-Ehrlich-Institut

2.5 Proteins and peptides

2.5.1 Enzymes and enzyme inhibitors

Enzyme	Cat. No.	Source
Antarctic phosphatase	M0289S	New England Biolabs, Ipswich (US)
KOD HotStart DNA Polymerase	71086-3	Merck KGaA, Darmstadt (GER)
Phosphatase inhibitor	4906845001	Merck KGaA, Darmstadt (GER)
Protease inhibitor cocktail (cOmplete)	04693124001	Roche, Basel (CH)
T4 polynucleotide kinase (PNK)	M0201S	New England Biolabs, Ipswich (US)
Ribonuklease A (RNase A)	7156.1	Carl Roth GmbH + Co. KG, Karlsruhe (GER)
RNase III	AM2290	Thermo Fisher Scientific Inc., Waltham (US)
RNasin® Ribonuclease Inhibitor	N2511	Promega, Fitchburg (US)
T4 DNA ligase	M0202S	New England Biolabs, Ipswich (US)

All restriction enzymes mentioned in the methods, including corresponding buffers, were purchased at New England Biolabs, Ipswich (US).

2.5.2 Primary antibodies

Western Blot antibody	Species/clonality	dilution	Product ID	Source
anti-ADAR1	rabbit (mc.)	1:1,000	14175	Cell Signaling Technology, Cambridge (UK)

anti-β-actin	mouse (mc.)	1:5,000	A5441	Sigma-Aldrich; Merck KGaA (GER)
anti-β-tubulin	mouse (mc.)	1:1,000	T4026	Sigma-Aldrich; Merck KGaA (GER)
anti-GAPDH	rabbit (mc.)	1:1,000	2118	Cell Signaling Technology, Cambridge (UK)
anti-IRF-3	rabbit (mc.)	1:2,000	ab76409	Abcam, Cambridge (UK)
anti-IRF-3 (phospho)	rabbit (mc.)	1:1,000	4947	Cell Signaling Technology, Cambridge (UK)
anti-MAVS	rabbit (pc.)	1:2,000	ab25084	Abcam, Cambridge (UK)
anti-PKR	rabbit (mc.)	1:1,000	12297	Cell Signaling Technology, Cambridge (UK)
anti-PKR (phospho)	rabbit (mc.)	1:1,000	ab32036	Abcam, Cambridge (UK)
anti-STAT1	Rabbit (mc.)	1:5,000	sc-346	Santa Cruz Biotechnology, Dallas (US)
anti-VP35	rabbit (pc.)	1:1,000	0301-040	IBT Bioservices, Rockville (US)

mc. = monoclonal, pc. = polyclonal

FACS antibody	**Clone**	**Volume per sample in µL**	**Attached fluorophore**	**Source**
CD1a	SK9	2	PE	BioLegend
IgG2b, κ	MG2b-57	2	PE	BioLegend
CD11c	N418	2	Vio Blue	Miltenyi
IgG2b	IS6-11E5.11	2	Vio Blue	Miltenyi

CD14	M5E2	1	Pacific Blue	BioLegend
IgG2b, κ	MOPC-173	1	Pacific Blue	BioLegend
CD163	GHI/61	2	PE	BD Bioscience
IgG1, κ	GHI/61 (RUO)	2	PE	Beckman Coulter
CD206	19.2 (RUO)	2	APC	BD Bioscience
IgG1, κ	MOPC-21	2	APC	BD Bioscience

Immunofluorescence antibody	**Species/clonality**	**dilution**	**Product ID**	**Source**
anti-dsRNA J2	mouse	1:1,000	10010200	Scicons, Szirák (HUN)
anti-IRF-3	rabbit	1:300	11904	Cell Signaling Technology, Cambridge (UK)

2.5.3 Secondary antibodies

Secondary antibody	**Species**	**Dilution**	**Product ID**	**Source**
anti-mouse IgG, HRP-linked antibody	horse	1:10,000	7076	Cell Signaling Technology, Cambridge (UK)
anti-rabbit IgG, HRP-linked antibody	goat	1:10,000	7074	Cell Signaling Technology, Cambridge (UK)
Alexa Fluor-488 anti-mouse IgG (H+L)	donkey	1:500	A11029	Thermo Fisher Scientific Inc., Waltham (US)
Alexa Fluor-555 anti-rabbit IgG	goat	1:300	A32732	Thermo Fisher Scientific Inc., Waltham (US)

2.5.4 Markers and dyes

Marker/Dye	Cat. No.	Source
CellMask™ Deep Red	H32721	Thermo Fisher Scientific Inc., Waltham (US)
DNA ladder	SM1331	GeneRuler™ 1 kb plus, Thermo Fisher Scientific Inc., Waltham (US)
Gel Loading Dye, Purple (6X)	B7024S	New England Biolabs, Ipswich (US)
GelRed®	B-41002	Hölzel, Darmstadt (GER)
Hoechst staining		Media kitchen, Paul-Ehrlich-Institut
Protein Marker PS10 PLUS	310004	GeneON, Ludwigshafen (GER)
Trypane blue	CN76.1	Carl Roth GmbH + Co. KG, Karlsruhe (GER)

2.6 Vectors and plasmids

Plasmid name	Properties	Origin
p4cis-vRNA-nanoluciferase	Expression plasmid for nanoluciferase (nluc), EBOV VP40, EBOV GP, EBOV VP24 for trVLP production	T. Hoenen*
pAX2	Packaging plasmid for lentiviruses	NG3
pCAGGS-EBOV-L	Expression plasmid for EBOV L for trVLP production	T. Hoenen*
pCAGGS-EBOV-NP	Expression plasmid of EBOV NP for trVLP production	T. Hoenen*
pCAGGS-T7	Expression plasmid of T7 polymerase for trVLP production	T. Hoenen*

pCAGGS-Tim1	Expression plasmid of Tim1 surface receptor for trVLP production	T. Hoenen*
pCAGGS-EBOV-VP30	Expression plasmid of EBOV VP30 for trVLP production	T. Hoenen*
pCAGGS-EBOV-VP35	Expression plasmid for EBOV VP35 for trVLP production	T. Hoenen*
pCAGGS-EBOV-VP35.R305A.K309A.R312A	Expression plasmid for EBOV VP35 for trVLP production with three mutations R305A, K309A, R312A	T. Hoenen* (Schümann et al., 2009)
pCAGGS-VP35.F239A.R305A.K309A.R312A.R322A.K339A	Expression plasmid for EBOV VP35 for trVLP production with six mutations F239A, R305A, K309A, R312A, R322A, K339A	J. Wildemann, cloned from plasmid above
pCMV-VSV-G	Expression plasmid encoding VSV-G for lentiviruses	NG3
pSP-Cas9(BB)-2A-GFP	Backbone for CRISPR/Cas9 plasmid-mediated knock-out	NG3
pSP-Cas9(BB)-2A-GFP-ADAR1-Eplus-ex2	Plasmid to introduce CRISPR/Cas9 knock-out in exon 2 of ADAR1	(Pfaller et al., 2018)
pSpCas9(BB)-2A-GFP_ MAVS (exon2)	Plasmid to introduce CRISPR/Cas9 knock-out in exon 2 of MAVS	NG3
pTsin-IRES-puro-p110 ADAR1	Lentiviral expression plasmid encoding ADAR1^{p110}	(Pfaller et al., 2018)
pTsin-IRES-puro-p150 ADAR1	Lentiviral expression plasmid encoding ADAR1^{p150}	(Pfaller et al., 2018)
pTsin-IRES-puro-p150 inactive ADAR1	Lentiviral expression plasmid encoding a mutated ADAR1^{p150} (H910Q/E912A)	(Pfaller et al., 2018)

*Plasmids received from Thomas Hoenen, Friedrich-Loeffler-Institut; unless stated otherwise, these plasmids are described in (Watt et al., 2014).

2.7 Nucleic acids and oligonucleotides

2.7.1 Oligonucleotides for cloning and mutagenesis

Introduced mutation	Sequence (5' – 3')	Use
F239A	GGATTTGAGAAACATTATGTATGATCACTTG CCTGGTTTTGGAACTGCT**GC**CCACCAATTAG TACAAGTGATTTGTAAATTGGG	Forward primer for site-directed mutagenesis of EBOV VP35
F239A	GGA**C**TTGAGAAA**T**ATTATGTATGATCACTTG CC**A**GGTTTTGGAACTGCT**GC**CCACCAATTAG TTCA**G**GT**T**AT**C**TGTAAATTGGG	Reverse primer for site-directed mutagenesis of EBOV VP35
R322A K339A	CCCGCGATTGAT**GC**AGGTTGGGTATGTGTTT TTCAGCTTCAAGATGGTAAAACACTTGGACT C**GC**AATT**TAG**ATGGTCTTCGCTAGCAGAT	Forward primer for site-directed mutagenesis of EBOV VP35
R322A K339A	CCCGCAATTGAT**GC**AGGTTGGGTATG**C**GT**C**T TTCAGCTTCA**G**GATGG**G**AAAACACTTGGACT C**GCG**ATTTAGATGGTCTTCGCTAGCAGAT	Reverse primer for site-directed mutagenesis of EBOV VP35

Underlined = restriction enzyme site; **bold and marked in grey** = mutation site; **bold** = silent mutations to avoid hairpins.

2.7.2 RNA interference

siRNA	Target gene	Sequence or order name
siRPS27a	RPS27a	AAGCTGGAAGATGGACGTACT
si1777	Non-targeting	AAGCGTTCGTCCTATGATCGA
Si177	Non-targeting	AAGGTAATTGCGCGTGCAACT
siMAVS	VISA	Hs_VISA_1 FlexiTube siRNA Hs_VISA_4 FlexiTube siRNA
siRIG-I	DDX58	Hs_DDX58_6 FlexiTube siRNA Hs_DDX58_8 FlexiTube siRNA
siMDA5	IFIH1	Hs_IFIH1_8 FlexiTube siRNA Hs_IFIH1_9 FlexiTube siRNA

All siRNAs were ordered at Qiagen as HP Custom siRNA without Modification (1027423).

2.7.3 Oligonucleotides for reverse transcription quantitative polymerase chain reaction

Name	Sequence forward & reverse (5' – 3')	Gene symbol	Use	Reference/ Source
hISG54	F: CAGCTGAGAATTGCACTGCAA R: GTAGGCTGCTCTCCAAGGAA	*ISG54 (IFIT2)*	Determination of ISG54 induction	(Yoh et al., 2015)
RPL13a	F: CCTGGAGGAGAAGAGGAAAGAGA R: TTGAGGACCTCTGTGTATTTGTCAA	*RPL13a*	Housekeeping gene for normalization	(Yoh et al., 2015)
EBOV p4cis-nluc	F: GGCTACAACCTGGACCAAGT R: TCCCGTATGAAGGTCTGAGC	EBOV p4cis-plasmid nluc	Quantification of EBOV RNA	J. Wildemann (Eurofins)
EBOV VP40	F: ATGTCATATCGGGCCCCAAA R: ATTGGTTGCCTTGCCGAAAT	EBOV wt	Quantification of EBOV RNA	J. Wildemann (Eurofins)
MAVS	F: GGTGCTCACCAAGGTGTCTG R: AGGAGGTGCTGGCACTGATG	*VISA*	Determination of siRNA knock-down	NG3 (Eurofins)
RIG-I	F: CCTACCTACATCCTGAGCTACAT R: TCTAGGGCATCCAAAAAGCCA	*DDX58*	Determination of siRNA knock-down	NG3 (Eurofins)
MDA5	F: AGAGTGGCTGTTTACATTGCC R: GCTGTTCAACTAGCAGTACCTT	*IFIH1*	Determination of siRNA knock-down	NG3 (Eurofins)
EBOV p4cis-nluc standard ssDNA	GGCTACAACCTGGACCAAGTCCTTGAACAGGGAGGTGTGTCCAGTTTCAGAATCTCGGGGTGTCCGTAACTCCGATCCAAAGGATTGTCCTGAGCGGTGAAAATGGGCTGAAGATCGACATCCATGTCATCATCCCGTATGAAGGTCTGAGC	EBOV p4cis-plasmid nluc	Standard for quantification of EBOV RNA	J. Wildemann (IDT)

EBOV VP40 standard ssDNA	ATGTCATATCGGGCCCAAAGTG CTAATGAAGCAAATTCCAATTTG GCTTCCTCTAGGTGTCGCTGATC AAAAGACCTACAGCTTTGACTC AACTACGGCCGCCATCATGCTT GCTTCATACACTATCACCCATTT CGGCAAGGCAACCAAT	EBOV wt	Standard for quantification of EBOV RNA	J. Wildemann (IDT)

F: forward primer, R: reverse primer

2.7.4 Guide RNA oligonucleotides to introduce CRISPR/Cas9 knock-out

Target gene	**Sequence (5' – 3')**
ADAR1	CACCGATGCCCTCCTTCTACAGTCA
MAVS	CACCGATTGCGGCAGATATACTTAT

2.7.5 Sequencing primers

Target	**Sequence (5' – 3')**
ADAR1	F: CCAGACCAGAACCAGCAAGA R: GAGGTTCATGGGGTGGTCC
MAVS	F: TCCAAAAAGTTGAGAAAGAATTGCC R: AGACACAGCAAGAGGAAGAAGGAA
VP35	F: GCGCGCGGCCGCCACAACTAGAACAAAGGGCAGGG R: GCGCTCAGACTAAATTTTGAGTCCAAGTGTTTTACC

2.8 Softwares

Software	Description	Supplier
CFX Maestro	RT-qPCR data processing	Bio-Rad Laboratories GmbH, Munich (GER)
FBS Express software	FACS data analysis	De Novo Software, Glendale, CA (US)
GraphPad Prism 8	Data processing	GraphPad Software, Inc.
Harmony	Microscopy data processing and analysis	PerkinElmer, Waltham (US)
LAS X	Microscopy data processing and analysis	Leica Microsystems, Wetzlar (GER)
Microsoft Office 2010	Basic writing and presentation programs	Microsoft Corporation, Washington (US)
Pherastar	Spectrophotometer data processing	BMG Labtech, Ortenberg (GER)
SnapGene Viewer	Cloning and plasmid organization system	GSL Biotech LLC, Chicago (US)
Vector NTI	Cloning and plasmid organization system	Thermo Fisher Scientific Inc., Waltham (US)

3 Methods

3.1 Molecular biological methods

3.1.1 DNA restriction

Restriction digests were conducted for 1 h at 37°C (5 µL 10x CutSmart buffer, 0.5 µL enzyme 1, 0.5 µL enzyme 2, 3 µg DNA, H_2O = 50 µL). 3 µL antarctic phosphatase (New England Biolabs) and 5.5 µL 10x phosphatase buffer were added to dephosphorylate the 5'-phosphates of the plasmid. Dephosphorylation was conducted for 30 min at 37°C and phosphatase was heat-inactivated for 5 min at 70°C.

3.1.2 Agarose gel electrophoresis and DNA extraction

In brief, for a 1% gel 100 mL TAE-buffer and 1 g agarose were cooked in a microwave and GelRed® dye (Hölzel) was added to a dilution of 1:12,500. Agarose gel was casted and 6x DNA gel loading dye (New England Biolabs) was added to the probes, 1 kb plus ladder (New England Biolabs) was taken along. Gels were connected to electricity for 75 min at 90 V. The correct size of the bands was determined under UV-light. Gel extraction was conducted with the NucleoSpin® Gel and PCR Clean-up Kit (Macherey-Nagel) according to the manufacturer's protocol.

3.1.3 DNA ligation

Ligations of backbones and inserts were conducted overnight at 16°C with 2 µL vector, 7 µL insert, 1 µL T4 DNA ligase (New England Biolabs), 1.5 µL 10x T4 ligase buffer, filled with H_2O to 15 µL.

3.1.4 Heat shock-transformation and bacteria growth

In short, 50 µL of chemically competent bacteria per plasmid were thawed on ice for 30 min and 1 µg of ligated plasmid was added. The mixture was incubated on ice for

30 min and then heated to 42°C for 45 s and subsequently incubated on ice for 2 min. 200 µL of SOC medium were added and the mixture was incubated in a thermomixer at 37°C at 350 rpm for 1 h. This mixture was used either to grow bacteria on 10 cm dishes with 1% agarose in LB medium with ampicillin or as a starter culture. For bacteria growth on LB-agar plates with ampicillin, 200 µL of the starter culture were spread on a 10 cm plate and the plate was incubated overnight at 37°C. Single clone colonies were picked with pipette tips the next day and cultures were grown in 5 mL LB-medium supplemented with 1 mg/L ampicillin on a shaker at 37°C with 225 rpm. Plasmids were isolated the next day with the NucleoBond® Xtra Midi Kit (Macherey-Nagel) according to the manufacturer's protocol. As a starter culture for an overnight culture, the mixture was added to 100 mL LB-medium supplemented with 1 mg/L ampicillin in an Erlenmeyer flask and incubated at 37°C and 225 rpm. Plasmids were isolated the next day with the NucleoBond® Xtra Midi Kit (Macherey-Nagel) according to the manufacturer's protocol.

3.1.5 Nucleic acid quantification

DNA was quantified by light absorbance at a wavelength of 260 nm at a NanoDrop® spectrophotometer (Thermo Fisher Scientific Inc.). Measurements were conducted with 1 µL sample in duplicates and the measurements were normalized to the DNA-free elution medium. The absorbance quotient of the measurements at 260 nm and 280 nm wavelength were calculated to qualify the DNA. Ratios around 1.8 are considered as clean DNA of good quality.

3.1.6 DNA sequencing

DNA sequencing was prepared with 10 µL DNA with a concentration of 100 ng/µL and 4 µL primer with a concentration of 5 µM. DNA was sequenced at LGC genomics by the Sanger sequencing method.

3.1.7 Ebola virus VP35 mutant cloning

In order to evaluate loss of IFN-antagonistic activity of VP35 mutants, mutations were inserted into a plasmid encoding an existing EBOV VP35 mutant. Three additional mutations were inserted into the VP35 R305A K309A R312A (VP35 m1) (Schümann et al., 2009). First, the plasmid for VP35 m1 was transformed with heat shock into *E. coli* GM33. This step was necessary because BclI-HF was used as one restriction enzyme for the cloning procedure, which is inhibited upon dam methylation. *E. coli* GM33 do not methylate the plasmid. Plasmids were isolated from bacteria cultures the next day. For site-directed mutagenesis, specific primers were designed to introduce mutations. Two forward primers and two reverse primers, one specific for the sequence and one optimized with silent mutations to avoid hairpin structures, respectively. A PCR was performed with all four possible primer combinations. In short, PCR was prepared as recommended by the iProof™ High-Fidelity DNA Polymerase (Bio-Rad) protocol (1x: 10 µL 5x HF-buffer, 2.5 µL each primer with a concentration of 10 µM, 20 ng DNA, 1 µL dNTPs, 0.5 µL $MgCl_2$, 1.5 µL DMSO, 0.5 µL iProof polymerase, H_2O = 50 µL). Following thermal cycler conditions were applied:

Step	Temp. [°C]	Time	Cycles
Initial denaturation	98	60 s	
Denaturation	98	10 sec	
Annealing	75	20 sec	30x
Extension	72	3 min	
Final extension	72	3 min	
Hold	4	∞	

Following the PCR, a gel electrophoresis was conducted, followed by gel extraction of the 377 bp product with the NucleoSpin® Gel and PCR Clean-up Kit (Macherey-Nagel). Next, a restriction for the product of the forward primer and the optimized reverse primer and the VP35 m1 vector was conducted with BclI-HF and NheI-HF. After another gel electrophoresis, respective bands were isolated and cleaned-up with the NucleoSpin® Gel and PCR Clean-up Kit (Macherey-Nagel). After ligation of backbone and insert, heat shock-transformation into competent XL1-blue bacteria followed. The

mixture was plated onto 10 cm dishes with 1% agarose in LB medium and ampicillin and the next day, 12 colonies were picked for further growth and transferred into tubes with 5 mL LB medium with ampicillin. The next day, plasmids were isolated with the GeneJET™ Plasmid Miniprep Kit (Thermo Fisher Scientific Inc.) according to the manufacturer's protocol. Plasmids were prepared to send in for sequencing. Sequences were analyzed and all tested plasmids contained following mutations: F239A R305A K309A R312A R322A K339A. This mutant was used for further experiments and is called in the following VP35 m2.

3.1.8 Cloning of plasmids for CRISPR/Cas9 knock-down

In order to prepare the plasmid to introduce a knock-out in cells, the vector pSpCas9(BB)-2A-GFP was digested with BbsI-HF. Agarose gel electrophoresis and DNA extraction by the NucleoSpin® Gel and PCR Clean-up Kit (Macherey-Nagel) followed. ADAR1 gRNA oligomers were phosphorylated for 30 min at 37°C (5 µL gRNA oligomer, 1.5 µL T4 PNK (New England Biolabs), 1.5 µL T4 10 x PNK buffer, filled with H_2O to 15 µL). The T4 PNK was inactivated for 5 min at 95°C. Vector and gRNA were ligated and 1 µL of the mix was heat shock-transformed into competent *E. coli* DH5α bacteria.

3.1.9 Cloning of polymerase chain reaction products to increase the amount for sequencing

TA-cloning is a convenient solution to clone PCR products, e.g. in order to increase the DNA amount. During PCR many polymerases add a single deoxyadenosine to the 3'-end of PCR products. For TA-cloning, a vector with single thymidine overhangs at the 3'-ends can easily be ligated to the insert without further restriction cuts. Here, TA-cloning was used to increase DNA amount of genes that were supposed to have a CRISPR/Cas9-mediated knock-out to check the sequence. To isolate total cellular DNA, the DNeasy Blood & Tissues kit (Qiagen) was applied according to the manufacturer's protocol. The pGEM®-T Easy Vector System I (Promega) provides a vector and a ligase. Ligation was conducted according to the manufacturer's protocol. After ligation, the plasmids were transformed into competent *E. coli* DH5α bacteria.

3.2 Cell biological and virological methods

3.2.1 Cultivation of cells

HEK 293T/17 cells (ATCC CRL-11268), HEK 293T/17 variants, A549 cells (ATCC CCL-185), and HepG2 cells (ATCC HB-8065) were cultivated in DMEM supplemented with 10% (v/v) heat-inactivated FBS and 2 mM L-glutamine (L-glut). THP-1 cells (ATCC TIB-202) and knock-out (KO) variants ΔMAVS (Mankan et al., 2014) and ΔSTING (Mankan et al., 2014) cells were cultivated in RPMI-1640 supplemented with 10% (v/v) heat-inactivated FBS and 2 mM L-glut.

3.2.2 Monocyte-derived dendritic cells and monocyte-derived macrophages

Human peripheral blood mononuclear cells (PBMCs) were isolated from buffy coats (German Red Cross Blood Donor Service, Baden-Württemberg Hessen). Blood was 1:1 diluted with PBS and 15 mL per 50 mL falcon tube layered onto 15 mL Histopaque-1077 (Sigma-Aldrich). Cell separation was carried out by Ficoll density gradient centrifugation (980 g, 30 min, RT, no brake). The white cell layer above the Histopaque-1777 was transferred into a new falcon tube and diluted with 45 mL PBS. PBMCs were centrifuged (550 g, 10 min, RT) and pellets were resuspended in 10 mL 0.86% (*w/v*) ammonium chloride to lyse erythrocytes (15 min, 37°C). Cells were washed twice in PBS and filtered (0.7 µM). Next, cells were counted by a Cellometer Auto T4 (Nexcelom Bioscience) and monocytes were purified using CD14 MicroBeads (Miltenyi Biotec) according to the manufacturer's protocol. In short, per $1x10^7$ cells 80 µL buffer and 20 µL MicroBeads were added. Mixture was incubated for 15 min at 4°C followed by washing in MACS buffer for 10 min at 300 g and the cell pellet was resuspended in 1.5 mL MACS buffer. Unlabeled cells were separated with an AutoMACS Pro Separator (Miltenyi Biotec) (Riess et al., 2017).

To generate monocyte-derived dendritic cells (MDDCs) or monocyte-derived macrophages (MDMs), isolated monocytes were cultured in RPMI-1640 supplemented with 10% FBS (*v/v*), 10 mM HEPES, 2 mM L-glut, 1 mM sodium pyruvate. The cytokines

granulocyte-macrophage colony-stimulating factor (GM-CSF; Leukine® Sargramostim, Genzyme, 280 Units/mL) and Interleukin-4 (IL-4) (800 Units/mL, PeproTech GmbH) were added for differentiation of MDDCs and GM-CSF only (560 Units/mL) for differentiation of MDMs. 72 h later, the respective cytokines were added again in the same concentrations with fresh medium. Another 48 h later, cells were harvested and counted by a Cellometer Auto T4 (Nexcelom Bioscience). Cells were plated for experiments and MDDCs were additionally checked for surface markers and differentiation status by flow cytometry analysis (Bergez et al., 2019).

3.2.3 Generation of CRISPR/Cas9 knock-out cell lines

HEK 293T/17 KO cell lines were generated by CRISPR/Cas9. For MAVS KO a pSpCas9(BB)-2A-GFP plasmid (Addgene) with a guide RNA (gRNA) insert specific for MAVS exon 2 was used (CACCG ATTGCGGCATATACTTAT). The plasmid with the specific insert was cloned previously in our group. Cells were seeded 24 h prior to transfection in a 6-well plate ($2.5x10^5$ cells/well) and 2 µg of plasmid were transfected with TransIT-LT1 (Mirus). 24 h after transfection, cells were checked for GFP expression under a fluorescence microscope and seeded into five 96-well plates with approximately 1 cell/well. GFP-expressing single cells were grown and checked for MAVS expression by Western Blot, in an infection assay with RT-qPCR readout, and by sequencing after TA-cloning (Promega) according to the manufacturer's protocol.

HEK 293T/17 ADAR1 KO cells were generated as described above for MAVS KO cells as a part of the bachelor thesis project of Carl Helmer under my supervision. A gRNA for ADAR1 Exon 2 (CACCG ATGCCCTCCTTCTACAGTCA) (Pfaller et al., 2018) was cloned into a pSpCas9(BB)-2A-GFP plasmid (Addgene). Disruption of the ADAR1 open reading frame was confirmed by Western Blot and sequencing after TA cloning. ADAR1 MAVS double-KO cells were generated from ADAR1 KO cells as described for MAVS KO cells. Stocks of all newly generated cell lines were amplified, mycoplasma tested and frozen in liquid nitrogen.

3.2.4 Generation of lentiviral particles

10 cm dishes were pre-coated with poly-l-lysine and washed with PBS. HEK 293T/17 cells were added and transfected with 4 µg pAX2, 2 µg pCMV-VSV-G and 8 µg pTsin-IRES-puro backbone containing the genetic information for either ADAR1^{p150}, ADAR1^{p110}, or catalytically inactive ADAR1^{p150in} (H910Q/E912A) using Lipofectamine 2000 (Invitrogen). 24 h post transfection (hpt), medium was renewed and another 24 h later, medium was collected and filtered through a syringe filter (0.45 µM), 9 mL fresh medium was added and 24 h later collected and filtered. Lentivirus-containing medium was aliquoted and stored at -80°C.

3.2.5 Generation of stable lentivirus-transduced cells

Generation of lentivirus-transduced cell lines for ADAR1^{p150}, ADAR1^{p110}, and catalytically inactive ADAR1^{p150} (H910Q/E912A) of HEK 293T/17 ADAR1 KO and HEK 293T/17 ADAR1 KO MAVS KO cells was done as described previously (Pfaller et al., 2018). In brief, 293T/17 ADAR1 KO and 293T/17 ADAR1 KO MAVS KO cells were seeded into a 6-well plate and 24 h later 1 mL of lentiviruses for ADAR1^{p150}, ADAR1^{p110}, and catalytically inactive ADAR1^{p150} (H910Q/E912A) was added. Plates were spinoculated for 1.5 h at 30°C (800 g), 24 h later again 1 mL of lentiviruses was added and spinoculated again. 24 h later, medium was exchanged to normal growth medium and on day 5 post seeding 5 µg/mL puromycin was added per well. Cells were grown to confluency with regular exchange of medium and addition of puromycin. Expression of lentiviral transduced proteins was confirmed by Western Blot analysis.

3.2.6 Transcription and replication competent virus-like particle system

The trVLPs were produced as described elsewhere (Watt et al., 2014). In brief, ¼ of a confluent T75 flask with HEK 293T/17 cells were seeded in 12 mL DMEM supplemented with 10% FBS into T75 flasks (p0 generation) and after 24 h (confluency of around 50%) they were transfected with following plasmid constructs: 2.2 µg p4cis-nanoluciferase (4cis-nluc), 2.2 µg T7-polymerase, and viral ribonucleoproteins (1.1 µg NP, 1.1 µg VP35,

9 µg L, 0.7 µg VP30) in 990 µL Opti-MEM using 54 µL TransIT-LT1 (Mirus) for 15 min. The mixture was added to the cells and medium was exchanged 24 h after transfection and twice the volume of DMEM supplemented with 5% FBS and 2 mM L-glut was added onto the cells. One day later (day 4) a second generation of cells (p1) was reverse transfected. Again, ¼ of a confluent T75 flask of HEK 293/17 cells were resuspended in a final volume of 8.8 mL DMEM supplemented with 10% FBS and 2 mM L-glut. Plasmids for following proteins were transfected: 1.1 µg NP, 1.1 µg VP35 (or mutants), 9 µg L, 0.7 µg VP30, and 2.2 µg Tim-1 (attachment factor). The plasmid mixture was added to 1.1 mL Opti-MEM and 47 µL TransIT-LT1 were added. 15 min later, the complexed plasmids were added to the cell suspension and cells were seeded into a T75 flask. 5 days after seeding of p0 cells, p1 cells were infected with 10 mL of trVLP-containing supernatant of p0 cells for 4 h and then medium of p1 cells was exchanged to twice the volume of DMEM supplemented with 5% FBS. The trVLPs from p1 cells were harvested 3 days post infection by centrifuging the supernatant (800 g, 5 min, RT), production was quantified by reporter readout of the luciferase nluc with the Nano-Glo® assay (Promega). In brief, cells of one T75 flask were lysed in 1.6 mL 1x passive lysis buffer (Promega) for 10 min and lysed cells were centrifuged for 3 min at 10,000 g. 30 µL of supernatant were transferred into a white 96-well plate and 30 µL of Nano-Glo® substrate were added. Readout was done with a Pherastar FS (BMG Labtech). TrVLP-containing supernatant was concentrated to isolate viral RNA, or aliquoted and frozen at -80°C for later purposes. Downscaling of the trVLP assay was done according to the seeding area.

3.2.7 Ebola virus VP35 transfection assay and Sendai virus infection

To test the IFN inhibitory capacity of VP35 and mutant versions, 60 µL with $5x10^5$ cells of HEK 293T/17 were prepared in DMEM with 20% FBS and 2 mM L-glut per well. 25 ng of plasmids were complexed with 0.75 µL TransIT-LT1 (Mirus) in 60 µL Opti-MEM/well according to the manufacturer's protocol. In a 96-well plate 60 µL of complexed plasmids were mixed with 60 µL cell suspension and incubated at 37°C with 5% CO_2. 48 hpt, SeV Cantell strain was 1:1,000 diluted in DMEM with 5% FBS and 2 mM L-glut and 120 µL were added per well (SeV final concentration of 1:500) and the plate was

incubated for 1 h. Medium was exchanged to 200 µL of DMEM with 5% FBS and 2 mM L-glut. 24 h after infection, cells were harvested in LBP buffer from the NucleoSpin RNA plus Kit (Macherey & Nagel). Samples were prepared according to the manufacturer's protocol and subjected to RT-qPCR to determine ISG54 levels. For Western Blot analysis, the protocol was scaled up to a 12-well plate.

3.2.8 Sensing assay with transcription and replication competent virus-like particles in primary cells

To determine sensing of primary transcription of trVLPs, fully differentiated MDDCs were seeded into 96-well plates with 30,000 cells/well and subsided for approximately 1 h. 100 µL trVLPs as well as SeV 1:500 diluted were added for 24 h. Cells were transferred into a 96-well V-plate and centrifuged for 5 min at 300 g. Supernatants were removed and cell pellets were resuspended in LBP buffer from the NucleoSpin RNA plus Kit (Macherey & Nagel) as preparation for whole cell RNA extraction for RT-qPCR.

3.2.9 Sensing assay with transcription and replication competent virus-like particles in cell lines

To determine sensing of secondary transcription and replication of trVLPs, cells were reverse transfected in 96-well plates according to a downscaled protocol for p1 trVLP production. In short, per well a mixture of 16 ng Tim1, 8 ng NP, 8 ng VP35 (or m1, m2, empty plasmid), 5 ng VP30, 63 ng L (or empty plasmid) was incubated with 6.6 µL Opti-MEM and 0.3 µL TransIT-LT1 for 15 min. A cell suspension was prepared of 3.5 x 10^5 cells/mL in DMEM supplemented with 10% FBS and 2 mM L-glut. 62.2 µL of cell suspension was added to the plasmid mixture and the whole cell-plasmid mix was seeded per well. 24 h later, medium was exchanged to 200 µL of p0 or p1 trVLPs for 6 h until medium was exchanged to DMEM supplemented with 5% FBS and 2 mM L-glut. 24 h after infection, cells were harvested in LBP buffer from the NucleoSpin RNA plus Kit (Macherey & Nagel) and subjected to RT-qPCR and as well harvested in 50 µL Nano-Glo® Luciferase assay substrate (Promega) and transferred into a 96-well white plate and measured at a Pherastar FS (BMG Labtech).

3.2.10 Concentration of transcription and replication competent virus-like particles and isolation of viral RNA

Two protocols were applied for the concentration of trVLPs. The first protocol was a sucrose cushion, which was used to concentrate trVLPs for further infection experiments. 20% (*w/v*) sucrose were diluted in PBS and stored at 4°C. Up to 30 mL (SW 32 rotor) of trVLPs were underlayed with 5 mL 20% sucrose. Tubes were weight-adjusted on a scale and centrifuged at 90,000 g (SW 32 rotor = 23,000 rpm) for 2 h at 4°C. Supernatant was discarded and tubes were dried. 100 µL DMEM with 5% FBS and 2 mM L-glut were added and tubes were covered with parafilm. After incubation overnight at 4°C, pellets were resuspended in 900 µL DMEM with 5% FBS and 2 mM L-glut.

The second protocol for trVLP concentration was a 50% solution of poly(ethylene)glycol (PEG)-8000 *(w/v)* in PBS, which was followed by RNA extraction from trVLPs. The trVLP-containing supernatant was mixed with PEG-8000 solution to a final concentration of 5% PEG-8000 and rotated over night at 4°C. Per T75 flask of trVLPs, one 50 mL falcon tube was filled with PEG-8000 and supernatants. Supernatants were centrifuged (3220 g, 90 min, 4°C) and pellets were resuspended in the remaining medium after discarding the supernatant. Viral nucleic acids were isolated with the Quick viral RNA kit (Zymo) according to the manufacturer's protocol. Per falcon tube one column was used. To remove possible plasmid DNA contamination, viral nucleic acids were subjected to a DNase-digest as described in the quick viral RNA kit protocol with the DNase I set (Zymo). Upon elution of viral RNA in 50 µL nuclease-free H_2O, 0.5 µL/10 µL RNA RNaseIN Ribonuclease Inhibitor (Promega) were added. Next, viral RNA was quantified by a qPCR. As negative control, one aliquot of viral RNA without RNaseIN was treated with RNase A (Carl Roth) with 1 µL/10 µL RNA for 2 h at 37°C, RNase A was inactivated for 10 min at 72°C.

3.2.11 Transfection of Ebola virus RNA into cells

Per well of a 96-well plate, $1.5x10^4$ of A549 cells were seeded one day prior to RNA transfection. The amount of 100 copies/cell of EBOV RNA was diluted in Opti-MEM at a total volume of 20 µL and complexed with 0.6 µL Metafectene (Biontex) in 30 µL Opti-MEM for 20 min. Medium of cells was removed and the whole 50 µL mix was added to one well. Cells were incubated at 37°C and 5% CO_2. 3 hpt, 50 µL DMEM supplemented with 20% FBS was added and cells were harvested 24 hpt. Total RNA from cells was extracted with the NucleoSpin® RNA Plus Kit (Macherey-Nagel) according to the manufacturer's protocol.

Primary cells were seeded 1 h prior to RNA transfection at $1.5x10^4$ cells/well. The amount of EBOV RNA for 100 copies/cell for one well of a 96-well plate was mixed with Opti-MEM in a total volume of 5 µL. 0.125 µL Lipofectamine 2000 (Thermo Fisher Scientific) in 5 µL Opti-MEM were added and complexed for 20 min. The whole 10 µL were added to one well.

THP-1 cells were activated to differentiate into macrophage-like cells with a final concentration of 60 ng/mL PMA for 48 h prior to experiments. RNA transfection was similar to primary cell transfection.

3.2.12 RNA interference

In order to optimize siRNA knock-down, three different protocols were evaluated (Table 3). In protocol 1, which was used for further siRNA knock-down experiments, for one well of a 96-well plate, 3 pmol siRNA in 30 µL fresh Opti-MEM were mixed with 0.15 µL Lipofectamine RNAimax (Thermo Fisher Scientific) in 30 µL Opti-MEM and incubated for 20 min. Meanwhile, around $2.2x10^5$ cells/mL were prepared in DMEM supplemented with 20% FBS (*v/v*) and 2 mM L-glut. 60 µL cell suspension were mixed with 60 µL of the siRNA mix in the well and incubated for 72 h at 37°C and 5% CO_2. Successful knock-down was visually and chemically determined by death of cells treated with siRPS27a. To determine the ATP levels of siRPS27a treated and untreated cells, the ATPlite

Luminescence Assay System (PerkinElmer) was used according to the manufacturer's protocol. In brief, 50 µL of mammalian cell lysis solution were added per well in a white 96-well plate and incubated for 5 min. Substrate solution was prepared and 50 µL were added and plate was incubated for 5 min in the dark. Readout was done with the Pherastar FS (BMG Labtech).

Table 3: RNAi protocols.

	Protocol 1	**Protocol 2**	**Protocol 3**
Cell preparation	216,000 cells/ml 20% FBS DMEM	216,000 cells/ml 10% FBS DMEM	108,000 cells/ml 10% FBS DMEM
Cells/well	13,000	25,000	13,500
Vol/well	60 µL	120 µL	125 µL
RNAimax	0.15 µL	0.3 µL	0.16 µL
In Opti-MEM	30 µL	5 µL	-
siRNA	3 pmol (0.15 µL)	1 pmol (0.05 µL)	1.5 pmol (0.075 µL)
In Opti-MEM	30 µL	5 µL	25 µL
Add per well	60 µL	10 µL	25 µL

The siRNA knock-down for subsequent EBOV RNA transfection was done as described above. Cells were siRNA-treated and incubated for 48 h at 37°C and 5% CO_2. Successful knock-down was visually determined by death of cells treated with siRPS27a. Two wells per siRNA were harvested in LBP buffer from the NucleoSpin RNA plus Kit (Macherey & Nagel) and subjected to RT-qPCR to determine the knock-down efficiency at the time point of EBOV RNA transfection. EBOV RNA was transfected as described above. Cells were harvested 24 h after EBOV RNA transfection in LBP buffer from the NucleoSpin RNA plus Kit (Macherey & Nagel) and as well subjected to ISG54 mRNA level determination by RT-qPCR.

3.2.13 Assay to confirm ADAR1 knock-out in cells

As an additional control for a successful knock-out of ADAR1 and MAVS, per well $1x10^6$ HEK 293T/17 cells were seeded into 6-well plates one day prior to IFN-α2 stimulation.

IFN-α2 (PBL Interferon) was prepared and added to cells at 1000 U/mL in 500 µL DMEM for 24 h. Cells were harvested and subjected to Western Blot analysis.

3.3 Biochemical and immunological methods

3.3.1 Protein concentration determination

For immunoblot analyses, cells of one well of a 6-well plate were resuspended in ice cold PBS, centrifuged (300 g, 5 min, 4°C) and lysed in 50 µL RIPA-lysis buffer containing a protease inhibitor cocktail (Roche) and for phosphorylation determination also a phosphatase inhibitor (Merck) for 30 min on ice. Lysates were centrifuged (15,000 g, 15 min, 4°C), and protein concentration was measured based on the Bradford assay (Protein Assay Dye Reagent Concentrate, Bio-Rad).

In brief, 5x protein assay dye reagent was prepared in distilled H_2O and samples and RIPA buffer were 1:5 diluted in distilled H_2O. 995 µL of diluted protein assay dye reagent were transferred into cuvettes and 5 µL diluted sample or RIPA buffer were added. After a mixing step, samples were incubated for 5 min in the dark and absorbance was measured in a UV-Vis spectrophotometer (Harvard Bioscience Inc.) at a wavelength of 595 nm. Protein concentration was determined by calculation from a standard curve.

3.3.2 Sodium dodecylsulfate polyacrylamide gel electrophoresis and Western Blot

For the sodium dodecylsulfate polyacrylamide gel electrophoresis (SDS-PAGE) 20 µg of protein per sample were prepared with 4x sample buffer and 10x reducing agent and denatured for 10 min at 70°C. Proteins were separated on pre-casted gels (NuPAGE 4-12% Bis-Tris gradient gels, Invitrogen) in 1x MOPS buffer supplemented with antioxidant (1:1,000; Thermo Fisher Scientific Inc.) in the inner chamber and MOPS buffer only in the outer chamber, at 200 V for 1 h 10 min. 500 mL transfer buffer were prepared with 20x transfer buffer (Bio-Rad), 50 mL methanol, 1 mL antioxidant, and H_2O. Proteins were transferred to a PVDF membrane (Thermo Fisher Scientific Inc.) with the transfer buffer

at 35 V for 1 h 50 min. Membranes were blocked in 0.01% (*w/v*) TBST supplemented with 5% (*w/v*) milk powder (Carl Roth) or 5% (*w/v*) BSA (Carl Roth) for detection of phosphorylation for 1 h at 4°C. Followed by incubation in the primary antibody dilutions in 0.01% (*w/v*) TBST supplemented with 5% (w/v) BSA and 1:2,000 sodium azide at 4°C overnight on a shaking plate. Horseradish-peroxidase (HRP)-linked horse anti-mouse IgG or goat anti-rabbit IgG secondary antibodies (Cell Signaling Technology) at a dilution of 1:10,000 in 0.01% (*w/v*) TBST supplemented with 5% (w/v) milk powder were applied for 1 h at RT. For detection, membranes were incubated in ECL Prime solution (GE Healthcare) for 5 min in the dark. The emitted chemiluminescence was detected at indicated exposure times.

3.3.3 Reverse transcription quantitative polymerase chain reaction

To determine the ISG54 induction, RNA from whole cell lysates was extracted with the NucleoSpin RNA plus Kit (Macherey & Nagel) according to the manufacturer's protocol. Expression of mRNA levels of ISG54 or RPL13a (housekeeping gene) as well as RNA quantification of EBOV trVLP nluc of the tetracistronic minigenome and the ssDNA templates were determined with the QuantiTect SYBR Green RT-PCR Kit (QIAGEN) with respective primers in a 384-well format on a CFX384 Touch Real-Time PCR Detection System (Bio-Rad). In brief, RT-qPCR mixture for one well was prepared with 5 µL SYBR green, 1.8 µL H_2O, 0.1 µL primer mix (including forward and reverse primer at a concentration of 5 mM each), and 0.1 µL RT mix. Per well of a 384-well plate 3 µL RNA and 7 µL RT-qPCR mixture were pipetted. Thermal cycling conditions were applied as following:

Step	Temp. [°C]	Time	Cycles
Polymerase activation	50	30 min	
Initial Denaturation	95	15 min	
Denaturation	95	15 sec	45x
Annealing	56	1 min	
Extension	72	1 min	
Final extension	95	15 sec	
Hold	4	∞	

Relative expression levels of ISG54 were normalized to RPL13a (housekeeping gene) and analyzed by the $2^{-\Delta\Delta C(T)}$ method (Livak and Schmittgen, 2001), depicted as fold inductions over mock, if indicated. Primer efficiencies were tested before in 10-fold serial dilutions and calculated to have an efficiency of >90%.

To quantify copy numbers of isolated viral RNA, specific primers (eurofins) for the nluc gene of the EBOV tetracistronic minigenome plasmid (4cis-nluc) and an ssDNA template for nluc (idt DNA) for concentration dilutions were designed. To determine the copy numbers of wt EBOV RNA, specific primers for VP40 (eurofins) and an ssDNA template for VP40 (idt DNA) were generated. Copy numbers were determined by one-step RT-qPCR and the results are expressed as cDNA-equivalent as we assume that the copy numbers of the viral RNAs are proportional to the respective specific cDNA quantification (Lauterbach-Rivière et al., 2020). In brief, isolated trVLP RNA was 1:10 diluted in H_2O. Per well of a 384-well plate 3 µL RNA and 7 µL RT-qPCR (as described above) were mixed. For the ssDNA dilution curve, 100 µM DNA were diluted from $1:10^6$ to $1:10^{12}$ and 3 µL of each dilution were mixed with 7 µL RT-qPCR mix. The formula for the standard curve was calculated with the natural logarithm of the median and the copy number per well. The equivalent of the RNA copy numbers was determined based on this formula.

As 1-step RT-qPCR quantifies both viral genomic RNA and mRNA, additionally a 2-step RT-qPCR to specifically quantify genomic RNA was conducted with a specific primer for cDNA synthesis (RT-step). For cDNA synthesis, the Maxima H Minus First Strand cDNA Synthesis Kit was used (Thermo Fisher Scientific) and cDNA was synthesized according to the manufacturer's protocol. In short, 1 µL RT-primer, 1 µL 10 mM dNTP mix, 3 µL H_2O, and 10 µL template were mixed. 4 µL RT buffer and 1 µL enzyme mix were added per sample. For each sample, a -RT control was carried along with 1 µL H_2O instead of enzyme mix. The mix was incubated for 10 min at 25°C followed by 15 min at 50°C. The reaction was terminated by heating at 85°C for 5 min. The qPCR was conducted with the Maxima SYBR Green qPCR Master Mix (2X) kit (Thermo Fisher Scientific) according to the manufacturer's protocol. In brief, per sample 6.25 µL Maxima SYBR green, 0.375 µL

of each forward and reverse primer (10 µM), and 4.25 µL H_2O were mixed and 10 µL were added to one well of a 384-well plate. 1 µL of the cDNA template was added. The -RT control for each sample was also measured by qPCR. Thermal cycling conditions were applied as following:

Step	Temp. [°C]	Time	Cycles
Initial Denaturation	95	10 min	
Denaturation	95	15 sec	
Annealing	60	30 sec	40x
Extension	72	30 sec	
Hold	4	∞	

The ssDNA dilution curve was carried along with 1 µL per well and the determination of the RNA equivalents to the ssDNA was done as described above. The underlying assumption for the measurement and calculation of the RNA equivalents was done as follows:

ssDNA concentration: 100 µM = 100 µM/L

Assumption: 1 mol = $6x10^{23}$ copies

$100x10^{-6}$ x $6x10^{23}$ copies/L = $6x10^{19}$ copies/L

$6x10^{19}$ copies/L / 10^6 µL

$6x10^{13}$ copies/µL

6 copies = $1:10^{13}$ dilution

A dilution curve of $1:10^6$ to $1:10^{12}$ was prepared which equals $6x10^7$ copies/µL to 60 copies/µL of ssDNA. After RT-qPCR, the natural logarithm (LN) of the copies/µL of the standard were applied to a graph with the median values of the RNA. A standard curve and formula were included. Based on this formula, the values of the RNA equivalents were calculated.

3.3.4 Enzyme-linked immunosorbent assay

The IFN-β enzyme-linked immunosorbent assay (ELISA) was conducted with the VeriKine Human Interferon Beta ELISA Kit (PBL Assay Science) according to the manufacturer's protocol. In short, reagents and standard curve were prepared and the trVLP-containing supernatants were pre-diluted 1:5 in DMEM with 5% FBS and stored on ice. Antibody concentrate and HRP solution were diluted in concentrate diluent according to the specific lot of the kit. Per well, 50 µL sample diluent and 50 µL pre-diluted sample were added, standard and blank (sample diluent only) were added accordingly. After 1 h incubation, the plate was washed 3x in the provided washing buffer. 100 µL of antibody dilution were added per well and after 1 h washed 3x. Next, 100 µL of HRP solution were added per well and after 1 h washed 3x. TMB substrate solution was pre-warmed to RT and 100 µL were added per well. A 15 min incubation step in the dark followed and 100 µL stop solution were added to each well. Absorbance was determined at 450 nm within 5 min after addition of the stop solution at the Pherastar FS (BMG Labtech).

3.3.5 Immunofluorescence assay

Prior to the immunofluorescence assay, samples were prepared. MeV DI-RNAs (kind gift of Christian Pfaller, Veterinary Medicine, Paul-Ehrlich-Institut, Langen) or EBOV wt RNA were treated with RNase III (Thermo Fisher Scientific). The enzyme was incubated with a concentration of 1 U/µL for 2 h at 37°C and inactivated for 10 min at 72°C. In a black 384-well plate with clear bottom, 5,000 cells in 20 µL of A549 cells were seeded and transfected with RNA 24 h later. In brief, 500 ng/well of RNA or RNase treated RNA in 10 µL Opti-MEM were mixed with 2.5 µL Metafectene (Biontex) in 10 µL Opti-MEM, incubated for 20 min and the complete 20 µL were added onto the cells. 6 hpt, cells were washed 3x with PBS and 20 µL/well of 2% paraformaldehyde in PBS were added for 20 min. After a washing step, 20 µL 0.5% Triton-X100 in PBS were added for 10 min. Following another washing step, 3% BSA in PBS were added for 1 h and next anti-dsRNA antibody (J2, Scicons) was added at 1:1,000 as well as anti-IRF-3 (Cell Signaling Technology) at 1:300 in 3% BSA PBS for 1 h. After a washing step, an anti-mouse IgG

AlexaFluor-488 antibody (Thermo Fisher Scientific) at a concentration of 1:500 as well as an anti-rabbit IgG AlexaFluor-555 antibody (Thermo Fisher Scientific) at a concentration of 1:300 was added in 3% BSA PBS for 1 h. Following a washing step, 20 µL of CellMask Deepred 1:5,000 diluted in PBS was added for 20 min and 1:5,000 Hoechst staining diluted in PBS were added for 2 min. A washing step followed and wells were filled with 40 µL PBS and the plate was closed airtight.

In order to quantify dsRNA spots per cell, the samples were analyzed with a high-content imaging system (Operetta) and the corresponding Harmony Software (PerkinElmer). Cells were counted based on cytoplasm (CellMask Deepred) staining and green spots for stained dsRNA within the cells were counted and green spots in the nuclei were subtracted. The ratio of spots per cytoplasm was calculated. Graphical analysis was conducted at the Leica SP8 microscope and the corresponding LAS X Software (Leica Microsystems).

3.3.6 Flow cytometry analysis

The differentiation status of MDDCs was assessed by flow cytometry analysis. The staining was conducted with $1x10^5$ cells in triplicates. CD1a, CD11c, CD14, CD163, and CD206 were stained including respective IgG controls as described elsewhere (Bergez et al., 2019). In short, 5 days after differentiation, MDDCs were detached from the flask by short incubation with PBS-EDTA on ice followed by resuspendation in PBS. Two washing cycles with FACS staining buffer (PBS containing 10% (v/v) FBS) were followed by addition of Fc-block (1:10, BD) for 10 min at RT. Cells were resuspended in dilutions with specific antibodies or respective isotype-controls and stained for 20 min on ice. Next, cells were washed twice in FACS staining buffer and fixed with 2% (w/v) paraformaldehyde for 20 min on ice and washed twice. Flow cytometry was conducted on the MACSQuant Analyzer 10 (Miltenyi) and analysis was performed with the FBS Express software (De Novo Software). Percentage of positive cells was calculated for each expression marker.

4 Results

4.1 Optimization of an RNA interference screening approach

To determine relevant, but yet unknown, sensors and co-factors of the innate immunity to EBOV, the initial plan was to conduct an RNAi screen with knock-down of sensors and factors in target cells and subsequent infection with trVLPs. The idea of this RNAi screen approach was to determine host factors that are involved in EBOV sensing. After siRNA transfection of target cells, EBOV trVLP infection follows. Upon knock-down of genes of interest, sensing of EBOV trVLPs could be increased or decreased. In order to conduct a high-throughput screening, every step was optimized beforehand.

4.1.1 Efficient RNA interference knock-down in HEK 293T/17 cells

To optimize siRNA knock-down of cells, three different protocols were compared. The protocols differed in the amount of cells per well, the total volume, amount of transfection reagent as well as the amount of siRNA applied. To determine effectiveness of the knock-down, a siRNA against an essential gene for cell survival - RPS27a was applied (Edinger et al., 2015). Accordingly, after siRNA knock-down of RPS27a, cell death can be observed under a microscope and can also be quantified by ATP readout. Here, cells were transfected with siRPS27a or a non-targeting control siRNA and 72 hpt cells were observed under a microscope as well as subjected to an ATPlite assay. Relative light units [RLUs] of luminescence triggered by an ATP reaction were calculated as fold reduction of siRPS27a treated cells to control siRNA treated cells. For all three protocols strong reduction of ATP amounts upon knock-down of RPS27a compared to control siRNA treatment was measured. The strongest effect of ATP reduction was observed for protocol 1. ATP values were reduced by around 35x after knock-down of RPS27a compared to negative control. ATP fold reduction of protocol 2 and 3 were approximately 18x and 20x, respectively (Figure 5). As cell death was assumed

equivalent to knock-down efficiency, it was concluded, that protocol 1 is the most effective for siRNA knock-down.

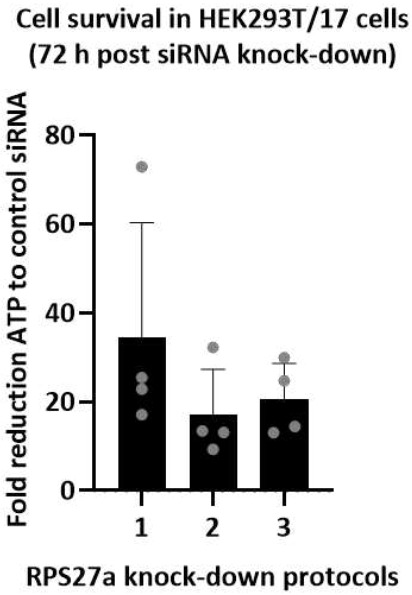

Figure 5: Optimization of siRNA transfection in HEK 293T/17. Cells were transfected with siRPS27a to knock-down an essential gene as well as a non-targeting control siRNA to compare three different protocols. The three protocols differ in the amount of cells per well, the amount of transfection reagent, the amount of siRNA, and the total volume. 72 hpt, an ATPlite assay was conducted to determine cell survival. Fold reduction of RLUs triggered by an ATP reaction in siRPS27a treated cells compared to RLU levels of control siRNA treated cells is displayed. The mean fold reduction of ATP values based on RLUs ± SD of four independent experiments each measured in duplicates is represented.

4.1.2 The transcription and replication competent virus-like particle assay is functional in different cell culture vessels

In order to research EBOV – host interactions the trVLP system is a convenient assay. The trVLP system can be used under BSL-1 conditions while it is able to resemble primary and secondary transcription as well as replication in cells. As outlined before, the tetracistronic minigenome (4cis) encoding for nluc and EBOV proteins VP40, GP, VP24, are transfected into HEK 293T/17 cells together with a T7-polymerase, and viral RNPs (NP, VP35, L, VP30), each on a separate plasmid. In this p0 generation of cells, the T7-polymerase drives replication of 4cis via a complementary RNA intermediate and transcription into mRNAs. Viral proteins are translated from these mRNAs and assemble

into trVLPs. Next, p1 cells are pre-transfected with plasmids encoding the viral proteins NP, VP35, L, VP30, as well as Tim-1 (attachment factor) and infected with trVLP-containing supernatant from p0 cells. The trVLPs from p1 can be used for further experiments or stored at -80°C for further use (Watt et al., 2014). Here, the trVLPs were produced in HEK 293T/17 cells in 96-well plates, 6-well plates, and T75 flasks. As control, the mixture of plasmids for trVLP production was supplemented with an empty vector plasmid instead of the plasmid for the polymerase L. The polymerase is essential for transcription and replication of the viral particles, therefore trVLPs cannot be produced without the polymerase. RLUs of nluc luminescence of wt trVLPs compared to –L controls are approximately 1000x higher for all cell culture vessels, representing substantial production and infectivity of wt trVLPs (Figure 6). The effectivity of the production of trVLPs showed only minor differences between the various cell culture vessels. These results indicate, that the assay was successfully established in the laboratory and is applicable in any size of cell culture vessel.

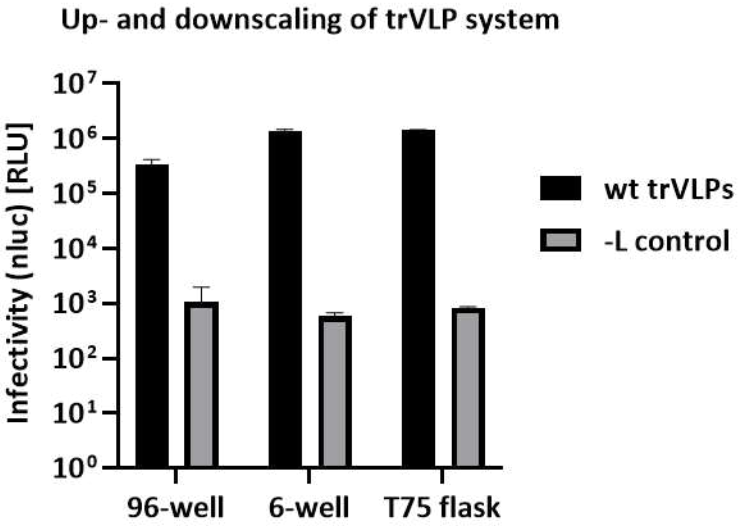

Figure 6: Luciferase-reporter gene activity of trVLPs during production in different cell culture vessels. HEK 293T/17 generation p0 cells were transfected with plasmids encoding 4cis, T7-polymerase, and viral RNPs (NP, VP35, L, VP30). Starting with T7-driven transcription, 4cis is replicated via a complementary RNA intermediate and transcribed into mRNAs. Viral proteins are translated from these mRNAs and assemble into trVLPs. Next, p1 cells were pre-transfected with plasmids for viral proteins NP, VP35, L (or empty vector as –L control), VP30, and Tim-1 (attachment factor) and infected with trVLP-containing supernatant from p0 cells. As the viral polymerase is essential for transcription and replication of trVLPs, the –L control serves as negative control. Infectivity was determined by readout of the nluc reporter gene. Mean ± SD of three technical replicates are shown.

4.1.3 Production of an Ebola virus VP35 mutant with less interferon-antagonistic activity

Due to the fact that VP35 possesses strong IFN-antagonistic activity, it is hardly possible to determine activation of the RLR innate sensing pathway in the presence of VP35 (summarized in 1.4.3.1). In order to overcome this issue, it is possible to research EBOV – host interactions with a VP35 mutated in the IID. One well described mutant is VP35 R305A K309A R312A (in the following called VP35 m1), which shows strong reduction of the IFN-antagonistic activity (Schümann et al., 2009). A second VP35 mutant was generated in order to further decrease IFN-antagonistic activity. To generate this second VP35 mutant, literature was studied to identify further essential amino acids in VP35 responsible for IFN-antagonism (Leung et al., 2010; Luthra et al., 2013; Zhang et al., 2017). Furthermore, the sequences of VP35 EBOV, RESTV, LLOV were compared and analyzed for conserved IFN-antagonistic amino acids (Leung et al., 2010), amino acids for the essential polymerase co-function of VP35 (Leung et al., 2010; Prins et al., 2010a), as well as for TBK1 and IKKε phosphorylation sites (Figure 7A). Based on these analyses, VP35 F239A R305A K309A R312A R322A K339A (in the following called VP35 m2) was cloned from VP35 m1 by inserting three additional point mutations. Successful introduction of the additional alanine substitutions on positions F239, R322, K339 was confirmed by sequencing (Figure 7B).

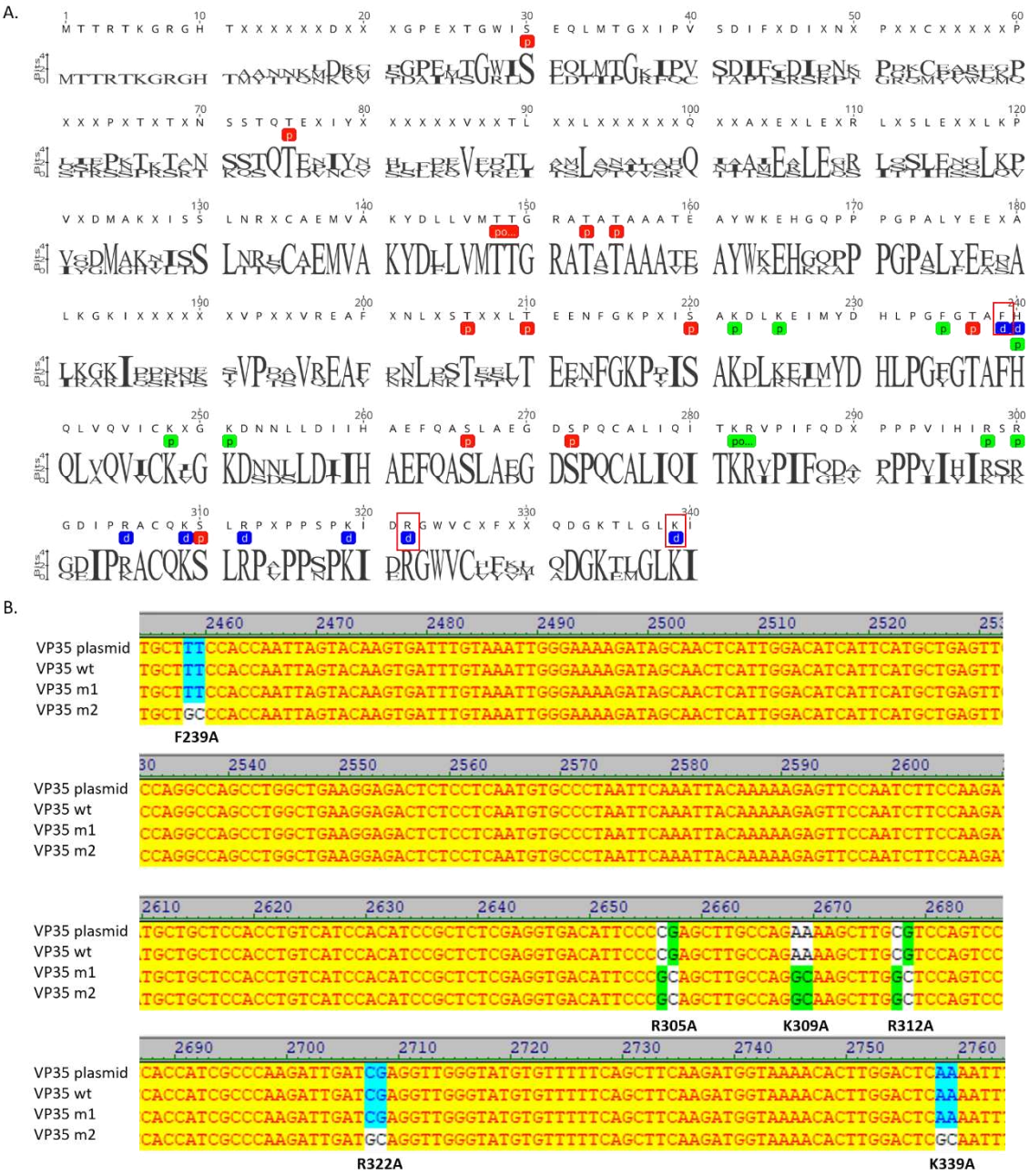

Figure 7: VP35 and mutant sequences. A) VP35 consensus sequence of EBOV, RESTV, and LLOV with different features marked with colors. Positions with one amino acid are highly conserved, whereas positions with several amino acids differ between the compared species. Blue marked amino acids are conserved IFN-antagonistic positions (Leung et al., 2010), green are essential for polymerase co-factor function (Prins et al., 2010a), and red are possible phosphorylation sites for TBK1 and IKKε (serines and threonines in the IID). Additional alanine substitutions for VP35 m2 were introduced on the red framed blue marked positions F239, R322, K339. This figure was adapted from T. Hoenen (Friedrich-Loeffler-Institut, Greifswald, Germany; personal exchange). B) Sequencing results for VP35 wt, m1, and m2 showed the successful introduction of mutations into VP35 m2, marked in light blue. Previous inserted mutations in VP35 m1 are marked in green.

4.1.4 Ebola virus VP35 mutants demonstrate decreased interferon-antagonistic activity

To test the IFN-antagonistic activity of VP35 wt and the mutants, an innate sensing activation assay was conducted. HEK 293T/17 cells were transfected with plasmids encoding VP35 wt, VP35 m1, VP35 m2, or an empty vector (EV). 48 h later, cells were infected with the highly immunostimulatory SeV Cantell strain (Cantell and Hirvonen, 1981). Innate sensing was monitored by measuring the expression of the IRF-3 target gene ISG54 as it represents a direct downstream transcriptional target of IRF-3 (Nakaya et al., 2001; Grandvaux et al., 2002). 24 h post infection (hpi), samples were collected for RT-qPCR of ISG54 and the housekeeping gene RPL13a as well as for Western Blot analysis. RT-qPCR results of ISG54 mRNA levels normalized to RPL13a for EV were set to 100% activation. Compared to EV, VP35 wt displayed decreased ISG54 induction of only 15% of full induction. Interestingly, VP35 m1 activation capacity was at approximately 50% of full ISG54 induction and VP35 m2 showed even less IFN-antagonistic activity and ISG54 mRNA levels were at around 55% of full activation (Figure 8A). A Western Blot was conducted to confirm similar expression levels for all three VP35 constructs (Figure 8B). These results confirmed that VP35 wt indeed inhibits the SeV-induced ISG54 response, whereas VP35 mutants partly alleviate the effect.

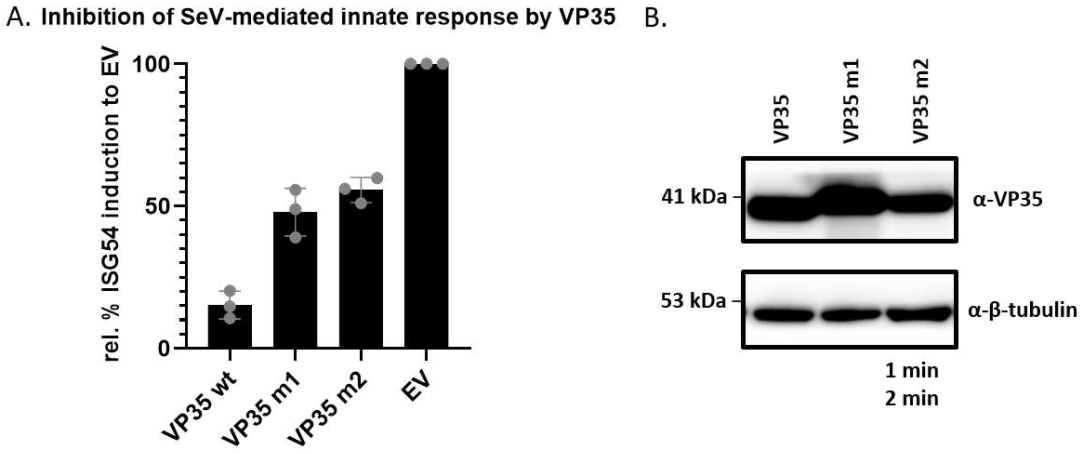

Figure 8: VP35 wt strongly inhibits SeV-induced sensing, whereas VP35 mutants partly alleviate the effect. A) In a 96-well plate, HEK 293T/17 cells were transfected with the indicated plasmids: VP35 wt, VP35 m1, VP35 m2, or empty vector (EV) followed by SeV infection 48 hpt. ISG54 and RPL13a mRNA levels were determined by RT-qPCR 24 h later and normalized. These values were calculated to % induction of

100% ISG54 induction with EV. The mean relative ISG54 induction ± SD of three independent experiments each measured in triplicates is represented. B) VP35 wt, VP35 m1, VP35 m2, or EV were transfected into HEK 293T/17 cells in a 6-well plate. 48 hpt, lysates were subjected to SDS-Page and Western blot to detect expression levels of VP35 by an anti-VP35 antibody. Tubulin served as a housekeeper control. One representative blot of three replications is shown.

4.1.5 Ebola virus VP35 mutants are slightly impaired as polymerase co-factors

To determine the function of the VP35 constructs regarding their properties as polymerase co-factor, trVLPs were produced with either VP35 wt, VP35 m1, VP35 m2, no VP35 (-VP35 control), no L (-L control), or no L and no VP35 (-L -VP35 control). Due to the crucial function of VP35 as well as L during transcription and replication of the viral genome, it is not possible to assemble trVLPs without VP35 or L. Naïve (not pre-transfected) HEK 293T/17 were infected with trVLPs of generation p0. The essential function of VP35 and L was reflected by the nluc reporter activity of the minigenome in the negative controls, which were almost 100x lower compared to infectivity of trVLPs containing VP35 wt. Infectivity of trVLPs with VP35 m2 was approximately 10x less compared to trVLPs with VP35 wt (Figure 9A). Nevertheless, infectivity rates with VP35 m1 and m2 trVLPs were higher compared to controls, indicating that trVLP production is possible with both VP35 mutants.

Infection of HEK 293T/17 cells with trVLPs with VP35 wt did not lead to an ISG54 induction, whereas trVLPs with VP35 m1 and m2 induced slight upregulation of ISG54 mRNA levels to approximately 3x and 6x, respectively (Figure 9B). Even stronger upregulation of ISG54 after infection with trVLPs containing the VP35 mutants was seen in MDDCs (Figure 9C). This reflects the reduced antagonistic function of the VP35 mutants compared to the wt. Nevertheless, upon infection of naïve target cells with supernatants of -VP35 as well as -L -VP35 controls very high ISG54 mRNA levels were detected of approximately 20x and 60x, respectively (Figure 9B). This suggests, that during p0 trVLP production and during preparation of negative controls, strong innate sensing is activated in producer cells. This effect was largely diminished when VP35 wt was present, which inhibited the IFN-response during production (Figure 9B). In fact, this effect was even stronger visible in MDDCs. ISG54 upregulation was more than 1000x

looking at the -VP35 and the -L -VP35 controls. As an additional control, MDDCs were treated with cell culture medium from cultured cells (used medium), which led only to a 2x upregulation of ISG54 mRNA levels compared to mock control. As expected, the -L control which contains VP35 wt only led to an ISG54 upregulation of around 10x compared to mock (Figure 9C). This indicates that steps of the trVLP and control preparation led to unwanted sensing in producer cells rather than sensing of trVLPs in target cells.

To further confirm that IFNs are present in trVLP-containing supernatants that unintentionally would activate the target cells and would confound our results, the supernatants were subjected to an IFN-β ELISA. Indeed, p0 trVLP controls which did not contain VP35 wt showed comparable IFN-β levels to trVLP supernatants containing VP35 m1 or VP35 m2 (with more than 100 pg/mL). In comparison, p0 trVLPs with VP35 wt showed a concentration of approximately 2 pg/mL of IFN-β. Interestingly, IFN-β secretion of all tested supernatants of p1 trVLPs was below detection (BD) (Figure 9D), suggesting that further experiments could be performed with supernatants from p1 trVLPs. Here, p1 trVLPs were generated by pre-transfecting cells with the respective VP35 versions (or for the negative controls without L, or VP35, or both) and infection with VP35 wt trVLP supernatant of p0. This resulted in p1 trVLP supernatant that did not contain any detectable IFN-β according to the ELISA (Figure 9D). In conclusion, both VP35 mutants are able to function as polymerase co-factor. In addition it was discovered that p0 trVLP production with the T7 DNA-dependent RNA-polymerase led to strong unwanted sensing activity and IFN secretion into the medium by producer cells, which was suppressed by VP35 wt, but not by VP35 mutants.

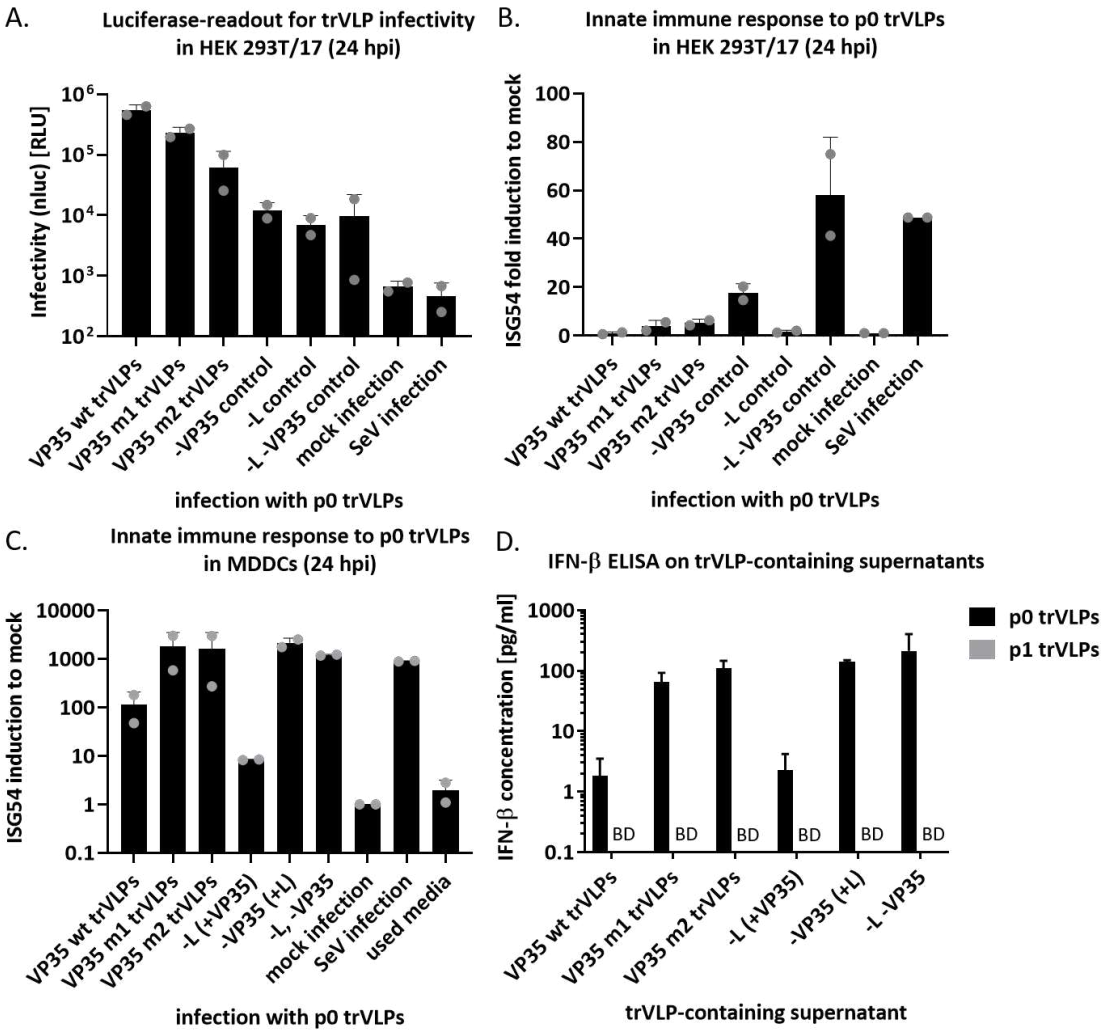

Figure 9: VP35 mutants are less IFN-antagonistic and able to function as a polymerase co-factor but the production process is sensed. P0 trVLPs were produced with VP35 wt, VP35 m1, VP35 m2, and controls without L, VP35, or both. Target cells were infected with p0 trVLP-containing supernatant, SeV or mock for 24 h. A) In HEK 293T/17 cells, infectivity was determined by luciferase-readout of the reporter-gene. The mean luciferase signal ± SD of two independent experiments each measured in duplicates is represented. B) For the same experiment depicted in A) ISG54 and RPL13a mRNA levels were determined by RT-qPCR 24 hpi and normalized to mock. The mean ISG54 induction ± SD of two independent experiments with three technical replicates for each is represented. C) PBMCs were isolated from blood donors, differentiated into MDDCs and infected with p0 trVLPs controls and additionally to A) and B) treated with used media from regular cell culture (negative control) for 24 h. ISG54 and RPL13a mRNA levels were determined by RT-qPCR 24 hpi and normalized to mock. The mean ISG54 induction ± SD of two independent donors each measured in technical triplicates is represented. D) ELISA determination of IFN-β concentrations in p0 and p1 trVLP-containing supernatants (for every sample BD = below detection). The mean IFN-β concentrations ± SD of two independent trVLP batches with two technical replicates for each is represented.

4.1.6 Generation of MAVS CRISPR/Cas9 knock-out cells

In order to avoid IFN production in producer cells, a CRISPR/Cas9-mediated knock-out (KO) of MAVS in HEK 293T/17 cells was performed. After transfection of the respective plasmid encoding the gRNA for the knock-out, single cell clones were grown and promising clones were subjected to functional analysis. Cells were infected with SeV and 24 h later ISG54 induction was determined by RT-qPCR. All tested cell clones showed significantly less (**** $p < 0.0001$) ISG54 induction compared to wt cells (Figure 10A). Next, Western Blot analysis was conducted to determine protein expression levels of MAVS. Several clones did not express MAVS at the expected size of 75 kDa (Figure 10B). Cell clones that did not show any ISG54 mRNA levels after infection as well as no Western Blot band for MAVS were sequenced (Figure 10C). MAVS KO clone 2A11 showed an insertion/deletion polymorphism on both alleles and was therefore determined as producer cell line for trVLPs. In conclusion, the trVLP system was adapted to MAVS KO producer cells. Furthermore, to determine host interactions with EBOV only p1 trVLPs were used.

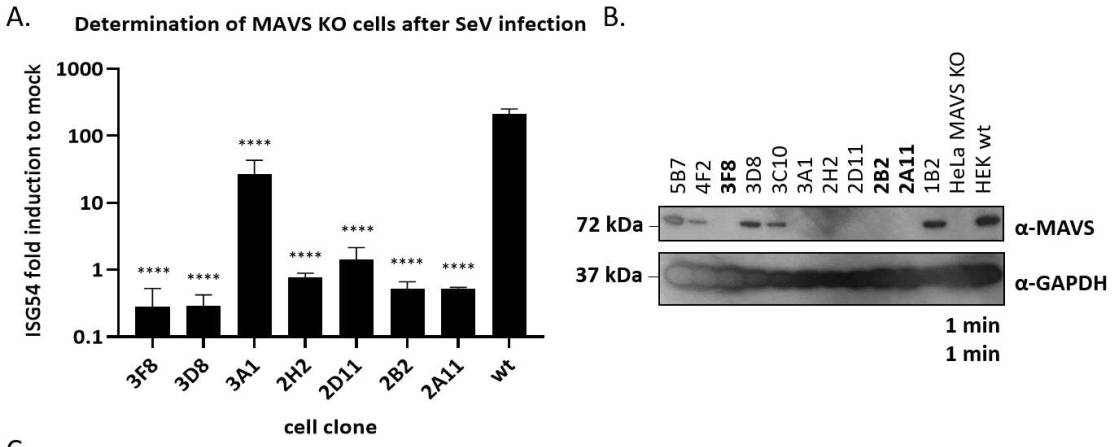

C.

293T/17 MAVS KO (2A11)

MAVS Exon 2		1 pSpCas9(BB)-2A-GFP-MAVS(ex2)		InDel	Stop
	Original:	5‘- ATGCCGTTTGCTGAAGACAAGACCTATAAGTATATCTGCCGCAATTTCAGCAATT -3‘			
		3‘- TACGGCAAACGACTTCTGTTCTGGATATTCATATAGACGGCGTTAAAGTCGTTAA -5‘			
2A11	Allele 1:	3‘- TACGGCAAACGACTTCTGTTCTGG -TAT - - -TATAGACGGCGTTAAAGTCGTTAA -5‘		-4	214
	Allele 2:	3‘- TACGGCAAACGACTTCTGTTCTGGATATTCATATAGACGGCGTTAAAGTCGTTAA -5‘		-5	-24

Figure 10: CRISPR/Cas9-mediated MAVS KO in HEK 293T/17 cells. HEK 293T/17 cells were seeded in 6-well plates and transfected with a plasmid encoding a gRNA to target MAVS exon 2. Successfully transfected clones were grown from single-cell colonies. A) In a functional assay, MAVS mediated signaling after knock-out was determined. Cells from different colonies were infected with SeV for 24 h and ISG54 and RPL13a mRNA levels were determined by RT-qPCR and normalized to mock (not shown). The mean ISG54 induction ± SD of technical triplicates is represented. **** $p < 0.0001$ (Dunnett's multiple comparisons test; induction of each cell clone was compared to induction of wt cells). B) Cell clones were subjected to Western Blot analysis to determine expression of MAVS. C) MAVS sequences of promising clones were amplified by PCR and cloned into a TA-vector system and transformed into competent bacteria. Genetic material was isolated and sequenced in order to determine both alleles of MAVS. Depicted are the original MAVS sequence of the target area of CRISPR/Cas9 KO and both alleles of clone 2A11, which was chosen based on the functional assay as well as the Western Blot results. Both alleles showed deletions of bases, leading to a frameshift and to a premature stop codon.

4.1.7 No sensing of entry and primary transcription of transcription and replication competent virus-like particles in monocyte-derived dendritic cells

To analyze EBOV trVLP interactions with innate sensing pathways, ISG54 induction in target cells after trVLP infection with the different VP35 constructs was determined. First, innate immune response in MDDCs to trVLPs was determined. MDDCs are especially interesting target cells as these cells are primary targets of EBOV and are an important intersection of innate and adaptive immunity (Geisbert et al., 2003). Interestingly, EBOV wt circumvents activation of MDDCs thus inhibiting stimulation of the adaptive immunity (Mahanty et al., 2003). The IFN-antagonist VP35 was identified as the main reason for lack of MDDC activation, whereas VP35 with mutations in the IID did activate MDDCs (Yen et al., 2014).

Infection with trVLPs in naïve cells (not pre-transfected with plasmids for EBOV RNPs) resembles EBOV entry and primary transcription (Hoenen et al., 2006). Sensing capacity and expression levels of sensors and regulators in MDDCs vary strongly depending on the donor, hence MDDCs of four different donors were infected. Reporter-activity for infectivity and ISG54 induction in naïve MDDCs was determined. Significantly higher (**** $p < 0.0001$) trVLP luciferase-reporter activity was measured 24 hpi with trVLPs containing VP35 wt and VP35 m1, compared to SeV infection not encoding any luciferase, indicating successful entry (Figure 11A). Whereas SeV infection led to an upregulation of ISG54 mRNA levels of up to 1000x compared to mock, all other samples

showed significantly lower (*** p < 0.0003) ISG54 induction. In fact, no increased ISG54 mRNA levels were determined upon infection with trVLPs compared to mock infection (Figure 11B), despite functional immune sensing pathways to RNA viruses as was seen with SeV infection.

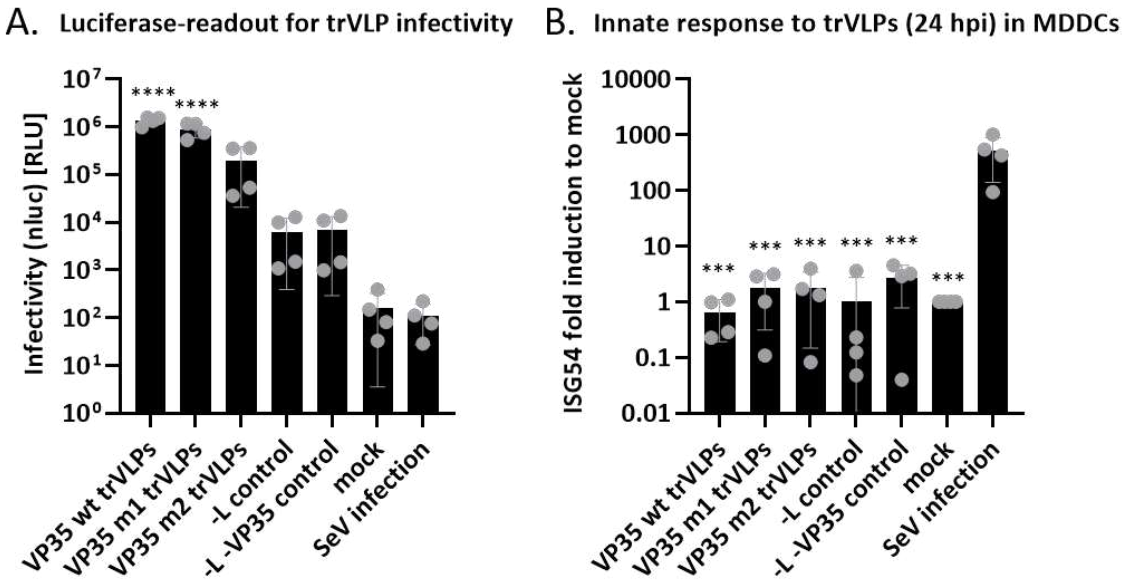

Figure 11: No sensing of p1 trVLP entry and primary transcription in MDDCs. PBMCs were isolated from blood of different donors, differentiated into MDDCs and infected with p1 trVLPs produced with VP35 wt, VP35 m1, or VP35 m2, -L, -L -VP35 or infected with SeV (positive control) or mock (negative control) for 24 h. A) Infectivity of trVLPs was determined by readout of the luciferase-reporter activity. The mean luciferase signal ± SD of four independent donors each measured in duplicates is represented. **** $p <$ 0.0001 (Dunnett's multiple comparisons test; RLUs of all samples were compared to RLUs of SeV infection). B) ISG54 and RPL13a mRNA levels were determined by RT-qPCR 24 hpi and normalized to mock. The mean ISG54 induction ± SD of four independent donors each measured in technical triplicates is represented. *** $p < 0.0003$ (Dunnett's multiple comparisons test; ISG54 induction values of all samples were compared to ISG54 induction of SeV infection).

To determine the right sensing window, a time course experiment was conducted. MDDCs of two different donors were infected with trVLPs and samples were taken 6 h, 24 h, and 48 h after infection. In none of these time points any sensing of trVLPs was detected (Figure 12A+B). In conclusion, in this setting, entry and primary transcription of trVLPs are not sensed in MDDCs, including VP35 mutants with strongly reduced IFN-antagonistic activity.

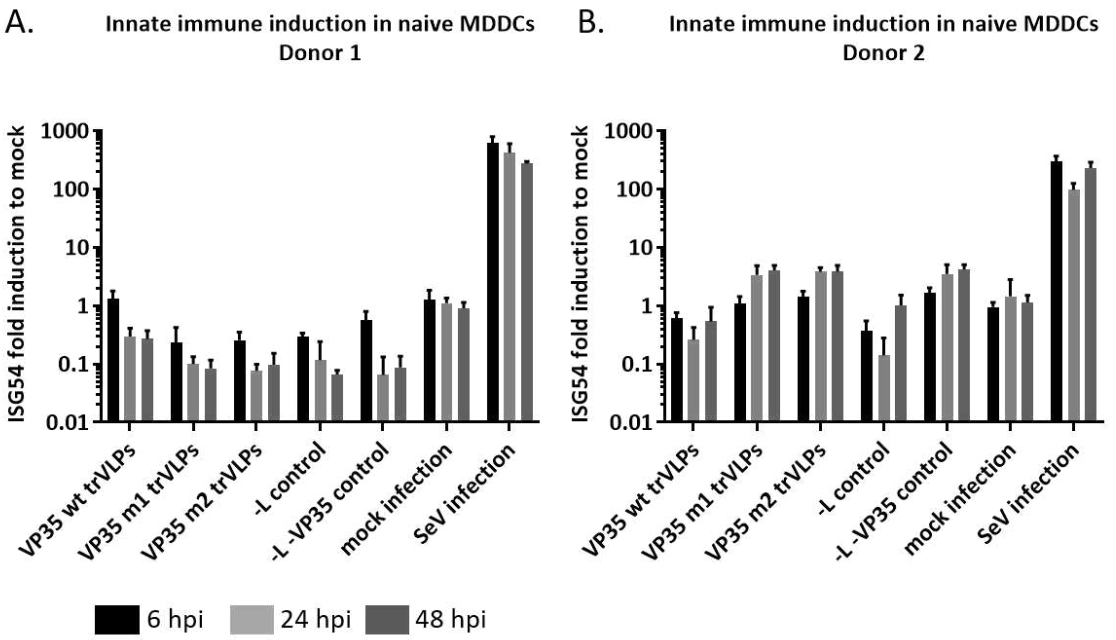

Figure 12: No sensing of p1 trVLP entry and primary transcription in MDDCs from two different donors at different time points. PBMCs were isolated from two different blood donors, differentiated into MDDCs and infected with p1 trVLPs produced with VP35 wt, VP35 m1, VP35 m2, -L control, -L -VP35 control, or treated with medium (mock infection) or infected with SeV (positive control) for 6, 24, and 48 h. A+B) ISG54 and RPL13a mRNA levels were determined by RT-qPCR and normalized to mock for two donors. The mean ISG54 induction ± SD of technical triplicates is represented.

4.1.8 No sensing of secondary transcription and replication of transcription and replication competent virus-like particles in target cells

Next, sensing of secondary transcription and replication of trVLPs by target cells was determined. To include all combinations of transfection and infection, two different set-ups were conducted. First, HEK 293T/17 wt cells were transfected prior to trVLP infection according to p1 generation trVLP producer cells, untransfected cells served as controls. In the next step, cells were infected according to the pre-transfection with p1 trVLPs for VP35 wt, VP35 m1, VP35 m2 as well as -VP35 control, SeV, or empty medium (mock) (Figure 13A). In the second set-up, infection was done with VP35 wt trVLPs after transfection of indicated plasmids (Figure 13B).

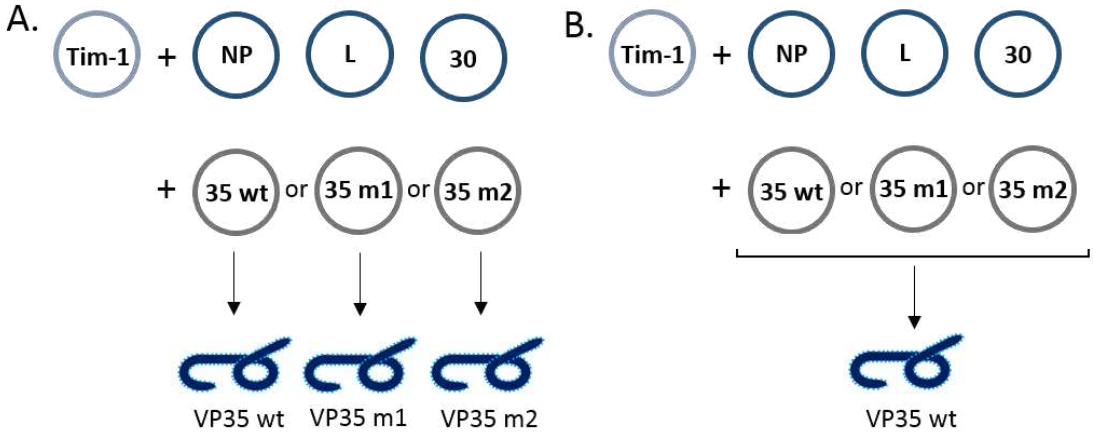

Figure 13: Schematic overview of pre-transfection and infection of trVLPs in target cells. HEK 293T/17 wt cells are transfected prior to trVLP infection according to p1 generation trVLP producer cells with Tim-1, NP, L, VP30 as well as VP35 wt or VP35 m1 or VP35 m2. A) Cells are infected with p1 trVLPs for VP35 wt, VP35 m1, VP35 m2 according to the pre-transfection of VP35. B) Cells are infected with VP35 wt trVLPs.

For the first set-up, substantial trVLP luciferase-reporter activity was measured 24 hpi for trVLPs with VP35 wt and for VP35 m1, indicating successful infection. In contrast, after pre-transfection with VP35 m2 and according infection with VP35 m2 trVLPs, decreased infectivity was measured (Figure 14A). However, no increased ISG54 mRNA levels were detected upon infection with VP35 m1 trVLPs whereas SeV infection elicited a very strong ISG54 mRNA upregulation of up to 300x compared to mock (Figure 14B). In the second set-up, infectivity was restored with VP35 m2 pre-transfection and VP35 wt trVLP infection (Figure 14C). Interestingly, very slight ISG54 mRNA upregulation was detected of around 8x for VP35 m1 compared to mock (Figure 14D).

In conclusion, in the second setting, slight sensing of secondary transcription and replication of trVLPs was measured. Due to the fact that VP35 m2 showed evidence of decreased activity as polymerase co-factor in this set-up, this mutant was excluded from further experiments.

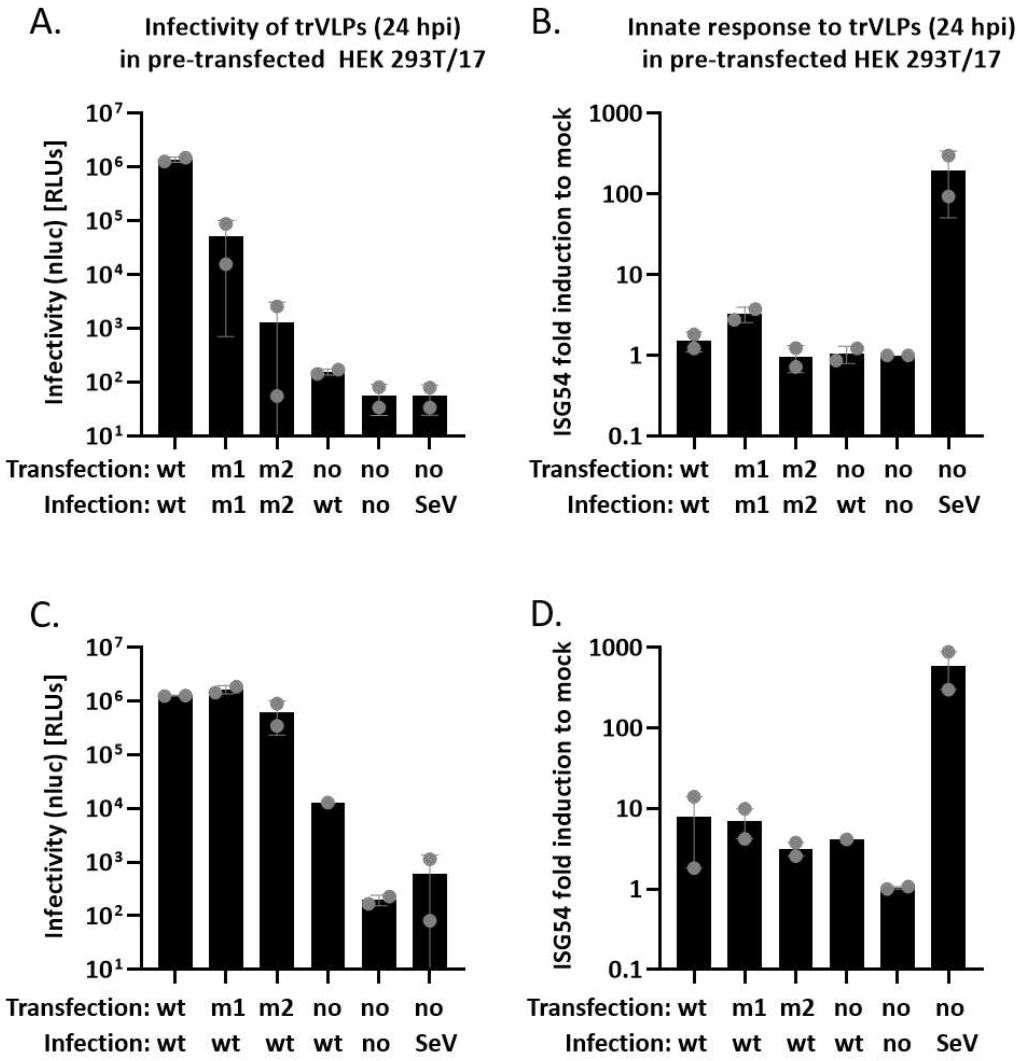

Figure 14: Generation p1 trVLP infection of HEK 293T/17 cells slightly elicits an ISG54 induction upon secondary transcription and replication. HEK 293T/17 cells were pre-transfected with Tim-1 and the RNPs L, VP30, NP, and VP35 versions (as indicated) and infected with p1 trVLPs including VP35 versions (as indicated) or infected with SeV (positive control), or medium (no) for 24 h. A) Pre-transfected cells were infected according to the transfection with trVLPs containing VP35 wt, VP35 m1, VP35 m2, or no VP35 or not infected or SeV infected. Infectivity of trVLPs was determined by luciferase-reporter activity. Mean ± SD of two independent experiments with duplicates each is represented. B) Pre-transfected cells were infected according to the transfection with trVLPs containing VP35 wt, VP35 m1, VP35 m2, or no VP35 or not infected or SeV infected. ISG54 and RPL13a mRNA levels were determined by RT-qPCR 24 hpi and normalized to mock. The mean ISG54 induction ± SD of two independent experiments with three technical replicates each is shown. C) Pre-transfected cells were infected with trVLPs containing VP35 wt, or mock infected, or SeV infected. Infectivity of trVLPs was determined by luciferase-reporter activity. Mean ± SD of two independent experiments with duplicates each is represented. D) Pre-transfected cells were infected with trVLPs containing VP35 wt, or mock infected, or SeV infected. ISG54 and RPL13a mRNA levels were determined by RT-qPCR 24 hpi and normalized to mock. The mean ISG54 induction ± SD of two independent experiments with three technical replicates each is shown.

As the slight upregulation of ISG54 hinted towards the possibility that sensing of trVLPs in a cell line is indeed possible, a higher concentration of trVLPs was prepared. The trVLPs were concentrated approximately 60x by a sucrose cushion, a commonly used method for virus concentration (Takamatsu et al., 2020). Unexpectedly, the infectivity of trVLPs in VP35 m1 pre-transfected HEK 293T/17 cells was only 100x higher than in mock infected cells (Figure 15A), which was comparable to infectivity of trVLPs which were not concentrated. Given the prior concentration of trVLPs, the infection rate was expected to be higher. No ISG54 induction was detected after infection with these trVLPs (Figure 15B).

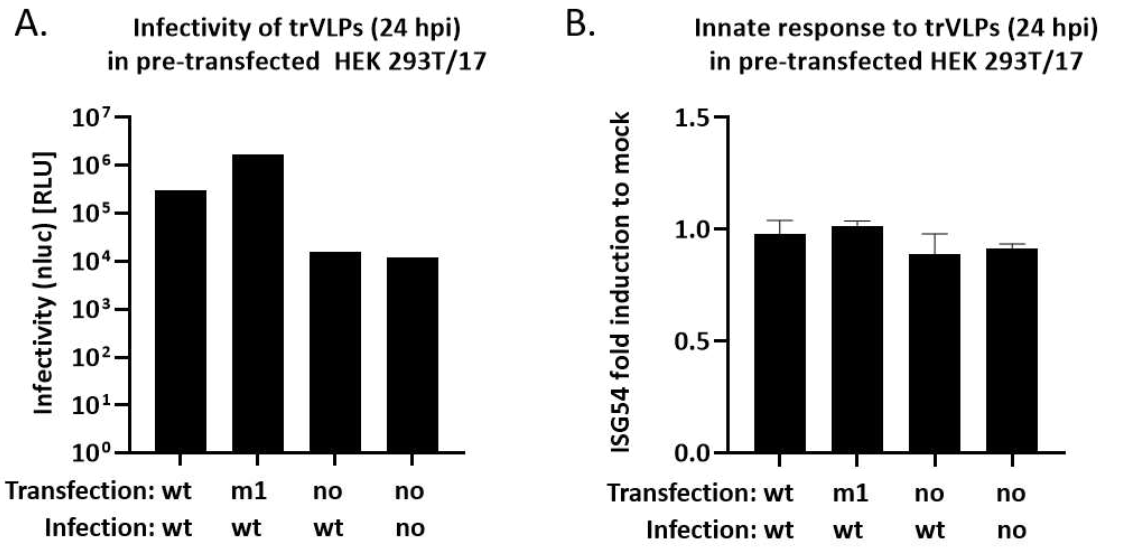

Figure 15: No sensing of concentrated trVLPs in HEK 293T/17 cells. Generation p1 trVLPs were approximately 60x concentrated. HEK 293T/17 cells were pre-transfected with Tim-1 and the RNPs L, VP30, NP and VP35 (as indicated) and infected with concentrated p1 trVLPs produced with VP35 wt or mock infected for 24 h. A) Infectivity of concentrated trVLPs was determined by readout of the luciferase-reporter activity. One representative experiment is shown. B) ISG54 and RPL13a mRNA levels were determined by RT-qPCR 24 hpi and normalized to mock. The mean ISG54 induction ± SD of three technical replicates of one representative experiment of three replicates is shown.

In addition, HepG2, a human liver cancer cell line was tested for the susceptibility to EBOV trVLPs. HepG2 cells were pre-transfected with RNPs including either VP35 wt or VP35 m1 and infected with trVLPs containing VP35 wt. 72 hpi, HepG2 reporter-activity was determined. Luciferase reporter values in HepG2 were comparable to similar

experiments with HEK 293T/17 cells (Figure 16A). Also in HepG2 cells, ISG54 induction was not considerably increased compared to mock infected cells with an induction of approximately 8x compared to mock. In contrast, SeV infection led to almost 1000x ISG54 induction, indicating intact RNA virus sensing pathways in HepG2 cells (Figure 16B).

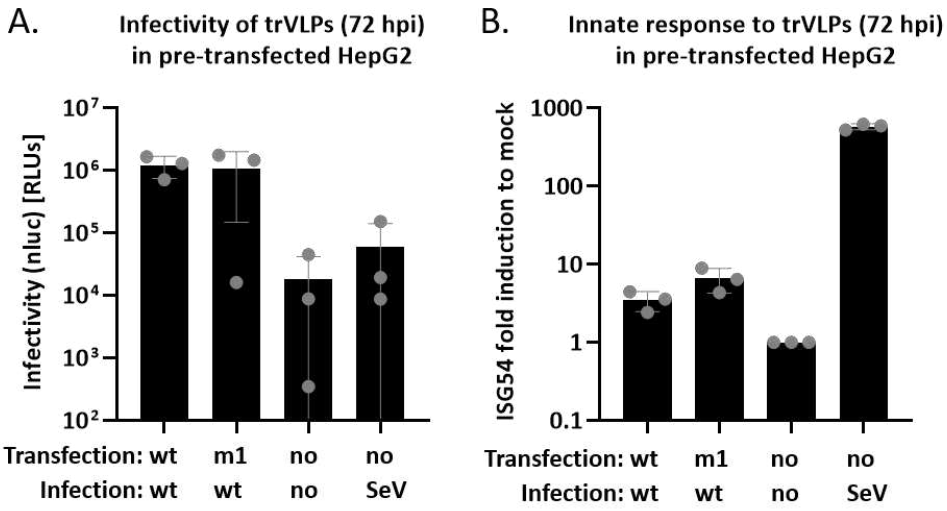

Figure 16: No sensing of p1 trVLPs in HepG2 cells. Cells were pre-transfected with Tim-1, and the RNPs L, VP30, NP, and VP35 (as indicated) and infected with p1 trVLPs produced with VP35 wt, mock infected or SeV infected. A) In HepG2 cells, infectivity of trVLPs was determined by readout of the luciferase-reporter activity 72 hpi. Mean ± SD of three independent experiments with duplicates each is represented. B) In HepG2 cells, ISG54 and RPL13a mRNA levels were determined by RT-qPCR 72 hpt and normalized to mock. The mean ISG54 induction ± SD of three independent experiments with three technical replicates each is represented.

In conclusion, the initial research plan of this study to perform an RNAi screen seemed not feasible due to the following reasoning: Production of p0 EBOV trVLPs activated IFN and sensing pathways in target cells unless VP35 wt was present. The supernatants of EBOV p0 trVLPs contained IFN and led to strong IFN pathway activation in target cells. To circumvent this problem, MAVS KO producer cells were generated and infection experiments were conducted with p1 trVLPs. Unfortunately, despite high infectivity, no ISG54 induction was detected in different target cells. The concentration of trVLPs and subsequent infection of target cells did also not result in increased ISG54 induction. Therefore, the system is not applicable to conduct a siRNA screen to determine sensors

and co-factors of sensing upon EBOV trVLP infection. Based on these insights, the focus of the project was adjusted to the question of the nature of the PAMPs that could be sensed by target cells and which PRRs are involved in sensing. Following this research question, we were interested in the question what role ADAR1 does play in EBOV sensing.

4.2 Determination of host sensors of Ebola virus RNA

To determine interactions of EBOV RNA with host sensors and regulators, the immunostimulatory capacity of EBOV nucleic acids was analyzed. Furthermore, the sensors of EBOV RNA and the nature of the PAMP were determined.

4.2.1 Ebola virus transcription and replication competent virus-like particles nucleic acids are highly immunostimulatory in primary myeloid cells

To determine the immunostimulatory capacity of EBOV trVLP nucleic acids, purified nucleic acids from trVLPs were transfected into primary cells. Again, the trVLP system was used as a model system for EBOV secondary transcription and replication. Therefore, different RNA intermediates that are potentially immunostimulatory can be found in trVLPs. For viral nucleic acid production, trVLPs of generation p1 were produced and infectivity was confirmed in a nluc reporter assay (data not shown). The trVLPs were collected, concentrated with the PEG-8000 method, and viral nucleic acids were isolated. Isolated nucleic acids were quantified by 1-step RT-qPCR with specific primers and standards to determine total viral RNA (genomic RNA, mRNA, and detectable intermediates). This process ensured that the copy numbers of transfected nucleic acids were controllable.

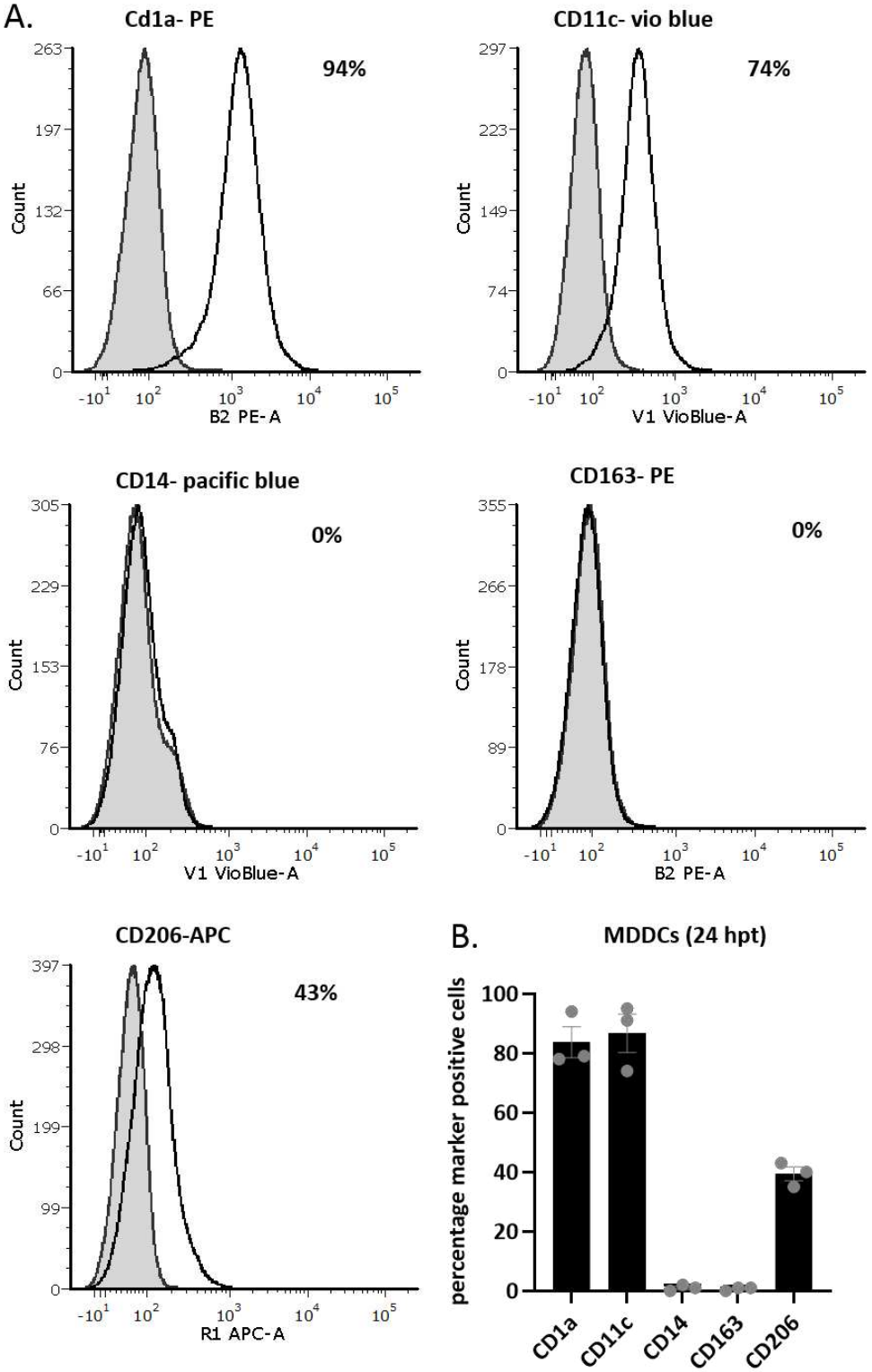

Figure 17: Characterization of differentiation status of MDDCs. MDDCs were differentiated for five days from $CD14^+$ monocytes and characterized by immunostaining of specific expression markers (CD1a, CD11c, CD14, CD163, CD206) and subsequent flow cytometry analysis. A) Flow cytometry gating examples for one donor for CD1a, CD11c, CD14, CD163, CD206 are shown. B) Means ± SD of expression marker positive cells, normalized to the corresponding IgG control are shown for n = 3 donors.

First, we used MDDCs as a model for highly sensitive immune cells to investigate whether EBOV nucleic acids are immunostimulatory. Differentiation and specific surface marker expression of MDDCs were confirmed by FACS analysis at the time point of RNA transfection into the cells. Upregulation of CD1a, CD11c, CD206 and concurrent downregulation of CD14 and CD163 surface expression markers confirmed MDDC differentiation (Figure 17).

MDDCs from three different donors were stimulated with the equivalent of 100 copies/cell of total viral RNA. As controls in MDDCs, the similar amount of RNase-treated nucleic acids was transfected and cells were SeV infected as well as mock transfected. ISG54 and RPL13a mRNA levels were determined 24 hpt by RT-qPCR. Strikingly, strong transcriptional upregulation of the ISG54 gene of around 800x were detected compared to mock transfection and transfection with RNase-treated EBOV trVLP nucleic acids, both leading to no upregulation of ISG54 mRNA. The SeV positive control showed ISG54 upregulation of around 1000x, underlining the strong immunostimulatory properties of EBOV nucleic acids in MDDCs (Figure 18A). As RNase-treatment completely diminished the ISG54 response, solely the EBOV RNA was responsible for the activation of innate sensing rather than DNA-contamination. To corroborate this finding, we furthermore analyzed MDMs from two donors that were stimulated with 100 copies/cell of total viral RNA. Here, ISG54 induction in MDMs was approximately 200x compared to mock (Figure 18B). In conclusion, EBOV RNAs isolated from particles are a potent immune stimulator in physiologically relevant cells.

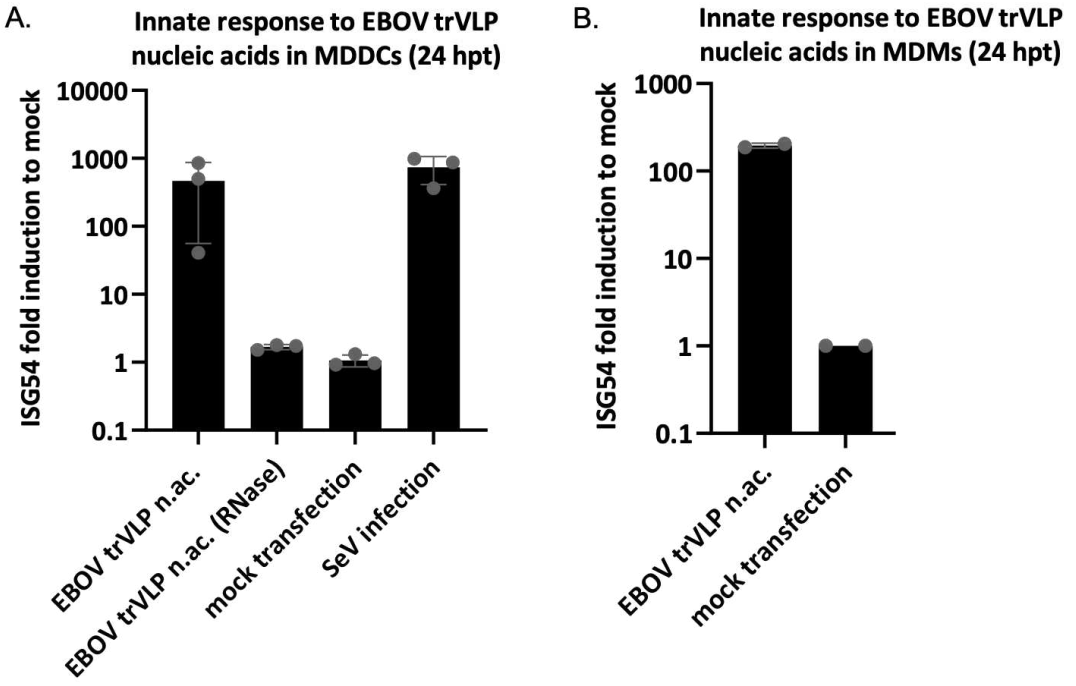

Figure 18: EBOV trVLP nucleic acids are immunostimulatory in MDDCs and MDMs. Total nucleic acids (n.ac.) were extracted from EBOV trVLPs (p1). The RNA copy number was determined by RT-qPCR using specific primers and standards. MDDCs and MDMs were isolated from human blood and differentiated from $CD14^+$ monocytes. A) The equivalent of 100 copies/cell of EBOV trVLP RNA and an RNase-digested control were transfected into MDDCs. SeV infection served as positive control and mock transfection as negative control. B) The equivalent of 100 copies/cell of EBOV trVLP RNA were transfected into MDMs and mock transfection served as negative control. 24 hpt ISG54 and RPL13a mRNA levels were determined by RT-qPCR and normalized to mock. Mean ISG54 induction ± SD of A) three different donors or B) two different donors each measured in technical triplicates is represented.

4.2.2 Ebola virus transcription and replication competent virus-like particle RNA is sensed via MAVS

To confirm the immunostimulatory capacity of EBOV RNA, THP-1 cells deficient in the key molecule of cytosolic RNA sensing MAVS, as well as THP-1 cells deficient in the key molecule of cytosolic DNA sensing STING and the parental wt cell line were exposed to different innate immune triggers. Upon PMA-induced differentiation into a macrophage-like phenotype, THP-1 cells were transfected with EBOV trVLP RNA, RNase-treated EBOV trVLP RNA, herring testis DNA (htDNA) as a strong activator of the STING-mediated DNA-sensing pathway, or SeV infected, as a strong RNA sensing pathway

activator via RLRs. The activation of the cytosolic DNA sensing pathway via STING as well as the RNA sensing pathway via MAVS lead to phosphorylation of TBK1 and IKKε, which further activate IRF-3. Subsequent translocation of activated IRF-3 into the nucleus activates expression of type I IFNs and ISGs. Strikingly, in STING KO cells and wt cells, an almost 100x and 50x ISG54 induction was detected respectively 24 h after stimulation with EBOV trVLP nucleic acids or infection with SeV, whereas there was no ISG54 induction upon stimulation with herring testis DNA in STING KO cells. In contrast, MAVS KO cells failed to mount an ISG54 response upon stimulation with EBOV trVLP nucleic acids or upon SeV infection, but a high induction was detectable after herring testis DNA transfection (Figure 19A). Western Blot analyses confirmed the protein expression and knock-out of MAVS and STING in the respective cell lines (Figure 19B). These findings confirm that specifically EBOV trVLP RNA elicits an innate immune induction and is sensed via the MAVS axis, presumably via the RLR pathway.

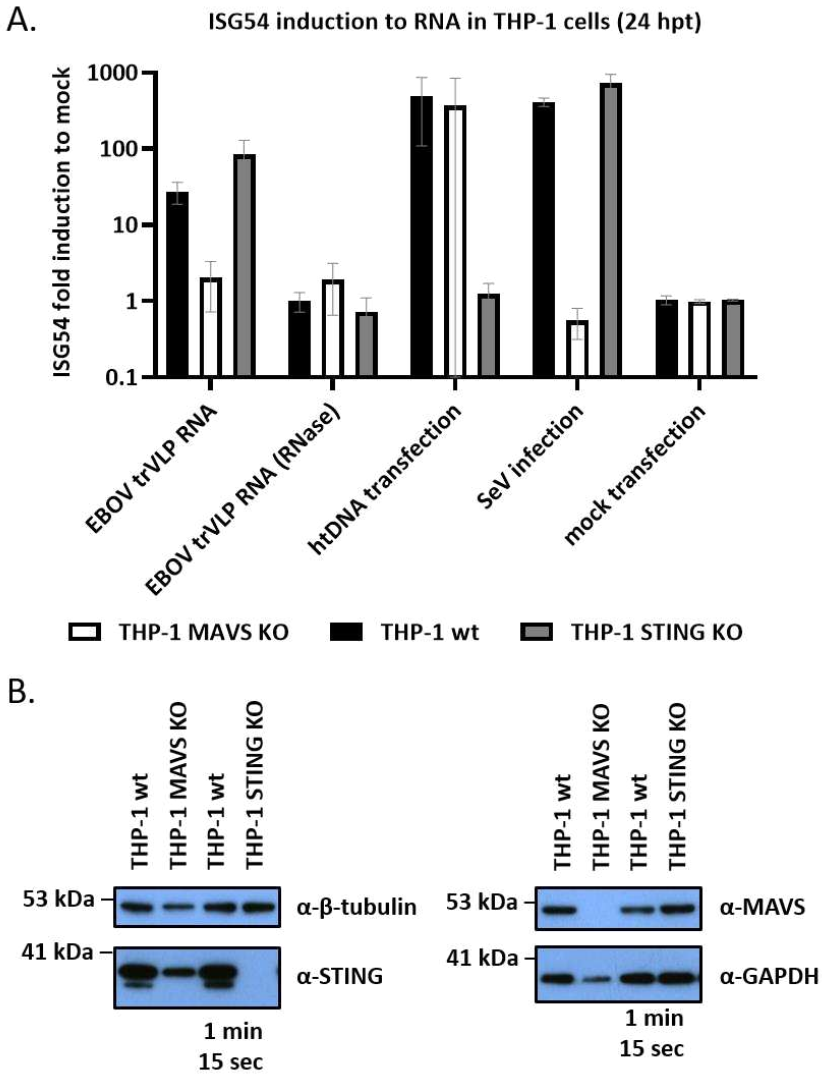

Figure 19: EBOV trVLP RNA induces a strong ISG54 response via MAVS. A) The trVLP nucleic acids produced in HEK 293T/17 wt cells were transfected into PMA-differentiated THP-1 wt, MAVS KO cells, or STING KO cells. As a control for the DNA-sensing pathway, htDNA was transfected and for the RNA-sensing pathway, cells were infected with SeV. Cells were harvested and subjected to RT-qPCR 24 hpt to determine ISG54 and RPL13a mRNA levels, values were normalized to mock. Mean ± SD of three different experiments with three technical replicates each are shown. B) Genome editing of THP-1 CRISPR/Cas9 KO for STING and MAVS was controlled by Western Blot analysis.

4.2.3 Ebola virus RNA is mainly sensed by RIG-I rather than MDA5

After determination of the cytosolic RNA-sensing pathway via the MAVS axis as the main pathway sensing wt EBOV RNA, the question arose whether sensing occurs via RIG-I or MDA5. In short, RIG-I mainly senses shorter dsRNA species with 5’-pp/ppp motifs or

blunt ends including panhandle structures, whereas MDA5 is known to sense longer dsRNAs with higher order structures (Liu and Gack, 2020). To determine the RLR for EBOV RNA, a siRNA assay following EBOV RNA transfection was established. EBOV (strain Mayinga) was grown on Vero E6 cells under BSL-4 conditions and RNA was isolated (Thomas Hoenen, Friedrich-Loeffler-Institut). As naked EBOV RNA is not pathogenic, it can be handled under BSL-1 conditions (Conzelmann, 2004). A549 cells were treated with two siRNAs for each target MAVS, RIG-I, MDA5, or with non-targeting control siRNAs and 48 h later, cells were transfected with wt EBOV RNA. 24 h after RNA transfection, ISG54 mRNA induction was measured by RT-qPCR. Knock-down efficiencies of siRNAs for specific targets were determined based on specific primers and normalized to mRNA levels in samples treated with control siRNAs. Knock-down efficiency for most targets was around 95% (Figure 20B). Interestingly, upon knock-down of MAVS as well as RIG-I, sensing was almost completely abrogated. Knock-down of MAVS reduced the sensing activity by 80-95%. Knock-down of RIG-I reduced the sensing activity by 75-85%. However, upon knock-down of MDA5 still high ISG54 induction were detected despite high knockdown efficiency (Figure 20B), suggesting that RIG-I indeed plays a major role in EBOV RNA sensing. As the results for MDA5 are inconsistent due to the high standard deviation, it cannot be ruled out that MDA5 also plays a role in EBOV RNA sensing to a certain degree (Figure 20A).

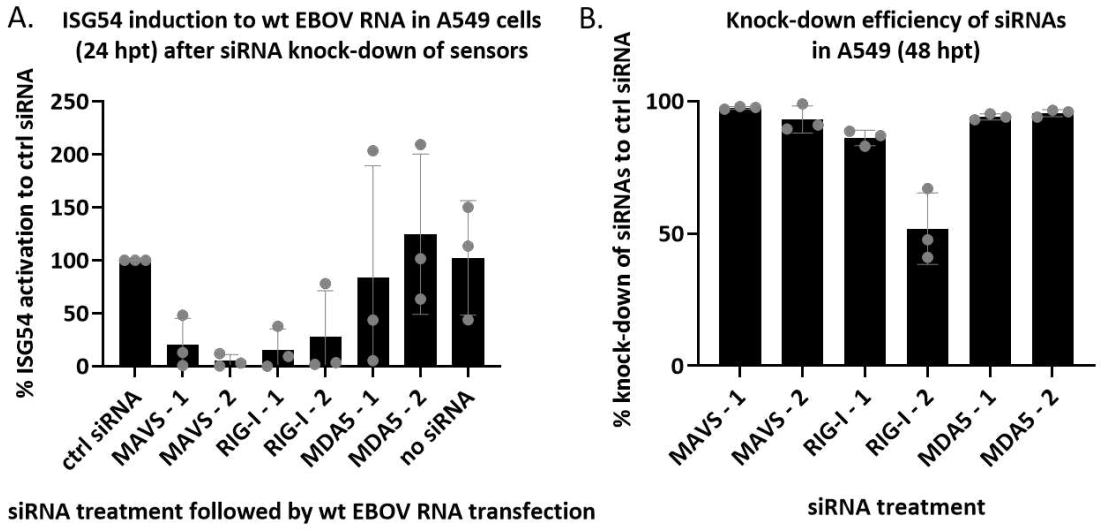

Figure 20: EBOV RNA is predominantly sensed by RIG-I. A) A549 cells were reverse transfected with specific siRNAs and 48 h later, wt EBOV RNA was transfected into siRNA-treated cells. Samples were harvested and subjected to RT-qPCR 72 h after siRNA transfection, values were normalized to control (ctrl) siRNA as 100% ISG54 activation. The mean ± SD of three independent experiments with technical triplicates for each is represented B) Knock-down efficiency of siRNAs was determined at the time point of EBOV RNA transfection by RT-qPCR using specific primers. The mean ± SD for all experiments depicted in A) are shown**.**

4.2.4 Immunofluorescence determination of double-stranded RNA patterns

To determine whether the main PAMP of EBOV RNA is dsRNA, an immunofluorescence assay was established. A549 cells were transfected with 500 ng/well of wt EBOV RNA (isolated at the BSL-4 laboratory facilities at the Friedrich-Loeffler-Institut). 500 ng of EBOV RNA equate around 1000 copies/cell. As positive controls MeV DI genomes were transfected, which are known to produce high amounts of dsRNA motifs. RNase III-treated EBOV RNA and MeV DI-RNAs as well as secondary antibody controls for dsRNA-staining and mock controls served as negative controls. 6 hpt, cells were fixated and stained with the dsRNA-specific J2 antibody followed by an Alexa-Flour 488 secondary antibody (green). Furthermore, IRF-3 nuclear translocation after cell stimulation with RNA was determined with an anti-IRF-3 antibody followed by an Alexa-Fluor 555 secondary antibody. The nucleus was stained with DAPI and the cell cytosol was stained with CellMask Deepred. Graphical analysis was conducted at the Leica SP8 microscope and the corresponding LAS X Software (Leica Microsystems). As expected, nuclear

translocation of the transcription factor IRF-3 was detected after MeV DI-RNAs and after EBOV RNA transfection, but not after RNase-treated RNA transfection (Figure 21A). In line with this, high amounts of spots/cell were detected for MeV DI-RNAs. Almost no spots were detected in the negative controls, including the RNase III-treated MeV DI-RNAs. However, only very few dsRNA spots were detected after EBOV RNA transfection (Figure 21A). Furthermore, the ratio of spots per cytoplasm was calculated. As expected, the amount of spots for EBOV RNA dsRNA was lower than for MeV DI-RNAs. In fact, the amount of spots was even lower than for mock controls. Nevertheless, after RNase-treatment of EBOV RNA, the ratio of spots/cytoplasm was lower compared to untreated EBOV RNA (Figure 21B). In conclusion, the set-up of the assay and the specificity of the antibodies were confirmed, but we were not able to detect significant amounts of spots for EBOV dsRNA.

A.

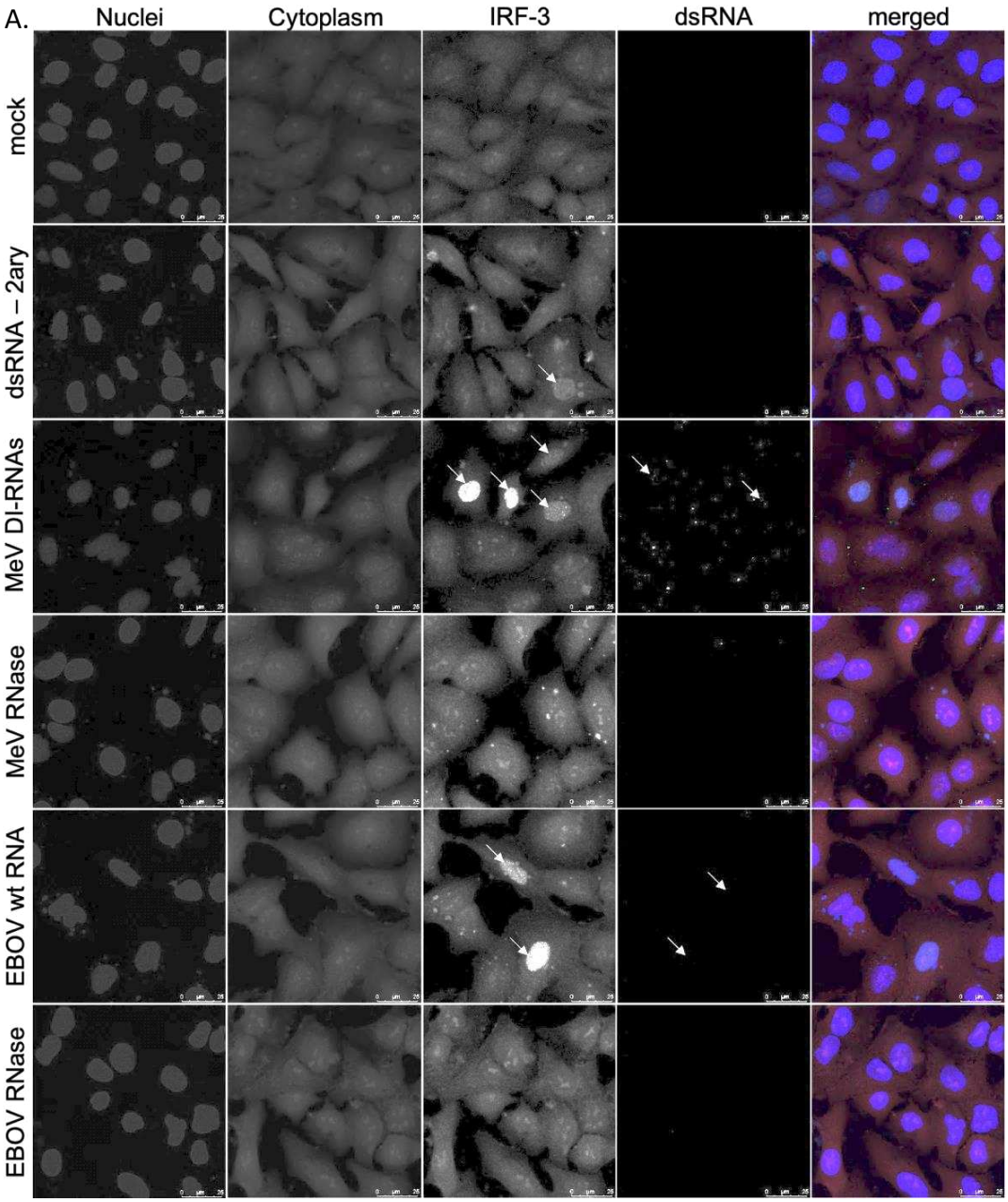
Nuclei
Cytoplasm
IRF-3
dsRNA
merged
mock
dsRNA – 2ary
MeV DI-RNAs
MeV RNase
EBOV wt RNA
EBOV RNase

B.

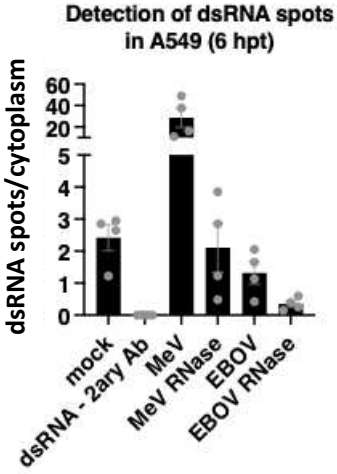
Detection of dsRNA spots
in A549 (6 hpt)
dsRNA spots/cytoplasm
60
40
20
5
4
3
2
1
0
mock
dsRNA - 2ary Ab
MeV
MeV RNase
EBOV
EBOV RNase

Figure 21: Determination of wt EBOV dsRNA by immunofluorescence. A549 cells were transfected with wt EBOV RNA, as well as *in vitro* transcribed MeV DI-RNAs as positive control. As negative controls served the transfection of RNase-treated MeV and EBOV RNA, a mock transfection, as well as a secondary antibody (2ary Ab) control for dsRNA. 6 hpt, cells were fixated and cell nuclei were stained with DAPI (blue), cytoplasms were stained with CellMask deepred (red), IRF-3 translocation was stained (Alexa Fluor-555 labeled), and dsRNA was stained with the J2 antibody (Alexa Fluor-488 labeled). A) Representative images are shown. B) Mean ± SD of four different experiments with technical duplicates each is represented.

4.3 Influence of ADAR1 on Ebola virus RNA sensing

The potential influence of the RNA-editing enzyme ADAR1 on EBOV RNA was evaluated. Therefore, sensing of EBOV trVLP RNA produced in cell lines depleted in ADAR1 isoforms or supplemented with ADAR1 isoforms was analyzed.

4.3.1 Generation of CRISPR/Cas9 ADAR1 knock-out and ADAR1 MAVS knock-out cell lines

To investigate the potential role of ADAR1 in innate sensing of EBOV trVLP RNA, HEK 293T/17 CRISPR/Cas9 ADAR1 KO cells were generated by targeting exon 2 of the ADAR1 locus. Single-cell clones were cultivated and subjected to Western Blot analysis (Figure 22A). Promising clones were subjected to TA-cloning with subsequent sequencing to confirm homozygous knock-out of ADAR1 (Figure 22D). As ADAR1 is essential to distinguish self-RNA from foreign RNA, ADAR1 KO can lead to aberrant IFN pathway activation (Rice et al., 2012). Therefore, a double KO (DKO) was performed to additionally target the MAVS locus. KO was confirmed by Western Blot and sequencing (Figure 22B+E). Additionally, self-activation by the KO of ADAR1 was analyzed by subjecting full cellular RNA to RT-qPCR for determination of ISG54 levels. Indeed, only a minimal upregulation of ISG54 was measured in almost all cell lines compared to wt cells (Figure 22C). In conclusion, for ADAR1 KO two clones were confirmed to have a homozygous KO – 5H11 and 1B8. Clone 4B12 showed a heterozygous KO and was removed (data not shown). Clone 5H11 was further used to generate ADAR1 MAVS KO cell lines and two cell lines were confirmed to have a homozygous KO – clone 5G9 and 2E3 (Figure 22E).

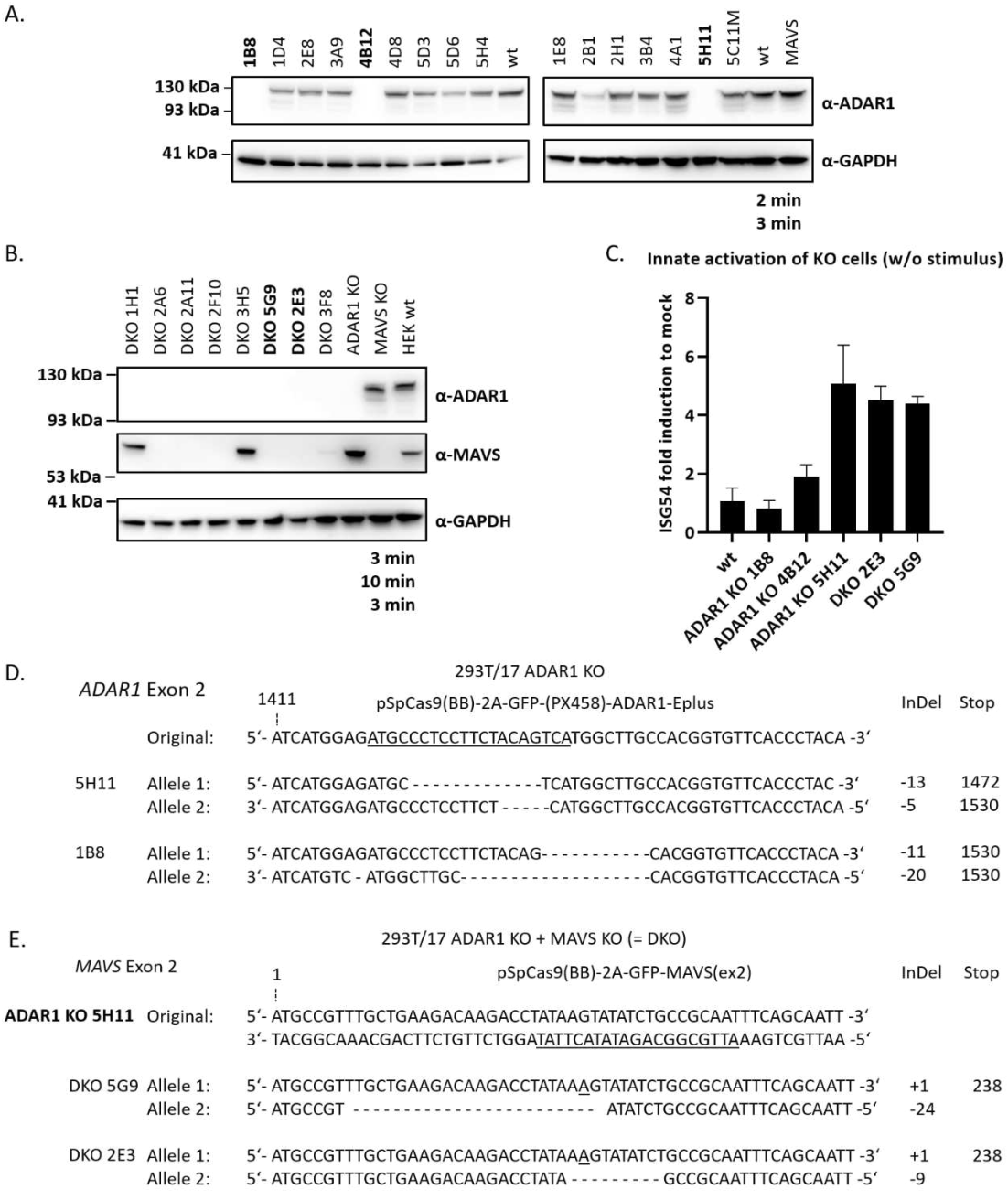

Figure 22: CRISPR/Cas9 mediated KO of ADAR1 and MAVS in HEK 293T/17 cells. HEK 293T/17 cells were seeded and transfected with plasmids including gRNAs targeting ADAR1 or MAVS. Single cell colonies were grown. A) Single cell clones were tested in a Western Blot analysis for expression of ADAR1. B) Single cell colonies of ADAR1 KO cells and transfected with a plasmid targeting MAVS were tested for MAVS expression. C) Cell clones that were identified as suitable were tested in a self-activation assay. Cells were seeded and 24 h later subjected to RT-qPCR on ISG54 levels without any stimulus. The mean ± SD for three technical replicates is shown. D) Promising clones for ADAR1 KO were sequenced and compared to the original. Mutation sites (InDel = Insertion/Deletion polymorphism) and premature stop position are depicted. E) Promising clones for ADAR1 KO MAVS KO were sequenced for the MAVS KO position and compared to the original. Mutation sites and premature stop position are depicted.

ADAR1 expresses two isoforms, the IFN-inducible ADAR1^{p150} that is mainly situated in the cytosol and the nuclear, constitutively active ADAR1^{p110}. To ensure that ADAR1^{p150} is indeed not expressed in ADAR1 KO cells as well as in DKO cells, cells were stimulated with IFN-α2a and subjected to Western Blot analysis (Figure 23A+B). High expression levels of STAT showed successful IFN-pathway activation, whereas there was no expression of the IFN-inducible ADAR1^{p150} neither in ADAR1 KO cells nor in DKO cells after activation of the IFN pathway. Furthermore, MAVS KO was also confirmed in IFN-pathway activated cells (Figure 23B).

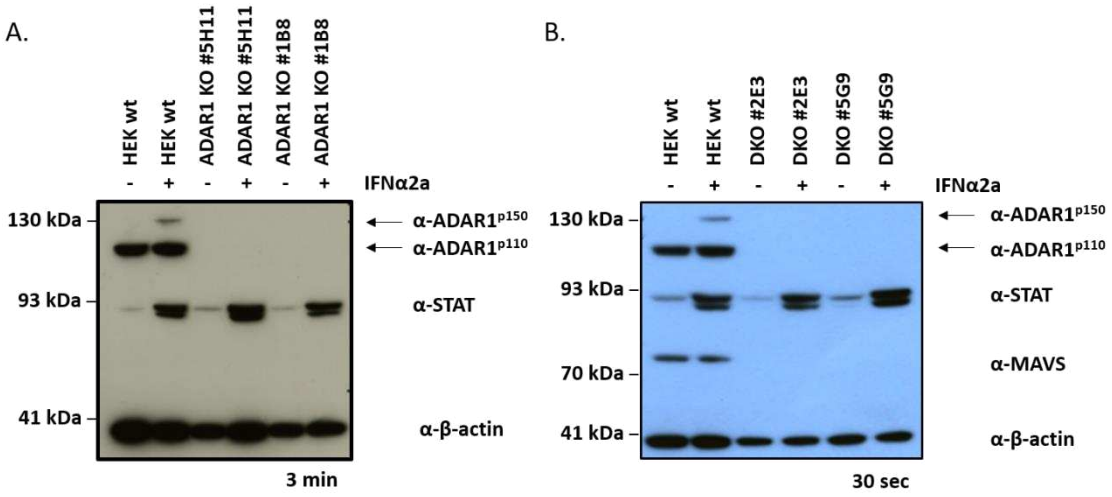

Figure 23: ADAR1 KO cell lines do not express ADAR1^{p150} after IFN stimulation. HEK 293T/17 wt cells and cell lines of A) ADAR1 KO and B) ADAR1 MAVS KO were seeded in 6-well plates and treated with IFN-α2a or not treated for 24h. Cell lysates were subjected to Western Blot analysis. Representative blots of three replicates are shown.

4.3.2 ADAR1 plays a role in innate sensing of Ebola virus transcription and replication competent virus-like particles RNA

To determine differential immunostimulatory potential of EBOV trVLP RNA produced in either wt or ADAR1 KO cells, and wt or DKO cells, trVLP RNA was isolated, DNase-digested, and quantified. Quantification was done by 1-step and 2-step RT-qPCR. Quantification with 1-step RT-qPCR is necessary to determine the total amount of viral RNA, including intermediates, mRNAs, and genomic RNA. With the 2-step RT-qPCR we

measured if and how much viral genomic RNA is present in the RNA samples (Figure 24A). For both methods, the values for copies/µL were calculated (Figure 24B) and quantity ratios of wt trVLP RNA and ADAR1 KO trVLP RNA as well as wt trVLP RNA and DKO trVLP RNA were compared for both methods (Figure 24C).

A.

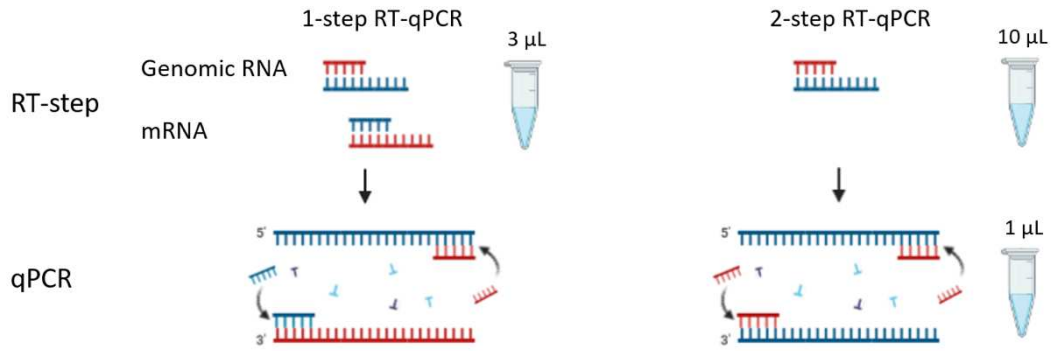

B.

Copies/µL	1-step RT-qPCR	2-step RT-qPCR
wt	$3.93x10^5$	$1.6x10^7$
ADAR1 KO	$4.66x10^5$	$2.75x10^7$

Copies/µL	1-step RT-qPCR	2-step RT-qPCR
wt	$1.7x10^6$	$9.93x10^7$
DKO	$5.83x10^5$	$2.58x10^7$

C.

Ratio to wt	1-step RT-qPCR	2-step RT-qPCR
wt	1	1
ADAR1 KO	1.2	1.7

Ratio to wt	1-step RT-qPCR	2-step RT-qPCR
wt	1	1
DKO	0.3	0.3

Figure 24: Schematic overview and results of EBOV RNA quantification. EBOV trVLPs were concentrated and RNA was isolated and quantified with specific primers and standards for the nluc gene on the 4cis minigenome. A) Schematic overview of 1-step RT-qPCR and 2-step RT-qPCR (the figure was assembled with BioRender). B) Calculated equivalent of RNA copies/µL based on a ssDNA standard curve for trVLP RNA isolated from wt cells, ADAR1 KO cells, as well as wt and DKO cells for 1-step and 2-step RT-qPCR. C) Calculation of quantity ratios based on calculation results depicted in B). ADAR1 and DKO values were normalized to the respective wt values.

Based on these calculations, the same equivalent of total RNA copy numbers per cell (measured by 1-step RT-qPCR) produced in wt cells or ADAR1 KO cells were transfected into A549 cells followed by determination of ISG54 mRNA level 24 hpt. Previous DNase-digestion of all RNA samples secured that no residual DNA was responsible for the ISG54 induction. Mock transfection (not shown) and RNase-treated EBOV trVLP RNA produced

in ADAR1 KO cells served as negative controls. Surprisingly, the same copy number per cell of EBOV trVLP RNA produced in ADAR1 KO cells led to an approximately 7x higher ISG54 response after transfection into A549 cells compared to EBOV trVLP RNA produced in wt cells (Figure 25A). To make sure that these results were not influenced by factors stemming from any kind of cellular self-activation due to ADAR1 manipulation, the same experiment was conducted with trVLP production in DKO cells. Strikingly, RNA stemming from EBOV trVLPs produced in DKO cells elicited an approximately 9x higher ISG54 response compared to EBOV trVLP RNA from wt cells (Figure 25B), comparable to EBOV trVLP RNA from ADAR1 KO cells. To control for sensors in A549 cells, Western Blot evaluation showed strong expression of MAVS whereas there was no expression of the DNA-sensor STING suggesting a crippled DNA sensing pathway in these cells (Figure 25C). This again, underlines the importance of the RLR pathway for EBOV sensing. Based on these results, we hypothesized that ADAR1 negatively influences trVLP RNA in wt cells, thus leading to reduced sensing of the RNA.

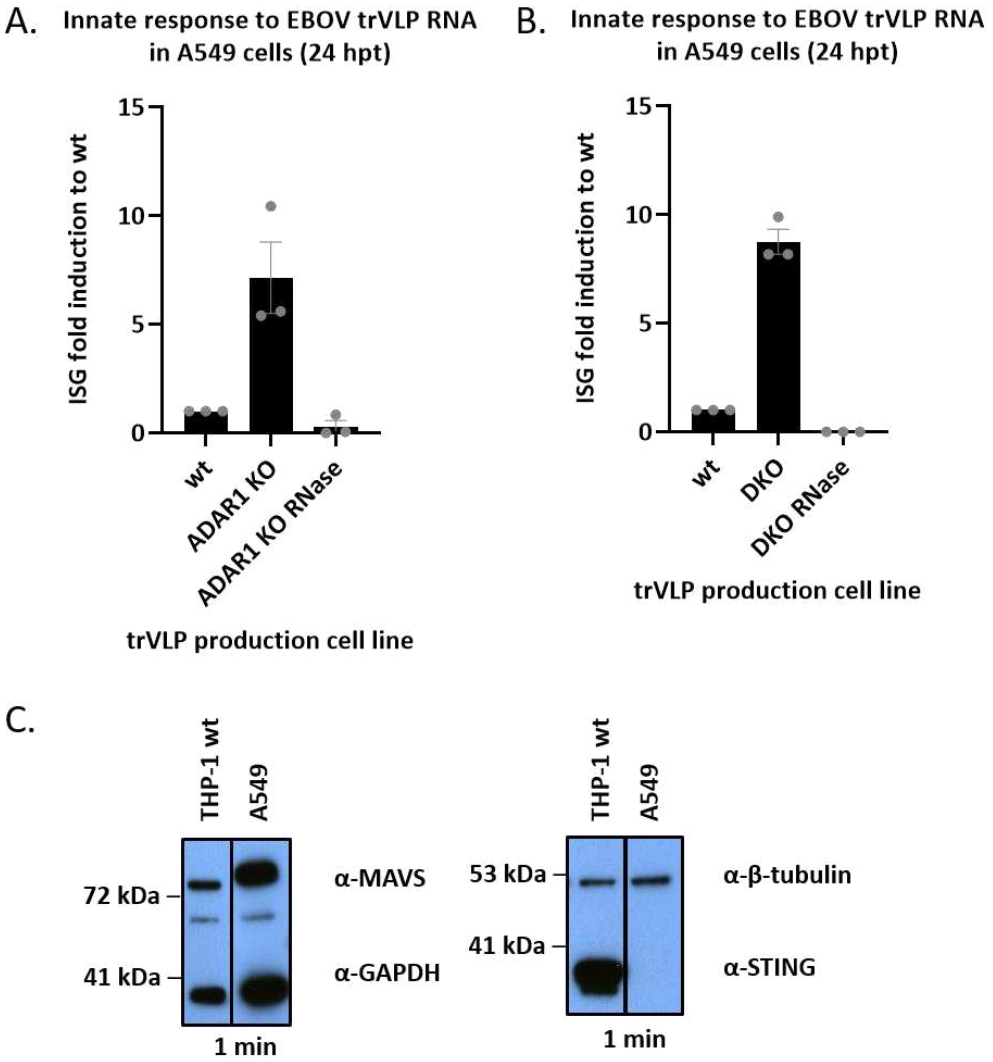

Figure 25: ADAR1 plays a role in innate sensing of EBOV RNA. A) EBOV trVLPs were produced in wt and ADAR1 KO cells and isolated trVLP RNA was transfected into A549 cells with 100 copies/cell. RNA isolated from ADAR1 KO cells was additionally RNase-digested and transfected. After 24 h, samples were harvested and ISG54 induction was determined by RT-qPCR. Mean ISG54 fold change to wt ± SD of three independent experiments each measured in triplicates is represented. B) EBOV trVLPs were produced in wt and DKO cells and isolated RNA was transfected into A549 cells with 100 copies/cell. RNA isolated from DKO cells was additionally RNase-digested and transfected. After 24 h, samples were harvested and ISG54 induction was determined by RT-qPCR. Mean ISG54 fold change to wt ± SD of three independent experiments each measured in triplicates is represented. C) Western Blot analysis of expression levels of the nucleic acid sensors MAVS and STING in THP-1 and A549 cells.

4.3.3 ADAR1^{p150} positively influences viral innate sensing escape

To further evaluate this finding of a potential suppressive role of ADAR1 in regulating sensing, we wanted to determine the responsible ADAR1 isoform. Therefore, ADAR1 KO cells were transduced with lentiviral vectors expressing either ADAR1^{p150}, a catalytically inactive ADAR1^{p150in} or ADAR1^{p110}. Stable expression of all three ADAR1 versions was confirmed by Western Blot analysis (Figure 26A). EBOV trVLPs were produced in these cell lines and quantification was again done by 1-step and 2-step RT-qPCR to determine total viral RNA species as well as viral genomic RNA. Quantity ratios of ADAR1^{p150} trVLP RNA, ADAR1^{p150in} trVLP RNA, and ADAR1^{p110} trVLP RNA were compared for both methods (Figure 26B). Intriguingly, the ISG54 mRNA in A549 recipient cells was decreased after transfection of EBOV trVLP RNA produced in ADAR1^{p150} cells compared to EBOV trVLP RNA produced in ADAR1^{p150in} or ADAR1^{p110}. EBOV trVLP RNA produced in ADAR1^{p150in} elicited an ISG54 response of approximately 10x higher and EBOV trVLP RNA produced in ADAR1^{p110} of approximately 25x higher compared to EBOV trVLP RNA produced in ADAR1^{p150}, respectively (Figure 26C). Furthermore, Western Blot analysis was performed with samples from these A549 RNA-transfected cells. Consistently, in A549 cells transfected with EBOV trVLP RNA stemming from ADAR1^{p150} cells, almost no phosphorylated IRF-3 was detected, whereas total IRF-3 levels were comparable in all samples (Figure 26D).

Next, DKO cells were also transduced with respective lentiviruses for stable expression of ADAR1^{p150}, ADAR1^{p150in} or ADAR1^{p110} (Figure 27A). Again, EBOV trVLP RNA was produced in these cells and quantified with 1-step and 2-step RT-qPCR and the ratio was determined (Figure 27B). In accordance with the previous results, EBOV trVLP RNA produced in DKO ADAR1^{p150} cells led to lower ISG54 mRNA levels compared to EBOV trVLP RNA stemming from DKO ADAR1^{p150in} or ADAR1^{p110} cells. EBOV trVLP RNA produced in ADAR1^{p150in} elicited an ISG54 response of approximately 15x higher and EBOV trVLP RNA produced in ADAR1^{p110} of approximately 35x higher compared to EBOV trVLP RNA produced in ADAR1^{p150}, respectively (Figure 27C).

A.

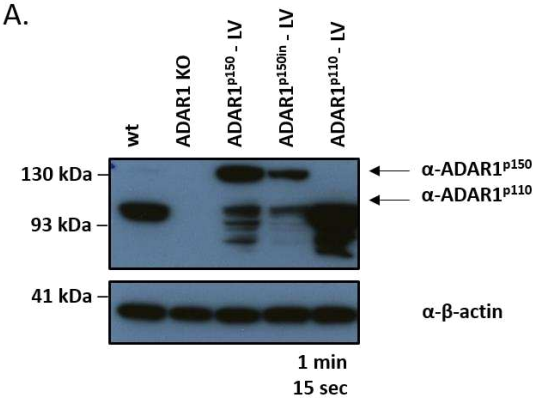

B.

Copies/µL	1-step RT-qPCR	2-step RT-qPCR
ADAR1^{p150} - LV	3.35x10^{6}	3.72x10^{8}
ADAR1^{p150in} - LV	5.74x10^{5}	4.35x10^{7}
ADAR1^{p110} - LV	1.3x10^{6}	3.65x10^{7}
Ratio to p150	**1-step RT-qPCR**	**2-step RT-qPCR**
ADAR1^{p150} - LV	1	1
ADAR1^{p150in} - LV	0.2	0.1
ADAR1^{p110} - LV	0.4	0.1

C.

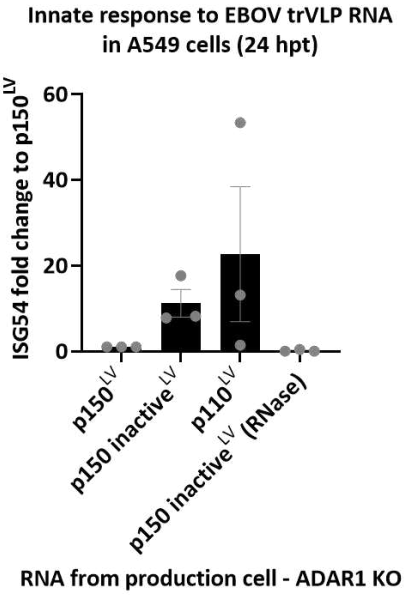

D.

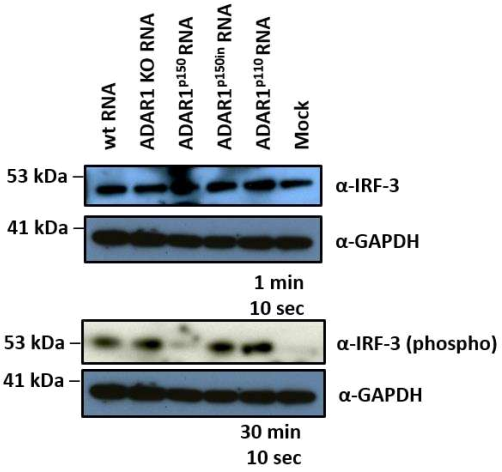

Figure 26: ADAR1^{p150} negatively regulates innate sensing of EBOV trVLP RNA. A) ADAR1 KO cells were transduced with lentiviruses (LV) introducing stable expression of ADAR1^{p150}, a catalytically inactive form ADAR1^{p150in} or ADAR1^{p110}. Cells were cultivated under puromycin selection pressure and Western Blot probes were harvested one week after cultivating without antibiotics. B) Calculated equivalent of RNA copies/µL based on a ssDNA standard curve for trVLP RNA isolated from ADAR1 KO^{p150} -LV cells, ADAR1 KO^{p150in} -LV cells and ADAR1 KO^{p110} -LV cells for 1-step and 2-step RT-qPCR and calculation of quantity ratios based on calculation results. ADAR1^{p150in} and ADAR1^{p110} values were normalized to the ADAR1^{p150} value. C) EBOV trVLPs were produced in ADAR1 KO^{p150} -LV cells, ADAR1 KO^{p150in} -LV cells and ADAR1 KO^{p110} -LV cells and viral RNA was isolated and with 100 copies/cell transfected into A549 cells. After 24 h, samples were harvested and ISG54 induction was determined by RT-qPCR. Shown are ISG54 fold changes to ADAR1^{p150} mean ± SD of three different experiments with technical triplicates for each. D) Isolated RNA from wt cells, ADAR1 KO cells, ADAR1 KO p150^{LV} cells, ADAR1 KO p150 inactive^{LV} cells and ADAR1 KO p110^{LV} cells was transfected into A549 cells and samples were subjected to Western Blot analysis to determine IRF-3 and phospho-IRF-3 levels. Representative blots are shown.

A.

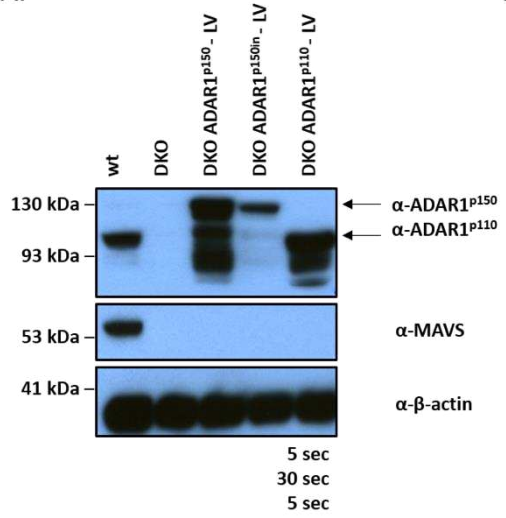

B.

Copies/µL	1-step RT-qPCR	2-step RT-qPCR
DKO ADAR1^{p150} - LV	8.18x10^5	9.55x10^7
DKO ADAR1^{p150in} - LV	8.97x10^5	1.5x10^8
ADAR1^{p110} - LV	7.6x10^5	6.84x10^7
Ratio to p150	1-step RT-qPCR	2-step RT-qPCR
DKO ADAR1^{p150} - LV	1	1
DKO ADAR1^{p150in} - LV	1.1	1.6
ADAR1^{p110} - LV	0.9	0.7

C.

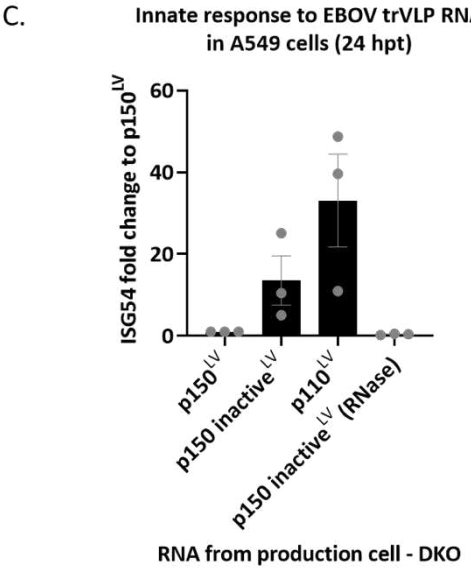

Figure 27: ADAR1^{p150} negatively regulates innate sensing of EBOV trVLP nucleic acids after trVLP RNA production in DKO cells. A) DKO cells were transduced with LV introducing stable expression of ADAR1^{p150}, a catalytically inactive form ADAR1^{p150in} or ADAR1^{p110}. Cells were cultivated under puromycin selection pressure and Western Blot probes were harvested one week after cultivating without antibiotics. B) Calculated equivalent of RNA copies/µL based on a ssDNA standard curve for trVLP RNA isolated from DKO ADAR1 KO^{p150} -LV cells, ADAR1 KO^{p150in} -LV cells and ADAR1 KO^{p110} -LV cells for 1-step and 2-step RT-qPCR and calculation of quantity ratios based on calculation results. DKO ADAR1^{p150in} and ADAR1^{p110} values were normalized to the ADAR1^{p150} value. C) EBOV trVLPs were produced in DKO ADAR1 KO^{p150} -LV cells, ADAR1 KO^{p150in} -LV cells and ADAR1 KO^{p110} -LV cells and viral RNA was isolated and 100 copies/cell were transfected into A549 cells. After 24 h, samples were harvested and ISG54 induction was determined by RT-qPCR. Shown are the fold changes to ADAR1^{p150} mean ± SD of three different experiments with technical triplicates for each.

Taken together, these results suggest that ADAR1^{p150} negatively regulates innate sensing of EBOV RNA, thereby supporting viral escape from innate immune sensing. Furthermore, we showed that the catalytic domain of ADAR1^{p150} is necessary to negatively regulate sensing of EBOV trVLP RNA.

5 Discussion

5.1 Optimization of an RNA interference screening approach

The early interactions of the innate immune system with pathogens are of great importance. The pathogenicity of an infection is determined by adequate recognition of the virus. On the one hand, lack of recognition leads to suppression of activation of the adaptive immunity. On the other hand, uncontrolled recognition, accompanied by excessive secretion of inflammatory cytokines and chemokines, leads to a cytokine storm with massive manifestations.

EBOV infection is responsible for both the lack of activation of the adaptive immunity and uncontrolled inflammation. Initial virus replication occurs in circulating DCs and macrophages, which are the sentinel cells of the immune system. Infection and subsequent block of the IFN-pathway by EBOV in these cells help spread the virus throughout the whole body, resulting in a systemic inflammatory response. However, infected DCs are not activated and therefore cannot mount an effective IFN immune response. Therefore, very early sensing events of EBOV in sentinel cells may be critical for disease progression. For the block of sensing and IFN activation particularly EBOV VP35 is responsible, which is a potent IFN-antagonist that has multiple mechanisms to counteract early sensing events.

This study addressed the early innate sensing events of EBOV. A better understanding of the interactions between the innate immune system and EBOV, as well as the characterization of innate sensors and regulators of RNA innate signaling pathways, are important not only for EBOV infections but also potentially for other pathogen infections as well.

5.1.1 Production of an Ebola virus VP35 mutant that has lost the interferon-antagonistic activity

VP35 is a potent IFN-antagonist, therefore infection does not elicit an IFN-mediated immune response from particles containing VP35 wt. To overcome this problem, it is possible to make use of a VP35 mutant to determine EBOV interactions with cellular sensing pathways. In order to be able to research innate sensing of EBOV, two different VP35 mutants were evaluated regarding their ability to antagonize the early sensing pathway. The first mutant has been described previously and contains the mutations R305A, K309A, R312A (Schümann et al., 2009). A mutation at position R312 has been shown to be essential for the dsRNA binding function of VP35 and consequently severely impairs the IFN-antagonistic function (Cárdenas et al., 2006; Hartman et al., 2006). However, a previous publication has teased that positions R305 and K309 are not responsible for dsRNA binding (Leung et al., 2010). This is in contrast to another publication, showing that K309 mediates dsRNA binding (Cárdenas et al., 2006). Nevertheless, mutations at both sites R305 and K309 simultaneously where shown to restore IFN activation better than a single mutation at either of these positions (Cárdenas et al., 2006; Hartman et al., 2006). However, none of these mutations completely restored e.g. SeV mediated IFN activation. Therefore, our goal was to introduce mutations in VP35 such that no IFN-antagonistic function was retained. Thus, the second mutant was cloned based on literature on VP35 and contains the additional mutations F239A, R322A, K339A. Position F239 represents an ‘end-cap’ for dsRNA and is thus essential for masking 5’-ppp ends on dsRNA from RIG-I. The same set of experiments also confirmed that positions R322 and K339 are also essential for dsRNA binding (Leung et al., 2010). These results were further supported by a molecular dynamics simulation, showing that particularly R312A, R322A, K339A alter biochemical properties compared to wt (Zhang et al., 2017).

This study presents a VP35 mutant (VP35 m2) with six mutations that indeed retains less antagonistic activity than the previously described VP35 triple mutant (m1) (Figure 8). Nevertheless, ISG54 mRNA activation was not fully restored. One reason for this could

be that despite the interaction with dsRNA and subsequent block of RLR activation, other amino acids are essential for further antagonistic functions. In line with this, VP35 has also been shown to interfere with the downstream signaling pathway. First, it acts as a decoy substrate for IRF-3 phosphorylation by IKKε and TBK-1 and second, it can directly interact with MAVS as well as IRF-3 and IRF-7, disrupting the interactions of these kinases (Prins et al., 2009). However, the exact amino acids of VP35 that enable these interactions have not yet been identified. Therefore, it is possible that phosphorylation of VP35 by IKKε and TBK-1 or direct interaction with these kinases are responsible for the residual block of IFN activation. In order to further explore these interactions, it is necessary to introduce additional mutations in VP35 and analyze them. In particular, kinase target sites such as serines or threonines are of interest. Nevertheless, VP35 has an essential role as polymerase co-factor that could be negatively affected by mutations.

5.1.2 Evaluation of Ebola virus VP35 mutants in the transcription and replication competent virus-like particle assay regarding the function as polymerase co-factor

VP35 is a crucial factor for transcription and replication of EBOV for several reasons (Mühlberger et al., 1999). Firstly, VP35-L interactions are essential for transcription and replication (Trunschke et al., 2013). Secondly, VP35 functions as a linker between NP-packaged EBOV RNA and L (Trunschke et al., 2013). In addition, VP35 directly interacts with NP in order to avoid homo-oligomerization of NPs, thus preventing early RNA binding (Kirchdoerfer et al., 2015; Leung et al., 2015) (Hume and Mühlberger, 2019). A look at the structure of VP35 reveals that the first basic patch and several basic amino acids outside the central basic patch of the VP35 IID (Leung et al., 2009) are essential for the interaction with NPs (Prins et al., 2010a). Furthermore, a coiled-coil domain is located at the amino terminal part of VP35, which facilitates the association to homo-oligomers of VP35 necessary for transcription and replication (Reid et al., 2005; Zinzula et al., 2019). Because critical residues for the polymerase co-function as well as the IFN-antagonism are concentrated in the same domain of VP35, it is inevitable to determine the ability of transcription and replication after introducing mutations into the VP35 IID.

Indeed, trVLPs containing either of the VP35 mutants slightly lost infectivity compared with VP35 wt containing trVLPs, with the effect being even stronger for VP35 m2. This is in concordance with previous observations with a related set-up (Woolsey et al., 2019). One possibility could be that the introduction of additional mutations leads to structural changes in VP35, preventing the coiled-coil domain from fully assembling. However, trVLP production was possible with both VP35 mutants and we showed less IFN-antagonistic activity of the two mutants compared with VP35 wt trVLPs. Production of trVLPs with the VP35 mutants results in a strong ISG54 and IFN-β response compared with wt VP35, confirming that the VP35 mutant proteins have partly lost their antagonistic activity (Figure 9). Nevertheless, during the production of p0 trVLPs as well as during the preparation of presumable negative controls, high amounts of IFN and ISGs were detected in the supernatants. We hypothesized that IFNs and ISGs from the sample preparation led to activation of additional sensing pathways as well as the IFNAR pathway of target cells. Interestingly, in the presence of the IFN-antagonist VP35, the sensing pathway activation in producer cells was blocked for the most part. Therefore, VP35 wt containing trVLP-supernatants or controls contained less IFNs or ISGs and subsequently activation of sensing pathways in target cells was mostly diminished.

Noteworthy, generation p1 trVLP supernatants did not contain any measurable amounts of IFNs, leading to the assumption that specifically p0 trVLP production or control preparation activates sensing. The main difference between p0 and p1 is the use of the bacteriophage T7 DNA-dependent RNA-polymerase for p0. For p0, the T7 polymerase transcribes the plasmid encoded tetracistronic minigenome into RNA, whereas in p1, the viral polymerase transcribes the minigenome from the incoming particles. In fact, T7-dependent activation of the RLR pathway has been observed previously. On the one hand, T7 adds 5’-ppp on synthesized RNAs which lead to a strong activation of RIG-I dependent sensing (Hornung et al., 2006). On the other hand, possible T7-driven promoter-independent transcription of long dsRNAs from the antisense strand leads to MDA5-dependent sensing (Mu et al., 2018). This suggests that the T7 polymerase synthesized unspecific RNAs from host or plasmid DNAs or modified the RNA, leading to strong sensing.

To completely avoid further IFN-pathway activation in producer and target cells, MAVS KO cells were generated (Figure 10). As MAVS is the joint downstream interaction partner of RIG-I and MDA5, any RLR dependent sensing is abrogated in MAVS KO cells. In addition, in further experiments target cells were infected with p1 trVLPs.

5.1.3 No sensing of Ebola virus transcription and replication competent virus-like particles in target cells

We wanted to determine sensing of EBOV trVLPs in physiologically relevant cells. Due to their essential role as connecting element between innate and adaptive immunity, MDDCs are important targets of EBOV (Geisbert et al., 2003). Usually, maturation of MDDCs by IFN is essential to activate the adaptive immunity. Due to the IFN-inhibitory function of EBOV VP35, maturation of MDDCs is circumvented (Mahanty et al., 2003; Yen et al., 2014). Therefore MDDCs are a reasonable choice to resemble sensing events of EBOV. Nevertheless, plasmid transfection rates in MDDCs are usually very low due to their sensitivity and slow dividing rate (Hamm et al., 2002). Therefore, naïve MDDCs were infected with p1. In order to determine whether secondary transcription and replication of EBOV trVLPs can be sensed, HEK 293T/17 cells are a convenient cell line model due to their robustness, their fast dividing rate, and their intact innate sensing system. Furthermore, siRNA knock-down as well as plasmid transfection can be easily conducted in these cells. Additionally, the hepatocyte cell line HepG2 was included. The liver is infested early during infection and plays an important role for pathogenesis of EBOV disease (Jankeel et al., 2020). Furthermore, HepG2 cells have been established previously in several studies to be a suitable cell line for the research of sensing of EBOV (Hartman et al., 2008b; Kuzmin et al., 2017).

Successful infection of target cells with recombinant EBOV and subsequent IFN response has been shown in previous publications. It was demonstrated that infection of HepG2 cells with recombinant EBOV including the VP35 R312A mutation elicits a robust ISG54 induction of 8-30x compared to wt infection which did not elicit an immune response (Kuzmin et al., 2017). Comparable results were published with recombinant EBOV harboring VP35 F239A K319A R322A mutations. Here, A549 cells were infected and IFN-

β induction was determined. 24 hpi the induction was around 10x, whereas 48 hpi the induction was approximately 350x (Woolsey et al., 2019). Nevertheless, innate sensing of EBOV trVLPs has not been shown, up to now. In this study, robust sensing of trVLPs was also not possible in any of the above-mentioned cells (Figure 11+14). This might be due to the fact that trVLP production is not as effective as wt EBOV replication in cells. Therefore, the infection rate of trVLPs might not have been high enough in target cells to elicit an immune response. It was previously shown that after p1 and p2 infection only a small portion of cells are infected (Schmidt et al., 2018). Another possibility might be a different way of sensing of trVLP RNA compared to wt EBOV RNA. The PAMPs might look different or the localization of RNA could differ.

In order to determine whether an increase in the amount of trVLPs for infection has an effect on sensing, trVLP supernatants were concentrated. Even though sucrose cushion has been used for EBOV concentration before successfully (Olejnik et al., 2017a; Takamatsu et al., 2020), here it was not possible to increase the infection rate of trVLPs after centrifugation over a sucrose cushion (Figure 15). As the shape of EBOV is filamentous, it might be possible that the pressure during ultracentrifugation ruptured the particles.

Not being able to detect trVLP sensing in target cells, the question arose whether EBOV RNA is immunostimulatory and therefore further experiments were performed with isolated EBOV trVLP RNA as well as isolated wt EBOV RNA.

5.2 Determination of host sensors of Ebola virus RNA

In this part of the study, the interaction of EBOV RNA with innate immune sensors was investigated. We determined the immunostimulatory capacity of EBOV RNA as well as the involved sensors.

5.2.1 Sensing of Ebola virus RNA

In order to isolate RNA from trVLPs, the trVLP concentration method was changed to PEG-8000, as was described earlier to isolate RNA from EBOV (Habjan et al., 2008; Deflubé et al., 2019). Here, we demonstrated that EBOV trVLP RNA is highly immunostimulatory in physiological relevant cells such as the primary cells MDDCs and MDMs (Figure 18) as well as in cell lines such as THP-1 (Figure 19) and A549 (Figure 20). Furthermore, this study confirmed that the RLR pathway is responsible for cytosolic EBOV RNA sensing leading to strong activation of ISG54 induction (Figure 19). In agreement to prior studies, RIG-I was determined as the main sensor of EBOV RNA (Habjan et al., 2008). Nevertheless, it cannot be completely ruled out that MDA5 does play a role in EBOV RNA sensing (Figure 20). The RIG-I activation suggests that 5'-ppp ends in combination with ds motifs are strong PAMPs of EBOV RNA. Indeed, incoming viral nucleocapsids containing 5’-ppp dsRNA panhandle structures triggered RIG-I signaling in previous studies. This was further supported by the fact that sensing was abrogated upon phosphatase treatment of the RNA (Weber et al., 2013). Furthermore, production of dsRNA motifs in the filoviral genomic RNA as well as mRNA were experimentally proven (Mühlberger et al., 1996; Bach et al., 2021). The highly conserved transcription start sequences and reinitiation sequences are able to form secondary structures. To further enlighten on the role of dsRNA motifs, we transfected wt EBOV RNA into target cells and stained using a specific anti-dsRNA antibody. Despite the detection of IRF-3 translocation into the nucleus, dsRNA was barely detectable (Figure 21). This is in line with a previous publication in which dsRNA from NSVs was not detected by immunofluorescence methods (Weber et al., 2006). One reason could be that an immunofluorescence assay might not be sensitive enough to detect low amounts

of dsRNA, which is underlined by the fact that already a reduction from 500 ng to 100 ng of MeV DI-RNAs was not detected anymore in our assay. Furthermore, transcription and replication of the viral genome are highly dynamic processes, and therefore secondary structures might only be present for very short or very specific time periods during infection. In addition, very low amounts of viral RNA are sufficient to activate RNA sensors and elicit an innate immune response (Marcus and Sekellick, 1977), therefore we hypothesized that the anti-dsRNA antibody is not sensitive enough despite dsRNA motifs being able to activate sensing pathways. In line with this, another publication described indeed detection of dsRNA produced by measles virus and other NSVs (Son et al., 2015).

5.3 Influence of ADAR1 on Ebola virus RNA sensing

In addition to the interaction of EBOV RNA with RLRs, the interaction with the RNA-modifying enzyme ADAR1 was of major interest in this study. ADAR1 is an RNA-editing enzyme that is essential for the discrimination between self and non-self RNA. A-to-I editing of dsRNA motifs leads to destabilization of the dsRNA motifs and therefore to diminished sensing by RLRs (Bass and Weintraub, 1988). Besides this, ADAR1 is also able to outcompete RIG-I for dsRNA binding (Vogel et al., 2020). For the first time, we could establish a correlation between ADAR1 expression and ISG induction as response to EBOV RNA. EBOV trVLP RNA produced in ADAR1 KO cells induced a higher ISG54 response after transfection in A549 cells than EBOV trVLP RNA produced in wt cells (Figure 25). This establishes ADAR1 as a negative regulator for sensing of EBOV trVLP RNA.

Two isoforms with different features are expressed: p110 is constitutively expressed and located in the nucleus, whereas p150 is upregulated as an ISG and situated mainly in the cytosol (Patterson and Samuel, 1995). To further research which isoform is involved in the differential sensing, we worked with lentiviral vectors to introduce stable expression of both isoforms as well as a catalytically inactive p150 isoform. Excitingly, the innate

response to particle-associated EBOV RNA stemming from cells overexpressing ADAR1^{p150} is significantly diminished in comparison to RNA stemming from cells overexpressing the catalytically inactive form of p150 or the nuclear isoform p110 (Figure 26). To exclude IFN-pathway activation by a positive feedback loop, a DKO cell line for ADAR1 and MAVS was generated. These cells ensured that no IFN production appeared during trVLP production, which could lead to JAK-STAT pathway activation in target cells. As expected, the results are comparable to these for ADAR1 KO cells and derived cells expressing the respective ADAR forms (Figure 27).

Compared to several previous publications (Liddicoat et al., 2015; Pestal et al., 2015), here we showed that ADAR1 negatively influences RIG-I mediated EBOV RNA sensing rather than MDA5-mediated sensing. In agreement, negative influence of ADAR1 on RIG-I sensing was shown previously in the context of IAV (Vogel et al., 2020). Nevertheless, the authors did not discriminate between editing-dependent negative influence on sensing and dsRNA-binding specific effects. Recently, a study determined ADAR1-editing of EBOV mRNA untranslated regions, revealing a possible positive function of ADAR1-editing for viral mRNA translation. This suggests a much more complex interplay between ADAR1-editing of viral RNA than previously assumed. It was shown, that ADAR1-edited untranslated regions significantly lose the ability to elicit an IFN-response compared to unedited mRNA (Khadka et al., 2021). In agreement, this study underlines the pro-viral function of ADAR1 on EBOV. Thus, we additionally reveal ADAR1^{p150} as the driver of this function and RIG-I as the main sensor of EBOV RNA. Furthermore, we wanted to determine whether it is possible that also viral genomic RNA sensing is influenced by ADAR1, rather than only mRNA. Therefore, total viral RNA as well as genomic RNA was quantified and high amounts of viral genomic RNA were present in the RNA samples that were transfected into target cells. Thus, we hypothesize that ADAR1 also interactions with viral genomic RNA.

In conclusion, this part of the study suggests that ADAR1^{p150} isoform interacts with EBOV trVLP RNA, leading to decreased sensing activity as determined by ISG54 mRNA levels as well as phosphorylated IRF-3 protein levels. This establishes ADAR1^{p150} as a negative

regulator of innate sensing of EBOV. This discovery is in line and further supports previous findings suggesting A-to-I editing in EBOV genomes as well as mRNA (Whitfield et al., 2020; Khadka et al., 2021). Two possibilities could explain this phenomenon: Firstly, independent from editing, ADAR1^{p150} might bind EBOV dsRNA features and therefore acts as a competitor to cytosolic RNA sensors. However, this possibility seems not to be the main function of ADAR1, as the catalytically inactive version of p150 used in this study expresses a functional RNA-binding motif and sensing of trVLP RNA produced in cells expressing the catalytically inactive form did not lead to completely diminished sensing. Nevertheless, compared to EBOV trVLP RNA stemming from ADAR1^{p110} cells, sensing of EBOV trVLP RNA from ADAR1^{p150in} cells was lower. Therefore, we think that ADAR1^{p150} edits EBOV dsRNA motifs, leading to destabilization of dsRNA features and therefore to less recognition by RLRs or that a joint function of editing and RNA-binding leads to the less sensing. We hypothesize that not only mRNA is edited by ADAR1, as was shown before (Khadka et al., 2021) but also viral genomic RNA, perhaps even EBOV DI-RNAs.

5.4 Open questions and future

5.4.1 Cellular localization of the interaction between RIG-I-like receptors and Ebola virus RNA

Given the plethora of antagonistic strategies EBOV has evolved and the restored strong immune activation to EBOV harboring mutations in the VP35 IID, there are still unanswered questions. Much research concentrates on the determination of additional sensors as well as co-sensors and modulators recognizing EBOV. As EBOV replicates in inclusion bodies in the cytoplasm, immunostimulatory RNA would need to leave these inclusion bodies to be freely available in the cytosol. The other possibility would be that RLRs are able to migrate into inclusion bodies as EBOV IFN-antagonistic strategies explicitly counteract RLR mediated sensing. For several viruses, such as human respiratory syncytial virus and severe fever with thrombocytopenia syndrome virus it

was shown that host proteins of the innate immunity pathways can be actively sequestered by viral proteins to inclusion bodies (Lifland et al., 2012; Ning et al., 2014; Wu et al., 2014). Presumably, this mechanism is another viral strategy to hinder innate signaling pathway member proteins from activating downstream signaling or from directly translocating to the nucleus and subsequent production of antiviral proteins and ISGs. Therefore, it would be of high interest to determine the site of interaction of EBOV with the IFN pathway members.

5.4.2 Possible pathogen-associated molecular patterns of Ebola virus RNA

The question of DI-RNA production during EBOV replication is not sufficiently researched, there is very scarce data on this topic, but would be of major interest to better understand the function of ADAR1 editing. Nevertheless, few publications have looked into the DI-RNA production during viral replication and indeed detected EBOV DI-RNAs (Calain et al., 1999; Calain et al., 2016). Furthermore, EBOV VP35 expresses a dsRNA-binding domain and is able to sequester RIG-I-mediated sensing. It was shown previously that VP35 is able to sequester EBOV derived *in vitro*-transcribed dsRNAs from RIG-I (Cárdenas et al., 2006). The exact function of this feature has not been determined yet, but it could be to capture DI-RNAs produced by EBOV to cover them from RIG-I. In line with this, usually transcription and replication of EBOV genomes takes place in specific inclusion bodies formed by the virus (Hoenen et al., 2012) and the full genome is encapsidated in the nucleoprotein. DI-RNAs are not encapsidated and might be freely available in the cytosol (Strahle et al., 2006). This suggests the question whether naked EBOV RNA intermediates are indeed able to escape the inclusion bodies and could interact with RIG-I.

5.4.3 Additional sensors and pathways that are potentially involved in Ebola virus RNA sensing

Apart from the discussed RLRs, several other RNA sensors and pathways might be of interest during EBOV infection of which several are shortly discussed in the following.

Toll-like-receptors (TLRs) are a group of intramembrane receptors, which are able to sense a variety of PAMPs, including but not restricted to specific pathogenic proteins, DNA, and RNA species. TLR signaling leads to the expression of pro-inflammatory cytokines and TLR3 signaling additionally leads to IRF-3 mediated IFN expression. TLRs are expressed in different cell types, including monocytes and DCs, and are expressed on the cell surface and the endosome (Takeda and Akira, 2015). RNA sensing TLRs are TLR3, TLR7, TLR8, and TLR13. Even though TLRs are not localized in the cytoplasm, involvement in EBOV sensing cannot be fully excluded.

The protein kinase PKR senses dsRNA and was proposed to sense also 5'-ppp and ssRNA structures (Nanduri et al., 1998; Nallagatla et al., 2007). The main effect of PKR activation is the inhibition of global protein synthesis mechanisms (Dar et al., 2005; Liu et al., 2020). The inhibitory effect of VP35 on PKR suggests a possible involvement of PKR in EBOV RNA sensing. During MeV infection, strong PKR activation was seen in response to DI-RNAs (Pfaller et al., 2018).

Oligoadenylate synthetases (OAS) sense RNA species and subsequently activate ribonuclease L, which degrades RNA (Chen and Hur, 2021). Involvement of OAS during EBOV infection remains to be elusive.

NOD-like receptors (NLRs) are a group of intracellular sensing proteins of which most lead to the assembly of inflammasomes after activation. Inflammasomes are multiprotein-complexes, which lead to the expression of pro-inflammatory cytokines as well as apoptosis signaling. Several NLRs are also able to activate IRF-3 via MAVS after binding RNA (Liu and Gack, 2020). As EBOV VP35 interferes on several stages with the IFN activation pathway, it would be of interest if EBOV RNA also activates NLR-mediated IFN responses as well as inflammasome signaling. Several NLRs might be able to recognize EBOV RNA, based on the patterns of other viruses, which have been shown to activate NLRs. For example, NLRC2 recognizes the (-)ssRNA of respiratory syncytial virus, leading to a MAVS-dependent IFN response (Sabbah et al., 2009). Furthermore, NLRP12 is a suppressor of RIG-I and is able to recognize 5'-ppp dsRNA features and viruses such as vesicular stomatitis virus. Viral RNA recognition leads to NLRP12 downregulation and

subsequent upregulation of RIG-I to allow activation, leading to an immune response (Chen et al., 2019). NLRP1 was recently shown to be able to sense dsRNA of (+)ssRNA viruses, resulting in inflammasome activation (Bauernfried et al., 2021).

Other RNA sensors include RNA helicases, which can also bind RNA. Many RNA helicases have different tasks during viral infection and function not only as direct RNA sensors but also support signaling of e.g. RLRs (Pattabhi et al., 2019). Here, several helicases are mentioned that would be interesting to research during EBOV infection. The helicase ZNFX1 can bind viral RNA, leading to a MAVS-dependent IFN response (Wang et al., 2019). Furthermore, DDX1 in a complex with DDX21 and DHX36 were shown to bind poly I:C as well as IAV RNA in DCs, resulting in IFN response and expression of pro-inflammatory cytokines (Zhang et al., 2011). Furthermore, DHX15 was shown to bind SeV RNA, leading to an IFN response (Lu et al., 2014). Additionally, a newly discovered mechanism is DHX16-mediated RIG-I activation. DHX16 was shown to bind specific features of IAV and is regulated by poly-ubiquitin, which ultimately leads to RIG-I activation (Hage et al., 2022).

Interestingly, an innate immune response to a pathogen can also be achieved by sensing of abnormal cellular RNA. It was shown, that HSV-1 infection triggers the relocalization of specific cellular RNA species to the cytosol, resulting in RIG-I dependent sensing, which in turn triggers an IFN response (Chiang et al., 2018). Furthermore, during the infection of KSHV misprocessed host noncoding RNAs with 5’-ppp ends triggered an IFN response (Zhao et al., 2018). If EBOV infection would trigger such relocalization of host RNAs, VP35 RNA-binding capacity would probably mask these RNA species from RLR sensing. Nevertheless, understanding such processes would not only be of high interest for EBOV infection, but also for other viral infections.

Lastly, a very novel discovered sensing activation mechanism might be of interest during EBOV infection. It was shown that TLR4 signaling leads to the activation of host transposable elements. Transposable elements are DNA sequences being able to change the position in the genome, but also able to produce dsRNA and dsDNA. The transposable elements led to sensing by the DNA sensor cGAS, which in turn activates

IFN expression via IRF-3 translocation (Macchietto et al., 2020; Rookhuizen et al., 2021). Interestingly, during EBOV infection GP triggers a strong TLR4 response, leading to the production of pro-inflammatory cytokines (Okumura et al., 2010; Lai et al., 2017). Therefore, it would be very interesting to better understand a possible involvement of transposable elements and cGAS-mediated sensing during EBOV infection.

In general, RLRs, TLRs, NLRs, RNA helicases, and other sensing mechanisms comprise a complex web of sensing pathways and are highly interconnected and somewhat redundant in order to facilitate a robust and strong antiviral response. In that manner, many proteins of different pathways and families interact to optimize the antiviral response, including IFN activation as well as expression of pro-inflammatory cytokines. To fully understand EBOV – host interactions a thorough screen of involved host sensors is necessary.

5.4.4 Adenosine to inosine editing of Ebola virus RNA and possible ADAR1 interaction with Ebola virus VP35

Despite exhibiting the negative regulation activity of ADAR1^{p150} on innate sensing, it was not possible to generate EBOV trVLP RNA for RNAseq. Due to the artificial trVLP system, virus production is limited, as was explained in detail for the first part of this thesis. Therefore, it is necessary to grow wt EBOV on the specific ADAR1 cell lines under BSL-4 conditions in order to collect enough RNA material for thorough RNAseq analysis. Consequently, future studies need to evaluate wt EBOV RNA produced in ADAR1 KO cells as well as supplemented ADAR1 cell lines and editing needs to be determined by RNAseq.

Recently, in a high throughput screen ADAR was identified as a potential interaction partner of VP35 (Batra et al., 2018). Here it would be of interest whether this is a true interaction or if this hit was identified by the shared dsRNA-binding potential of both proteins. Furthermore, it would be interesting to analyze whether VP35 recruits ADAR1 to mediate dsRNA editing.

In summary, open questions include the nature of the PAMP, the interplay of various sensors, the influence of localization on sensing, and the consequence of proteins such as ADAR1 on sensing. Novel insights will be gained from future studies in order to better understand virus – host interactions with focus on EBOV and might help to improve therapeutic strategies.

6 Summary

6.1 Summary

Ebola virus is a negative sense RNA virus and belongs to the family of Filoviridae. It can cause severe disease including hemorrhagic fever and multiorgan failure. Initial Ebola virus replication occurs in dendritic cells and macrophages, the sentinel cells of our immune system. However, infected dendritic cells fail to orchestrate an effective immune response. Virulence is partly associated to Ebola virus protein VP35, an interferon-antagonist which effectively counteracts the activation of RNA receptors from the RIG-I-like receptor pathway family. Furthermore, potential editing of viral RNA could have pro-viral effects, avoiding interferon induction. ADAR1 is an RNA editing enzyme, which modifies double-stranded RNA by adenosine-to-inosine editing, essential for differentiation between self and foreign RNA. This crucial negative regulator of the interferon response is expressed in two isoforms: the interferon-inducible p150 present in both the cytoplasm and nucleus, and the constitutively expressed p110, which is restricted to the nucleus. Potential adenosine-to-inosine editing of Ebola virus genomes was shown recently in different approaches and in samples from Ebola virus disease survivors.

Therefore, the early immune response to Ebola virus seems to be crucial for disease outcome. The aim of this thesis was to determine and analyze innate sensors and regulators of the innate signaling pathways relevant for Ebola virus infections. The goal was to research innate sensors of Ebola virus transcription and replication competent virus-like particles as well as to analyze sensing of Ebola virus RNA in cell-based assays and to investigate a link to altered innate sensing depending on the presence or absence of ADAR1 isoforms.

The transcription and replication competent virus-like particle system allows life cycle modeling of Ebola virus under biosafety level-1 conditions. Innate sensing was measured by monitoring expression of the direct IRF3-target gene ISG54. Two different VP35

mutants were analyzed regarding their interferon antagonistic function as well as their function in replication and transcription. Production of transcription and replication competent virus-like particles including the VP35 mutants in HEK 293T cells, leads to a strong interferon-β response compared to wildtype VP35, suggesting that mutant VP35 proteins lost their antagonistic activity compared to wildtype VP35. Nevertheless, infection of cells with mutant VP35 virus-like particles does not lead to an immune response. To further investigate the lack of innate response to particles infection, the immunostimulatory potential of naked Ebola virus RNAs isolated from particles was assessed in a quantitative assay using monocyte-derived dendritic cells and monocyte-derived macrophages as a model for highly immunocompetent cells. Upon transfection of viral nucleic acids into immunocompetent cells, high sensing inductions are observed, suggesting that viral RNA components are sensed. To identify the particular innate pathways that are triggered by Ebola RNA, THP-1 knock-out cell lines deficient for key molecules of RNA and DNA sensing pathways were exposed to Ebola virus RNA. As expected, THP-1 cells deficient in the key molecule of the RNA sensing pathway lose the ability to trigger an immune response upon stimulation with Ebola virus RNA, suggesting members of the RIG-I like receptor family as initial sensors. Indeed, in gene knock-down experiments sensing of Ebola virus RNA was abrogated upon knock-down of RIG-I.

Furthermore, ADAR1 knock-out HEK 293T cells, as well as knock-out cells stably expressing ADAR1^{p150}, catalytically inactive ADAR1^{p150in}, and the ADAR1^{p110} isoform were generated. Ebola virus particles were produced in respective cells or wildtype cells, followed by Ebola virus RNA extraction. Target cells were transfected with respective Ebola virus RNA and innate sensing was measured by monitoring the expression of the IRF-3 target gene ISG54 as well as by Western Blots for IRF-3 activation.

Here, it was shown that Ebola virus RNA extracted from particles produced in wildtype cells induce an IRF-3-dependent response after transfection in primary myeloid cells. Interestingly, Ebola virus RNA produced in ADAR1 knock-out cells induce a higher immune response after transfection in A549 cells than RNA produced in wildtype cells. This suggests ADAR1 as a negative regulator for sensing. In addition, the innate response

to particle-associated RNA stemming from cells overexpressing ADAR1^{p150} is strongly diminished in comparison to RNA stemming from ADAR1 knock-out cells or cells overexpressing the catalytically inactive form of p150 or the nuclear isoform p110. This suggests that strong RNA editing activity by the active interferon-stimulated p150, but not p110 influences the capacity for Ebola virus RNA sensing.

In conclusion, this work leads to a better understanding of Ebola virus-host interactions and established ADAR1 as a pro-viral factor during Ebola virus infection and as a negative regulator of innate sensing of Ebola virus RNA. A better understanding of the first interactions between Ebola virus and innate regulators can help to advance therapeutic strategies.

6.2 Zusammenfassung

Das Ebolavirus ist ein RNA-Virus mit negativer Orientierung und gehört zur Familie der Filoviridae. Es kann schwere Krankheiten verursachen und zu hämorrhagischem Fieber und Multiorganversagen führen. Dendritische Zellen und Makrophagen gehören zu den ersten Zielzellen von Ebola und sind eine wichtige Verbindung zwischen angeborener und erlernter Immunität. Infizierte dendritische Zellen sind jedoch nicht mehr in der Lage eine wirksame Immunreaktion auszulösen. Die Virulenz basiert hauptsächlich auf dem Ebola-Protein VP35, einem Interferon-Antagonisten, der der Aktivierung von RNA-Rezeptoren aus der Familie der RIG-I-ähnlichen Rezeptoren entgegenwirkt. Darüber hinaus könnte eine mögliche Veränderung der viralen RNA durch Proteine von Wirtszellen zusätzliche pro-virale Effekte haben, die die Unterdrückung von Interferon unterstützen. ADAR1 ist ein RNA-Editierungsenzym, das doppelsträngige RNA durch Adenosin-zu-Inosin-Editierung modifiziert, was für die Unterscheidung zwischen eigener und fremder RNA wesentlich ist. Die ADAR1-Editierung von viraler RNA wurde für andere RNA-Viren mit negativer Orientierung nachgewiesen, z. B. für das Masernvirus. Dieser wichtige negative Regulator des Interferonweges wird in zwei Isoformen exprimiert: das Interferon-induzierbare p150, das sowohl im Zytoplasma als auch im Zellkern vorkommt, und das konstitutiv exprimierte p110, das auf den Zellkern beschränkt ist. Eine mögliche Adenosin-zu-Inosin-Editierung von Ebolavirus-Genomen wurde kürzlich durch verschiedene Ansätze sowie in Proben von Überlebenden der Ebolavirus-Erkrankung nachgewiesen. Daher scheinen die Prozesse während der frühen angeborenen Immunantwort auf das Ebolavirus entscheidend für den Krankheitsverlauf zu sein. Das Ziel dieser Arbeit war es, die Interaktionen des angeborenen Immunsystems des Wirts mit dem Ebolavirus zu untersuchen und zu analysieren. Diese Arbeit befasst sich mit der Immun-Erkennung von transkriptions- und replikationskompetenten virusähnlichen Partikeln des Ebolavirus sowie mit der Erkennung von Ebolavirus-RNA durch das Immunsystem in zellbasierten Assays. Weiterhin wurde in dieser Arbeit die Verbindung zu einer veränderten angeborenen Immun-Erkennung untersucht in Abhängigkeit vom Vorhandensein oder Fehlen verschiedener Isoformen von ADAR1.

Das transkriptions- und replikationskompetente virusähnliche Partikelsystem ermöglicht die Modellierung des Lebenszyklus von Ebola unter Laborsicherheitsbestimmungen der Stufe 1. Die angeborene Immunantwort wurde durch Messung der Expression des direkten IRF-3-Zielgens ISG54 determiniert. Zwei verschiedene VP35-Mutanten wurden auf ihre interferon-antagonistische Funktion sowie auf ihre Funktion bei der Replikation und Transkription untersucht. Es konnte gezeigt werden, dass die Produktion von virus-ähnlichen Partikeln einschließlich der VP35-Mutanten in HEK 293T-Zellen zu einer starken Interferon-β-Antwort im Vergleich zu Wildtyp VP35 führt, was darauf hindeutet, dass die mutierten VP35-Proteine ihre antagonistische Aktivität im Vergleich zu Wildtyp VP35 verloren haben. Dennoch führt die Infektion von Zellen mit mutierten VP35 Partikeln nicht zu einer Immunantwort. Um das Fehlen einer angeborenen Reaktion auf eine Partikel-Infektion weiter zu untersuchen, wurde das immunstimulierende Potenzial nackter Ebolavirus-RNAs, die aus Partikeln isoliert wurden, in einem quantitativen Assay unter Verwendung von aus Monozyten gewonnenen dendritischen Zellen und aus Monozyten gewonnenen Makrophagen als Modell für hoch immunkompetente Zellen untersucht. Nach der Transfektion von viralen Nukleinsäuren in immunkompetente Zellen wurde eine hohe Interferon-Antwort beobachtet, was darauf hindeutet, dass virale RNA-Komponenten erkannt werden. Um die speziellen angeborenen Signalwege zu identifizieren, die durch Ebola-RNA ausgelöst werden, wurden THP-1 Knock-out-Zelllinien, denen Schlüsselmoleküle der RNA- und DNA-Erkennungs-Wege fehlen, Ebolavirus-RNA ausgesetzt. Wie erwartet verlieren THP-1-Zellen, denen das Schlüsselmolekül des RNA-Erkennungsweges fehlt, die Fähigkeit, bei Stimulation mit Ebolavirus-RNA eine Immun-Reaktion auszulösen, was auf Mitglieder der RIG-I-ähnlichen Rezeptorfamilie als erste Sensoren hindeutet. In Protein Knockdown-Experimenten führte Ebolavirus-RNA Stimulierung nach Knockdown von RIG-I tatsächlich nicht mehr zu einer Immunantwort.

Weiterhin wurden ADAR1 Knock-out-Zellen sowie Knock-out-Zellen erzeugt, die ADAR1^{p150}, katalytisch inaktives ADAR1^{p150in} und die ADAR1^{p110}-Isoform stabil exprimieren. Ebolavirus-Partikel wurden in den entsprechenden Zellen oder Wildtyp-Zellen produziert, gefolgt von einer Ebolavirus-RNA-Extraktion. Die Zielzellen wurden

mit der entsprechenden Ebolavirus-RNA transfiziert, und die angeborene Immun-Erkennung wurde gemessen, indem die Expression des IRF-3-Zielgens ISG54 überwacht wurde, sowie durch einen Western Blot für die IRF-3 Aktivierung. Es konnte gezeigt werden, dass Ebolavirus RNA, die aus Partikeln extrahiert wurde, die in Wildtyp-Zellen produziert wurden, nach Transfektion in primären myeloiden Zellen eine IRF-3-abhängige Reaktion auslöst. Interessanterweise induziert Ebolavirus-RNA, die in ADAR1 Knock-out-Zellen produziert wurde, nach der Transfektion in A549-Zellen eine stärkere Immun-Reaktion als RNA, die in Wildtyp-Zellen produziert wurde. Dies deutet darauf hin, dass ADAR1 ein negativer Regulator für die Immun-Erkennung von viraler RNA ist. Darüber hinaus ist die angeborene Reaktion auf Partikel-assoziierte RNA, die von Zellen stammt, die ADAR1^{p150} überexprimieren, im Vergleich zu RNA, die von ADAR1 Knock-out-Zellen oder Zellen stammt, die die katalytisch inaktive Form von p150 oder die nukleäre Isoform p110 überexprimieren, deutlich geringer. Dies deutet darauf hin, dass eine starke RNA-Editierungsaktivität durch das aktive, durch Interferon stimulierte p150, aber nicht durch p110, die Fähigkeit zur Erkennung von Ebolavirus-RNA beeinflusst.

Zusammenfassend lässt sich sagen, dass diese Arbeit zu einem besseren Verständnis der Wechselwirkungen zwischen Ebolavirus und Wirt führt und ADAR1 als proviraler Faktor während der Ebolavirusinfektion und als negativer Regulator der angeborenen Erkennung von Ebolavirus-RNA etabliert. Ein besseres Verständnis der ersten Interaktionen zwischen Ebolavirus und angeborenen Regulatoren kann dazu beitragen, bessere therapeutische Strategien zu entwickeln.

7 References

Aden, D.P., Fogel, A., Plotkin, S., Damjanov, I., and Knowles, B.B. (1979). Controlled synthesis of HBsAg in a differentiated human liver carcinoma-derived cell line. Nature *282*, 615-616. https://doi.org/10.1038/282615a0.

Ahmad, S., Mu, X., Yang, F., Greenwald, E., Park, J.W., Jacob, E., Zhang, C.-Z., and Hur, S. (2018). Breaching Self-Tolerance to Alu Duplex RNA Underlies MDA5-Mediated Inflammation. Cell *172*, 797-810.e13. https://doi.org/10.1016/j.cell.2017.12.016.

Aleksandrowicz, P., Marzi, A., Biedenkopf, N., Beimforde, N., Becker, S., Hoenen, T., Feldmann, H., and Schnittler, H.-J. (2011). Ebola virus enters host cells by macropinocytosis and clathrin-mediated endocytosis. The Journal of infectious diseases *204 Suppl 3*, S957-67. https://doi.org/10.1093/infdis/jir326.

Alvarez, C.P., Lasala, F., Carrillo, J., Muñiz, O., Corbí, A.L., and Delgado, R. (2002). C-type lectins DC-SIGN and L-SIGN mediate cellular entry by Ebola virus in cis and in trans. Journal of virology *76*, 6841-6844. https://doi.org/10.1128/jvi.76.13.6841-6844.2002.

Amarasinghe, G.K., Ayllón, M.A., Bào, Y., Basler, C.F., Bavari, S., Blasdell, K.R., Briese, T., Brown, P.A., Bukreyev, A., and Balkema-Buschmann, A., et al. (2019). Taxonomy of the order Mononegavirales: update 2019. Archives of virology *164*, 1967-1980. https://doi.org/10.1007/s00705-019-04247-4.

Atherstone, C., Diederich, S., Pickering, B., Smith, G., Casey, G., Fischer, K., Ward, M.P., Ndoboli, D., Weingartl, H., and Alonso, S., et al. (2021). Investigation of Ebolavirus exposure in pigs presented for slaughter in Uganda. Transboundary and emerging diseases *68*, 1521-1530. https://doi.org/10.1111/tbed.13822.

Bach, S., Demper, J.-C., Biedenkopf, N., Becker, S., and Hartmann, R.K. (2021). RNA secondary structure at the transcription start site influences EBOV transcription initiation and replication in a length- and stability-dependent manner. RNA biology *18*, 523-536. https://doi.org/10.1080/15476286.2020.1818459.

Baize, S., Leroy, E.M., Georges-Courbot, M.C., Capron, M., Lansoud-Soukate, J., Debré, P., Fisher-Hoch, S.P., McCormick, J.B., and Georges, A.J. (1999). Defective humoral responses and extensive intravascular apoptosis are associated with fatal outcome in Ebola virus-infected patients. Nature medicine *5*, 423-426. https://doi.org/10.1038/7422.

Bartok, E., and Hartmann, G. (2020). Immune Sensing Mechanisms that Discriminate Self from Altered Self and Foreign Nucleic Acids. Immunity *53*, 54-77. https://doi.org/10.1016/j.immuni.2020.06.014.

Basler, C.F. (2015). Innate immune evasion by filoviruses. Virology *479-480*, 122-130. https://doi.org/10.1016/j.virol.2015.03.030.

Basler, C.F. (2017). Molecular pathogenesis of viral hemorrhagic fever. Seminars in immunopathology *39*, 551-561. https://doi.org/10.1007/s00281-017-0637-x.

Basler, C.F., Mikulasova, A., Martinez-Sobrido, L., Paragas, J., Mühlberger, E., Bray, M., Klenk, H.-D., Palese, P., and García-Sastre, A. (2003). The Ebola virus VP35 protein inhibits activation

of interferon regulatory factor 3. Journal of virology *77*, 7945-7956. https://doi.org/10.1128/jvi.77.14.7945-7956.2003.

Basler, C.F., Wang, X., Mühlberger, E., Volchkov, V., Paragas, J., Klenk, H.D., García-Sastre, A., and Palese, P. (2000). The Ebola virus VP35 protein functions as a type I IFN antagonist. Proceedings of the National Academy of Sciences of the United States of America *97*, 12289-12294. https://doi.org/10.1073/pnas.220398297.

Bass, B.L., and Weintraub, H. (1988). An unwinding activity that covalently modifies its double-stranded RNA substrate. Cell *55*, 1089-1098. https://doi.org/10.1016/0092-8674(88)90253-x.

Bass, B.L., Weintraub, H., Cattaneo, R., and Billeter, M.A. (1989). Biased hypermutation of viral RNA genomes could be due to unwinding/modification of double-stranded RNA. Cell *56*, 331. https://doi.org/10.1016/0092-8674(89)90234-1.

Batra, J., Hultquist, J.F., Liu, D., Shtanko, O., Dollen, J. von, Satkamp, L., Jang, G.M., Luthra, P., Schwarz, T.M., and Small, G.I., et al. (2018). Protein Interaction Mapping Identifies RBBP6 as a Negative Regulator of Ebola Virus Replication. Cell *175*, 1917-1930.e13. https://doi.org/10.1016/j.cell.2018.08.044.

Bauernfried, S., Scherr, M.J., Pichlmair, A., Duderstadt, K.E., and Hornung, V. (2021). Human NLRP1 is a sensor for double-stranded RNA. Science (New York, N.Y.) *371*. https://doi.org/10.1126/science.abd0811.

Baum, A., Sachidanandam, R., and García-Sastre, A. (2010). Preference of RIG-I for short viral RNA molecules in infected cells revealed by next-generation sequencing. Proceedings of the National Academy of Sciences *107*, 16303-16308. https://doi.org/10.1073/pnas.1005077107.

Bausch, D.G., Nichol, S.T., Muyembe-Tamfum, J.J., Borchert, M., Rollin, P.E., Sleurs, H., Campbell, P., Tshioko, F.K., Roth, C., and Colebunders, R., et al. (2006). Marburg hemorrhagic fever associated with multiple genetic lineages of virus. The New England journal of medicine *355*, 909-919. https://doi.org/10.1056/NEJMoa051465.

Bazak, L., Haviv, A., Barak, M., Jacob-Hirsch, J., Deng, P., Zhang, R., Isaacs, F.J., Rechavi, G., Li, J.B., and Eisenberg, E., et al. (2014). A-to-I RNA editing occurs at over a hundred million genomic sites, located in a majority of human genes. Genome research *24*, 365-376. https://doi.org/10.1101/gr.164749.113.

Beniac, D.R., Melito, P.L., Devarennes, S.L., Hiebert, S.L., Rabb, M.J., Lamboo, L.L., Jones, S.M., and Booth, T.F. (2012). The organisation of Ebola virus reveals a capacity for extensive, modular polyploidy. PloS one *7*, e29608. https://doi.org/10.1371/journal.pone.0029608.

Bergez, M., Weber, J., Riess, M., Erdbeer, A., Seifried, J., Stanke, N., Munz, C., Hornung, V., König, R., and Lindemann, D. (2019). Insights into Innate Sensing of Prototype Foamy Viruses in Myeloid Cells. Viruses *11*. https://doi.org/10.3390/v11121095.

Bharat, T.A.M., Noda, T., Riches, J.D., Kraehling, V., Kolesnikova, L., Becker, S., Kawaoka, Y., and Briggs, J.A.G. (2012). Structural dissection of Ebola virus and its assembly determinants using cryo-electron tomography. Proceedings of the National Academy of Sciences *109*, 4275-4280. https://doi.org/10.1073/pnas.1120453109.

Bhattacharyya, S., Hope, T.J., and Young, J.A.T. (2011). Differential requirements for clathrin endocytic pathway components in cellular entry by Ebola and Marburg glycoprotein pseudovirions. Virology *419*, 1-9. https://doi.org/10.1016/j.virol.2011.07.018.

Biedenkopf, N., and Hoenen, T. (2017). Modeling the Ebolavirus Life Cycle with Transcription and Replication-Competent Viruslike Particle Assays. Methods in molecular biology (Clifton, N.J.) *1628*, 119-131. https://doi.org/10.1007/978-1-4939-7116-9_9.

Boonyaratanakornkit, J., Bartlett, E., Schomacker, H., Surman, S., Akira, S., Bae, Y.-S., Collins, P., Murphy, B., and Schmidt, A. (2011). The C proteins of human parainfluenza virus type 1 limit double-stranded RNA accumulation that would otherwise trigger activation of MDA5 and protein kinase R. Journal of virology *85*, 1495-1506. https://doi.org/10.1128/JVI.01297-10.

Bosio, C.M., Aman, M.J., Grogan, C., Hogan, R., Ruthel, G., Negley, D., Mohamadzadeh, M., Bavari, S., and Schmaljohn, A. (2003). Ebola and Marburg viruses replicate in monocyte-derived dendritic cells without inducing the production of cytokines and full maturation. The Journal of infectious diseases *188*, 1630-1638. https://doi.org/10.1086/379199.

Bradley, J.H., Harrison, A., Corey, A., Gentry, N., and Gregg, R.K. (2018). Ebola virus secreted glycoprotein decreases the anti-viral immunity of macrophages in early inflammatory responses. Cellular immunology *324*, 24-32. https://doi.org/10.1016/j.cellimm.2017.11.009.

Bray, M., and Geisbert, T.W. (2005). Ebola virus: the role of macrophages and dendritic cells in the pathogenesis of Ebola hemorrhagic fever. The international journal of biochemistry & cell biology *37*, 1560-1566. https://doi.org/10.1016/j.biocel.2005.02.018.

Brody, T., Yavatkar, A.S., Park, D.S., Kuzin, A., Ross, J., and Odenwald, W.F. (2017). Flavivirus and Filovirus EvoPrinters: New alignment tools for the comparative analysis of viral evolution. PLoS neglected tropical diseases *11*, e0005673. https://doi.org/10.1371/journal.pntd.0005673.

Bruns, A.M., Pollpeter, D., Hadizadeh, N., Myong, S., Marko, J.F., and Horvath, C.M. (2013). ATP hydrolysis enhances RNA recognition and antiviral signal transduction by the innate immune sensor, laboratory of genetics and physiology 2 (LGP2). The Journal of biological chemistry *288*, 938-946. https://doi.org/10.1074/jbc.M112.424416.

Burk, R., Bollinger, L., Johnson, J.C., Wada, J., Radoshitzky, S.R., Palacios, G., Bavari, S., Jahrling, P.B., and Kuhn, J.H. (2016). Neglected filoviruses. FEMS microbiology reviews *40*, 494-519. https://doi.org/10.1093/femsre/fuw010.

Bwaka, M.A., Bonnet, M.J., Calain, P., Colebunders, R., Roo, A. de, Guimard, Y., Katwiki, K.R., Kibadi, K., Kipasa, M.A., and Kuvula, K.J., et al. (1999). Ebola hemorrhagic fever in Kikwit, Democratic Republic of the Congo: clinical observations in 103 patients. The Journal of infectious diseases *179 Suppl 1*, S1-7. https://doi.org/10.1086/514308.

Calain, P., Monroe, M.C., and Nichol, S.T. (1999). Ebola virus defective interfering particles and persistent infection. Virology *262*, 114-128. https://doi.org/10.1006/viro.1999.9915.

Calain, P., Roux, L., and Kolakofsky, D. (2016). Defective interfering genomes and Ebola virus persistence. The Lancet *388*, 659-660. https://doi.org/10.1016/S0140-6736(16)31272-7.

Cantell, K., and Hirvonen, S. (1981). Preparation and assay of Sendai virus. Methods in enzymology *78*, 299-301. https://doi.org/10.1016/0076-6879(81)78131-x.

Cárdenas, W.B., Loo, Y.-M., Gale, M., Hartman, A.L., Kimberlin, C.R., Martínez-Sobrido, L., Saphire, E.O., and Basler, C.F. (2006). Ebola virus VP35 protein binds double-stranded RNA and inhibits alpha/beta interferon production induced by RIG-I signaling. Journal of virology *80*, 5168-5178. https://doi.org/10.1128/JVI.02199-05.

Carette, J.E., Raaben, M., Wong, A.C., Herbert, A.S., Obernosterer, G., Mulherkar, N., Kuehne, A.I., Kranzusch, P.J., Griffin, A.M., and Ruthel, G., et al. (2011). Ebola virus entry requires the cholesterol transporter Niemann-Pick C1. Nature *477*, 340-343. https://doi.org/10.1038/nature10348.

Cattaneo, R., Schmid, A., Eschle, D., Baczko, K., Meulen, V. ter, and Billeter, M.A. (1988). Biased hypermutation and other genetic changes in defective measles viruses in human brain infections. Cell *55*, 255-265. https://doi.org/10.1016/0092-8674(88)90048-7.

CDC (2022). Diagnosis | Ebola (Ebola Virus Disease). https://www.cdc.gov/vhf/ebola/diagnosis/index.html. 22.03.2022.

Chan, S.Y., Empig, C.J., Welte, F.J., Speck, R.F., Schmaljohn, A., Kreisberg, J.F., and Goldsmith, M.A. (2001). Folate Receptor-α Is a Cofactor for Cellular Entry by Marburg and Ebola Viruses. Cell *106*, 117-126. https://doi.org/10.1016/S0092-8674(01)00418-4.

Chandran, K., Sullivan, N.J., Felbor, U., Whelan, S.P., and Cunningham, J.M. (2005). Endosomal proteolysis of the Ebola virus glycoprotein is necessary for infection. Science (New York, N.Y.) *308*, 1643-1645. https://doi.org/10.1126/science.1110656.

Chang, T.-H., Kubota, T., Matsuoka, M., Jones, S., Bradfute, S.B., Bray, M., and Ozato, K. (2009). Ebola Zaire virus blocks type I interferon production by exploiting the host SUMO modification machinery. PLoS pathogens *5*, e1000493. https://doi.org/10.1371/journal.ppat.1000493.

Chassey, B. de, Aublin-Gex, A., Ruggieri, A., Meyniel-Schicklin, L., Pradezynski, F., Davoust, N., Chantier, T., Tafforeau, L., Mangeot, P.-E., and Ciancia, C., et al. (2013). The interactomes of influenza virus NS1 and NS2 proteins identify new host factors and provide insights for ADAR1 playing a supportive role in virus replication. PLoS pathogens *9*, e1003440. https://doi.org/10.1371/journal.ppat.1003440.

Chen, S.-T., Chen, L., Lin, D.S.-C., Chen, S.-Y., Tsao, Y.-P., Guo, H., Li, F.-J., Tseng, W.-T., Tam, J.W., and Chao, C.-W., et al. (2019). NLRP12 Regulates Anti-viral RIG-I Activation via Interaction with TRIM25. Cell host & microbe *25*, 602-616.e7. https://doi.org/10.1016/j.chom.2019.02.013.

Chen, Y.G., and Hur, S. (2021). Cellular origins of dsRNA, their recognition and consequences. Nature reviews. Molecular cell biology. https://doi.org/10.1038/s41580-021-00430-1.

Chiang, J.J., Sparrer, K.M.J., van Gent, M., Lässig, C., Huang, T., Osterrieder, N., Hopfner, K.-P., and Gack, M.U. (2018). Viral unmasking of cellular 5S rRNA pseudogene transcripts induces RIG-I-mediated immunity. Nature immunology *19*, 53-62. https://doi.org/10.1038/s41590-017-0005-y.

Christie, A., Davies-Wayne, G.J., Cordier-Lasalle, T., Blackley, D.J., Laney, A.S., Williams, D.E., Shinde, S.A., Badio, M., Lo, T., and Mate, S.E., et al. (2015). Possible Sexual Transmission of Ebola Virus — Liberia, 2015. Morbidity and Mortality Weekly Report *64*, 479-481.

Chung, H., Calis, J.J.A., Wu, X., Sun, T., Yu, Y., Sarbanes, S.L., Dao Thi, V.L., Shilvock, A.R., Hoffmann, H.-H., and Rosenberg, B.R., et al. (2018). Human ADAR1 Prevents Endogenous RNA from Triggering Translational Shutdown. Cell *172*, 811-824.e14. https://doi.org/10.1016/j.cell.2017.12.038.

Conzelmann, K.K. (2004). Reverse genetics of mononegavirales. Current topics in microbiology and immunology *283*, 1-41. https://doi.org/10.1007/978-3-662-06099-5_1.

Côté, M., Misasi, J., Ren, T., Bruchez, A., Lee, K., Filone, C.M., Hensley, L., Li, Q., Ory, D., and Chandran, K., et al. (2011). Small molecule inhibitors reveal Niemann-Pick C1 is essential for Ebola virus infection. Nature *477*, 344-348. https://doi.org/10.1038/nature10380.

Cox, N.J., McCormick, J.B., Johnson, K.M., and Kiley, M.P. (1983). Evidence for two subtypes of Ebola virus based on oligonucleotide mapping of RNA. The Journal of infectious diseases *147*, 272-275. https://doi.org/10.1093/infdis/147.2.272.

Dar, A.C., Dever, T.E., and Sicheri, F. (2005). Higher-order substrate recognition of eIF2alpha by the RNA-dependent protein kinase PKR. Cell *122*, 887-900. https://doi.org/10.1016/j.cell.2005.06.044.

Darnell, J.E., Kerr, I.M., and Stark, G.R. (1994). Jak-STAT pathways and transcriptional activation in response to IFNs and other extracellular signaling proteins. Science (New York, N.Y.) *264*, 1415-1421. https://doi.org/10.1126/science.8197455.

Deddouche, S., Goubau, D., Rehwinkel, J., Chakravarty, P., Begum, S., Maillard, P.V., Borg, A., Matthews, N., Feng, Q., and van Kuppeveld, F.J.M., et al. (2014). Identification of an LGP2-associated MDA5 agonist in picornavirus-infected cells. eLife *3*, e01535. https://doi.org/10.7554/eLife.01535.

Deflubé, L.R., Cressey, T.N., Hume, A.J., Olejnik, J., Haddock, E., Feldmann, F., Ebihara, H., Fearns, R., and Mühlberger, E. (2019). Ebolavirus polymerase uses an unconventional genome replication mechanism. Proceedings of the National Academy of Sciences of the United States of America *116*, 8535-8543. https://doi.org/10.1073/pnas.1815745116.

Di Giorgio, S., Martignano, F., Torcia, M.G., Mattiuz, G., and Conticello, S.G. (2020). Evidence for host-dependent RNA editing in the transcriptome of SARS-CoV-2. Science advances *6*, eabb5813. https://doi.org/10.1126/sciadv.abb5813.

Dilley, K.A., Voorhies, A.A., Luthra, P., Puri, V., Stockwell, T.B., Lorenzi, H., Basler, C.F., and Shabman, R.S. (2017). The Ebola virus VP35 protein binds viral immunostimulatory and host RNAs identified through deep sequencing. PloS one *12*, e0178717. https://doi.org/10.1371/journal.pone.0178717.

Dokubo, E.K., Wendland, A., Mate, S.E., Ladner, J.T., Hamblion, E.L., Raftery, P., Blackley, D.J., Laney, A.S., Mahmoud, N., and Wayne-Davies, G., et al. (2018). Persistence of Ebola virus after the end of widespread transmission in Liberia: an outbreak report. The Lancet Infectious Diseases *18*, 1015-1024. https://doi.org/10.1016/S1473-3099(18)30417-1.

Dudas, G., Carvalho, L.M., Bedford, T., Tatem, A.J., Baele, G., Faria, N.R., Park, D.J., Ladner, J.T., Arias, A., and Asogun, D., et al. (2017). Virus genomes reveal factors that spread and sustained the Ebola epidemic. Nature *544*, 309-315. https://doi.org/10.1038/nature22040.

Eckmann, C.R., Neunteufl, A., Pfaffstetter, L., and Jantsch, M.F. (2001). The human but not the Xenopus RNA-editing enzyme ADAR1 has an atypical nuclear localization signal and displays the characteristics of a shuttling protein. Molecular biology of the cell *12*, 1911-1924. https://doi.org/10.1091/mbc.12.7.1911.

Edinger, T.O., Pohl, M.O., Yángüez, E., and Stertz, S. (2015). Cathepsin W Is Required for Escape of Influenza A Virus from Late Endosomes. mBio *6*, e00297. https://doi.org/10.1128/mBio.00297-15.

Edwards, M.R., Liu, G., Mire, C.E., Sureshchandra, S., Luthra, P., Yen, B., Shabman, R.S., Leung, D.W., Messaoudi, I., and Geisbert, T.W., et al. (2016). Differential Regulation of Interferon Responses by Ebola and Marburg Virus VP35 Proteins. Cell reports *14*, 1632-1640. https://doi.org/10.1016/j.celrep.2016.01.049.

Emanuel, J., Marzi, A., and Feldmann, H. (2018). Filoviruses: Ecology, Molecular Biology, and Evolution. Advances in virus research *100*, 189-221. https://doi.org/10.1016/bs.aivir.2017.12.002.

Feldmann, H., Bugany, H., Mahner, F., Klenk, H.D., Drenckhahn, D., and Schnittler, H.J. (1996). Filovirus-induced endothelial leakage triggered by infected monocytes/macrophages. Journal of virology *70*, 2208-2214. https://doi.org/10.1128/JVI.70.4.2208-2214.1996.

Feng, Z., Cerveny, M., Yan, Z., and He, B. (2007). The VP35 protein of Ebola virus inhibits the antiviral effect mediated by double-stranded RNA-dependent protein kinase PKR. Journal of virology *81*, 182-192. https://doi.org/10.1128/JVI.01006-06.

García-Sastre, A. (2017). Ten Strategies of Interferon Evasion by Viruses. Cell host & microbe *22*, 176-184. https://doi.org/10.1016/j.chom.2017.07.012.

Geisbert, T.W., Hensley, L., Larsen, T., Young, H.A., Reed, D.S., Geisbert, J.B., Scott, D.P., Kagan, E., Jahrling, P.B., and Davis, K.J. (2003). Pathogenesis of Ebola hemorrhagic fever in cynomolgus macaques: Evidence that dendritic cells are early and sustained targets of infection. American Journal of Pathology, 2347-2370. https://doi.org/10.1016/S0002-9440(10)63591-2.

Geisbert, T.W., and Jahrling, P.B. (1995). Differentiation of filoviruses by electron microscopy. Virus Research *39*, 129-150. https://doi.org/10.1016/0168-1702(95)00080-1.

George, C.X., and Samuel, C.E. (1999). Human RNA-specific adenosine deaminase ADAR1 transcripts possess alternative exon 1 structures that initiate from different promoters, one constitutively active and the other interferon inducible. Proceedings of the National Academy of Sciences *96*, 4621-4626. https://doi.org/10.1073/pnas.96.8.4621.

Giard, D.J., Aaronson, S.A., Todaro, G.J., Arnstein, P., Kersey, J.H., Dosik, H., and Parks, W.P. (1973). In vitro cultivation of human tumors: establishment of cell lines derived from a series of solid tumors. Journal of the National Cancer Institute *51*, 1417-1423. https://doi.org/10.1093/jnci/51.5.1417.

Goldstein, T., Anthony, S.J., Gbakima, A., Bird, B.H., Bangura, J., Tremeau-Bravard, A., Belaganahalli, M.N., Wells, H.L., Dhanota, J.K., and Liang, E., et al. (2018). The discovery of Bombali virus adds further support for bats as hosts of ebolaviruses. Nature microbiology *3*, 1084-1089. https://doi.org/10.1038/s41564-018-0227-2.

Goubau, D., Schlee, M., Deddouche, S., Pruijssers, A.J., Zillinger, T., Goldeck, M., Schuberth, C., van der Veen, A.G., Fujimura, T., and Rehwinkel, J., et al. (2014). Antiviral immunity via RIG-I-mediated recognition of RNA bearing 5'-diphosphates. Nature *514*, 372-375. https://doi.org/10.1038/nature13590.

Gramberg, T., Hofmann, H., Möller, P., Lalor, P.F., Marzi, A., Geier, M., Krumbiegel, M., Winkler, T., Kirchhoff, F., and Adams, D.H., et al. (2005). LSECtin interacts with filovirus glycoproteins and the spike protein of SARS coronavirus. Virology *340*, 224-236. https://doi.org/10.1016/j.virol.2005.06.026.

Grandvaux, N., Servant, M.J., tenOever, B., Sen, G.C., Balachandran, S., Barber, G.N., Lin, R., and Hiscott, J. (2002). Transcriptional profiling of interferon regulatory factor 3 target genes: direct involvement in the regulation of interferon-stimulated genes. Journal of virology *76*, 5532-5539. https://doi.org/10.1128/jvi.76.11.5532-5539.2002.

Gupta, M., Mahanty, S., Ahmed, R., and Rollin, P.E. (2001). Monocyte-derived human macrophages and peripheral blood mononuclear cells infected with ebola virus secrete MIP-1alpha and TNF-alpha and inhibit poly-IC-induced IFN-alpha in vitro. Virology *284*, 20-25. https://doi.org/10.1006/viro.2001.0836.

Habjan, M., Andersson, I., Klingström, J., Schümann, M., Martin, A., Zimmermann, P., Wagner, V., Pichlmair, A., Schneider, U., and Mühlberger, E., et al. (2008). Processing of genome 5' termini as a strategy of negative-strand RNA viruses to avoid RIG-I-dependent interferon induction. PloS one *3*, e2032. https://doi.org/10.1371/journal.pone.0002032.

Hage, A., Bharaj, P., van Tol, S., Giraldo, M.I., Gonzalez-Orozco, M., Valerdi, K.M., Warren, A.N., Aguilera-Aguirre, L., Xie, X., and Widen, S.G., et al. (2022). The RNA helicase DHX16 recognizes specific viral RNA to trigger RIG-I-dependent innate antiviral immunity. Cell reports *38*, 110434. https://doi.org/10.1016/j.celrep.2022.110434.

Hamm, A., Krott, N., Breibach, I., Blindt, R., and Bosserhoff, A.K. (2002). Efficient Transfection Method for Primary Cells. Tissue Engineering *8*, 235-245. https://doi.org/10.1089/107632702753725003.

Han, Z., Boshra, H., Sunyer, J.O., Zwiers, S.H., Paragas, J., and Harty, R.N. (2003). Biochemical and functional characterization of the Ebola virus VP24 protein: implications for a role in virus assembly and budding. Journal of virology *77*, 1793-1800. https://doi.org/10.1128/jvi.77.3.1793-1800.2003.

Harcourt, B.H., Sanchez, A., and Offermann, M.K. (1998). Ebola virus inhibits induction of genes by double-stranded RNA in endothelial cells. Virology *252*, 179-188. https://doi.org/10.1006/viro.1998.9446.

Harcourt, B.H., Sanchez, A., and Offermann, M.K. (1999). Ebola virus selectively inhibits responses to interferons, but not to interleukin-1beta, in endothelial cells. Journal of virology *73*, 3491-3496. https://doi.org/10.1128/JVI.73.4.3491-3496.1999.

Hartman, A.L., Bird, B.H., Towner, J.S., Antoniadou, Z.-A., Zaki, S.R., and Nichol, S.T. (2008a). Inhibition of IRF-3 activation by VP35 is critical for the high level of virulence of ebola virus. Journal of virology *82*, 2699-2704. https://doi.org/10.1128/JVI.02344-07.

Hartman, A.L., Dover, J.E., Towner, J.S., and Nichol, S.T. (2006). Reverse genetic generation of recombinant Zaire Ebola viruses containing disrupted IRF-3 inhibitory domains results in attenuated virus growth in vitro and higher levels of IRF-3 activation without inhibiting viral transcription or replication. Journal of virology *80*, 6430-6440. https://doi.org/10.1128/JVI.00044-06.

Hartman, A.L., Ling, L., Nichol, S.T., and Hibberd, M.L. (2008b). Whole-genome expression profiling reveals that inhibition of host innate immune response pathways by Ebola virus can be reversed by a single amino acid change in the VP35 protein. Journal of virology *82*, 5348-5358. https://doi.org/10.1128/JVI.00215-08.

Hartman, A.L., Towner, J.S., and Nichol, S.T. (2004). A C-terminal basic amino acid motif of Zaire ebolavirus VP35 is essential for type I interferon antagonism and displays high identity with the RNA-binding domain of another interferon antagonist, the NS1 protein of influenza A virus. Virology *328*, 177-184. https://doi.org/10.1016/j.virol.2004.07.006.

Harty, R.N., Brown, M.E., Wang, G., Huibregtse, J., and Hayes, F.P. (2000). A PPxY motif within the VP40 protein of Ebola virus interacts physically and functionally with a ubiquitin ligase: implications for filovirus budding. Proceedings of the National Academy of Sciences of the United States of America *97*, 13871-13876. https://doi.org/10.1073/pnas.250277297.

Hoenen, T., Groseth, A., and Feldmann, H. (2019). Therapeutic strategies to target the Ebola virus life cycle. Nature reviews. Microbiology *17*, 593-606. https://doi.org/10.1038/s41579-019-0233-2.

Hoenen, T., Groseth, A., Kok-Mercado, F. de, Kuhn, J.H., and Wahl-Jensen, V. (2011). Minigenomes, transcription and replication competent virus-like particles and beyond: reverse genetics systems for filoviruses and other negative stranded hemorrhagic fever viruses. Antiviral research *91*, 195-208. https://doi.org/10.1016/j.antiviral.2011.06.003.

Hoenen, T., Groseth, A., Kolesnikova, L., Theriault, S., Ebihara, H., Hartlieb, B., Bamberg, S., Feldmann, H., Ströher, U., and Becker, S. (2006). Infection of naive target cells with virus-like particles: implications for the function of ebola virus VP24. Journal of virology *80*, 7260-7264. https://doi.org/10.1128/JVI.00051-06.

Hoenen, T., Shabman, R.S., Groseth, A., Herwig, A., Weber, M., Schudt, G., Dolnik, O., Basler, C.F., Becker, S., and Feldmann, H. (2012). Inclusion bodies are a site of ebolavirus replication. Journal of virology *86*, 11779-11788. https://doi.org/10.1128/JVI.01525-12.

Hoenen, T., Watt, A., Mora, A., and Feldmann, H. (2014). Modeling the lifecycle of Ebola virus under biosafety level 2 conditions with virus-like particles containing tetracistronic minigenomes. Journal of visualized experiments : JoVE, 52381. https://doi.org/10.3791/52381.

Hornung, V., Ellegast, J., Kim, S., Brzózka, K., Jung, A., Kato, H., Poeck, H., Akira, S., Conzelmann, K.-K., and Schlee, M., et al. (2006). 5'-Triphosphate RNA is the ligand for RIG-I. Science (New York, N.Y.) *314*, 994-997. https://doi.org/10.1126/science.1132505.

Hume, A.J., and Mühlberger, E. (2019). Distinct Genome Replication and Transcription Strategies within the Growing Filovirus Family. Journal of molecular biology *431*, 4290-4320. https://doi.org/10.1016/j.jmb.2019.06.029.

Hunt, C.L., Kolokoltsov, A.A., Davey, R.A., and Maury, W. (2011). The Tyro3 receptor kinase Axl enhances macropinocytosis of Zaire ebolavirus. Journal of virology *85*, 334-347. https://doi.org/10.1128/JVI.01278-09.

Jacob, S.T., Crozier, I., Fischer, W.A., Hewlett, A., Kraft, C.S., La Vega, M.-A.d., Soka, M.J., Wahl, V., Griffiths, A., and Bollinger, L., et al. (2020). Ebola virus disease. Nature reviews. Disease primers *6*, 13. https://doi.org/10.1038/s41572-020-0147-3.

Jacobs, M., Rodger, A., Bell, D.J., Bhagani, S., Cropley, I., Filipe, A., Gifford, R.J., Hopkins, S., Hughes, J., and Jabeen, F., et al. (2016). Late Ebola virus relapse causing meningoencephalitis: a case report. The Lancet *388*, 498-503. https://doi.org/10.1016/S0140-6736(16)30386-5.

Jahrling, P.B., Geisbert, T.W., Johnson, E.D., Peters, C.J., Dalgard, D.W., and Hall, W.C. (1990). Preliminary report: isolation of Ebola virus from monkeys imported to USA. The Lancet *335*, 502-505. https://doi.org/10.1016/0140-6736(90)90737-p.

Jankeel, A., Menicucci, A.R., Woolsey, C., Fenton, K.A., Mendoza, N., Versteeg, K., Cross, R.W., Geisbert, T.W., and Messaoudi, I. (2020). Early Transcriptional Changes within Liver, Adrenal Gland, and Lymphoid Tissues Significantly Contribute to Ebola Virus Pathogenesis in Cynomolgus Macaques. Journal of virology *94*. https://doi.org/10.1128/JVI.00250-20.

Jemielity, S., Wang, J.J., Chan, Y.K., Ahmed, A.A., Li, W., Monahan, S., Bu, X., Farzan, M., Freeman, G.J., and Umetsu, D.T., et al. (2013). TIM-family proteins promote infection of multiple enveloped viruses through virion-associated phosphatidylserine. PLoS pathogens *9*, e1003232. https://doi.org/10.1371/journal.ppat.1003232.

Johnson, E.D., Johnson, B.K., Silverstein, D., Tukei, P., Geisbert, T.W., Sanchez, A.N., and Jahrling, P.B. (1996). Characterization of a new Marburg virus isolated from a 1987 fatal case in Kenya. Archives of virology. Supplementum *11*, 101-114. https://doi.org/10.1007/978-3-7091-7482-1_10.

Judson, S., Prescott, J., and Munster, V. (2015). Understanding ebola virus transmission. Viruses *7*, 511-521. https://doi.org/10.3390/v7020511.

Kato, H., Takeuchi, O., Mikamo-Satoh, E., Hirai, R., Kawai, T., Matsushita, K., Hiiragi, A., Dermody, T.S., Fujita, T., and Akira, S. (2008). Length-dependent recognition of double-stranded ribonucleic acids by retinoic acid-inducible gene-I and melanoma differentiation-associated gene 5. The Journal of experimental medicine *205*, 1601-1610. https://doi.org/10.1084/jem.20080091.

Kawai, T., Takahashi, K., Sato, S., Coban, C., Kumar, H., Kato, H., Ishii, K.J., Takeuchi, O., and Akira, S. (2005). IPS-1, an adaptor triggering RIG-I- and Mda5-mediated type I interferon induction. Nature immunology *6*, 981-988. https://doi.org/10.1038/ni1243.

Kawakubo, K., and Samuel, C.E. (2000). Human RNA-specific adenosine deaminase (ADAR1) gene specifies transcripts that initiate from a constitutively active alternative promoter. Gene *258*, 165-172. https://doi.org/10.1016/s0378-1119(00)00368-1.

Keita, A.K., Koundouno, F.R., Faye, M., Düx, A., Hinzmann, J., Diallo, H., Ayouba, A., Le Marcis, F., Soropogui, B., and Ifono, K., et al. (2021). Resurgence of Ebola virus in 2021 in Guinea suggests a new paradigm for outbreaks. Nature *597*, 539-543. https://doi.org/10.1038/s41586-021-03901-9.

Khadka, S., Williams, C.G., Sweeney-Gibbons, J., and Basler, C.F. (2021). 3' untranslated regions of Marburg and Ebola virus mRNAs possess negative regulators of translation that are modulated by ADAR1 editing.

Kirchdoerfer, R.N., Abelson, D.M., Li, S., Wood, M.R., and Saphire, E.O. (2015). Assembly of the Ebola Virus Nucleoprotein from a Chaperoned VP35 Complex. Cell reports *12*, 140-149. https://doi.org/10.1016/j.celrep.2015.06.003.

Kok, K.-H., Lui, P.-Y., Ng, M.-H.J., Siu, K.-L., Au, S.W.N., and Jin, D.-Y. (2011). The double-stranded RNA-binding protein PACT functions as a cellular activator of RIG-I to facilitate innate antiviral response. Cell host & microbe *9*, 299-309. https://doi.org/10.1016/j.chom.2011.03.007.

Kondratowicz, A.S., Lennemann, N.J., Sinn, P.L., Davey, R.A., Hunt, C.L., Moller-Tank, S., Meyerholz, D.K., Rennert, P., Mullins, R.F., and Brindley, M., et al. (2011). T-cell immunoglobulin and mucin domain 1 (TIM-1) is a receptor for Zaire Ebolavirus and Lake Victoria Marburgvirus. Proceedings of the National Academy of Sciences *108*, 8426-8431. https://doi.org/10.1073/pnas.1019030108.

König, R., Stertz, S., Zhou, Y., Inoue, A., Hoffmann, H.-H., Bhattacharyya, S., Alamares, J.G., Tscherne, D.M., Ortigoza, M.B., and Liang, Y., et al. (2010). Human host factors required for influenza virus replication. Nature *463*, 813-817. https://doi.org/10.1038/nature08699.

Kortepeter, M.G., Bausch, D.G., and Bray, M. (2011). Basic clinical and laboratory features of filoviral hemorrhagic fever. The Journal of infectious diseases *204 Suppl 3*, S810-6. https://doi.org/10.1093/infdis/jir299.

Ksiazek, T.G., Rollin, P.E., Williams, A.J., Bressler, D.S., Martin, M.L., Swanepoel, R., Burt, F.J., Leman, P.A., Khan, A.S., and Rowe, A.K., et al. (1999). Clinical virology of Ebola hemorrhagic fever (EHF): virus, virus antigen, and IgG and IgM antibody findings among EHF patients in Kikwit, Democratic Republic of the Congo, 1995. The Journal of infectious diseases *179 Suppl 1*, S177-87. https://doi.org/10.1086/514321.

Kubota, T., Matsuoka, M., Chang, T.-H., Tailor, P., Sasaki, T., Tashiro, M., Kato, A., and Ozato, K. (2008). Virus infection triggers SUMOylation of IRF3 and IRF7, leading to the negative regulation of type I interferon gene expression. The Journal of biological chemistry *283*, 25660-25670. https://doi.org/10.1074/jbc.M804479200.

Kuhn, J.H., Amarasinghe, G.K., Basler, C.F., Bavari, S., Bukreyev, A., Chandran, K., Crozier, I., Dolnik, O., Dye, J.M., and Formenty, P.B.H., et al. (2019). ICTV Virus Taxonomy Profile: Filoviridae. The Journal of general virology *100*, 911-912. https://doi.org/10.1099/jgv.0.001252.

Kumar, H., Kawai, T., and Akira, S. (2011). Pathogen recognition by the innate immune system. International reviews of immunology *30*, 16-34. https://doi.org/10.3109/08830185.2010.529976.

Kuzmin, I.V., Schwarz, T.M., Ilinykh, P.A., Jordan, I., Ksiazek, T.G., Sachidanandam, R., Basler, C.F., and Bukreyev, A. (2017). Innate Immune Responses of Bat and Human Cells to Filoviruses: Commonalities and Distinctions. Journal of virology *91*. https://doi.org/10.1128/JVI.02471-16.

Lai, C.-Y., Strange, D.P., Wong, T.A.S., Lehrer, A.T., and Verma, S. (2017). Ebola Virus Glycoprotein Induces an Innate Immune Response In vivo via TLR4. Frontiers in microbiology *8*, 1571. https://doi.org/10.3389/fmicb.2017.01571.

Lauterbach-Rivière, L., Bergez, M., Mönch, S., Qu, B., Riess, M., Vondran, F.W.R., Liese, J., Hornung, V., Urban, S., and König, R. (2020). Hepatitis B Virus DNA is a Substrate for the cGAS/STING Pathway but is not Sensed in Infected Hepatocytes. Viruses *12*. https://doi.org/10.3390/v12060592.

Le Guenno, B., Formenty, P., Wyers, M., Gounon, P., Walker, F., and Boesch, C. (1995). Isolation and partial characterisation of a new strain of Ebola virus. The Lancet *345*, 1271-1274. https://doi.org/10.1016/S0140-6736(95)90925-7.

Leendertz, S.A.J., Gogarten, J.F., Düx, A., Calvignac-Spencer, S., and Leendertz, F.H. (2016). Assessing the Evidence Supporting Fruit Bats as the Primary Reservoirs for Ebola Viruses. EcoHealth *13*, 18-25. https://doi.org/10.1007/s10393-015-1053-0.

Leung, D.W., Borek, D., Luthra, P., Binning, J.M., Anantpadma, M., Liu, G., Harvey, I.B., Su, Z., Endlich-Frazier, A., and Pan, J., et al. (2015). An Intrinsically Disordered Peptide from Ebola Virus VP35 Controls Viral RNA Synthesis by Modulating Nucleoprotein-RNA Interactions. Cell reports *11*, 376-389. https://doi.org/10.1016/j.celrep.2015.03.034.

Leung, D.W., Ginder, N.D., Fulton, D.B., Nix, J., Basler, C.F., Honzatko, R.B., and Amarasinghe, G.K. (2009). Structure of the Ebola VP35 interferon inhibitory domain. Proceedings of the National Academy of Sciences *106*, 411-416. https://doi.org/10.1073/pnas.0807854106.

Leung, D.W., Prins, K.C., Borek, D.M., Farahbakhsh, M., Tufariello, J.M., Ramanan, P., Nix, J.C., Helgeson, L.A., Otwinowski, Z., and Honzatko, R.B., et al. (2010). Structural basis for dsRNA recognition and interferon antagonism by Ebola VP35. Nature structural & molecular biology *17*, 165-172. https://doi.org/10.1038/nsmb.1765.

Levanon, E.Y., Eisenberg, E., Yelin, R., Nemzer, S., Hallegger, M., Shemesh, R., Fligelman, Z.Y., Shoshan, A., Pollock, S.R., and Sztybel, D., et al. (2004). Systematic identification of abundant A-to-I editing sites in the human transcriptome. Nature biotechnology *22*, 1001-1005. https://doi.org/10.1038/nbt996.

Li, Z., Okonski, K.M., and Samuel, C.E. (2012). Adenosine deaminase acting on RNA 1 (ADAR1) suppresses the induction of interferon by measles virus. Journal of virology *86*, 3787-3794. https://doi.org/10.1128/JVI.06307-11.

Licata, J.M., Johnson, R.F., Han, Z., and Harty, R.N. (2004). Contribution of ebola virus glycoprotein, nucleoprotein, and VP24 to budding of VP40 virus-like particles. Journal of virology *78*, 7344-7351. https://doi.org/10.1128/JVI.78.14.7344-7351.2004.

Licht, K., Hartl, M., Amman, F., Anrather, D., Janisiw, M.P., and Jantsch, M.F. (2019). Inosine induces context-dependent recoding and translational stalling. Nucleic acids research *47*, 3-14. https://doi.org/10.1093/nar/gky1163.

Liddicoat, B.J., Piskol, R., Chalk, A.M., Ramaswami, G., Higuchi, M., Hartner, J.C., Li, J.B., Seeburg, P.H., and Walkley, C.R. (2015). RNA editing by ADAR1 prevents MDA5 sensing of endogenous dsRNA as nonself. Science (New York, N.Y.) *349*, 1115-1120. https://doi.org/10.1126/science.aac7049.

Lifland, A.W., Jung, J., Alonas, E., Zurla, C., Crowe, J.E., and Santangelo, P.J. (2012). Human respiratory syncytial virus nucleoprotein and inclusion bodies antagonize the innate immune response mediated by MDA5 and MAVS. Journal of virology *86*, 8245-8258. https://doi.org/10.1128/JVI.00215-12.

Liu, G., and Gack, M.U. (2020). Distinct and Orchestrated Functions of RNA Sensors in Innate Immunity. Immunity *53*, 26-42. https://doi.org/10.1016/j.immuni.2020.03.017.

Liu, G., Park, H.-S., Pyo, H.-M., Liu, Q., and Zhou, Y. (2015). Influenza A Virus Panhandle Structure Is Directly Involved in RIG-I Activation and Interferon Induction. Journal of virology *89*, 6067-6079. https://doi.org/10.1128/JVI.00232-15.

Liu, Y., George, C.X., Patterson, J.B., and Samuel, C.E. (1997). Functionally distinct double-stranded RNA-binding domains associated with alternative splice site variants of the interferon-inducible double-stranded RNA-specific adenosine deaminase. The Journal of biological chemistry *272*, 4419-4428. https://doi.org/10.1074/jbc.272.7.4419.

Liu, Y., Wang, M., Cheng, A., Yang, Q., Wu, Y., Jia, R., Liu, M., Zhu, D., Chen, S., and Zhang, S., et al. (2020). The role of host eIF2α in viral infection. Virology journal *17*, 112. https://doi.org/10.1186/s12985-020-01362-6.

Liu, Y.-J. (2001). Dendritic Cell Subsets and Lineages, and Their Functions in Innate and Adaptive Immunity. Cell *106*, 259-262. https://doi.org/10.1016/s0092-8674(01)00456-1.

Livak, K.J., and Schmittgen, T.D. (2001). Analysis of relative gene expression data using real-time quantitative PCR and the 2(-Delta Delta C(T)) Method. Methods (San Diego, Calif.) *25*, 402-408. https://doi.org/10.1006/meth.2001.1262.

Lu, H., Lu, N., Weng, L., Yuan, B., Liu, Y.-J., and Zhang, Z. (2014). DHX15 senses double-stranded RNA in myeloid dendritic cells. Journal of immunology (Baltimore, Md. : 1950) *193*, 1364-1372. https://doi.org/10.4049/jimmunol.1303322.

Lubaki, N.M., Ilinykh, P., Pietzsch, C., Tigabu, B., Freiberg, A.N., Koup, R.A., and Bukreyev, A. (2013). The lack of maturation of Ebola virus-infected dendritic cells results from the cooperative effect of at least two viral domains. Journal of virology *87*, 7471-7485. https://doi.org/10.1128/JVI.03316-12.

Luthra, P., Ramanan, P., Mire, C.E., Weisend, C., Tsuda, Y., Yen, B., Liu, G., Leung, D.W., Geisbert, T.W., and Ebihara, H., et al. (2013). Mutual antagonism between the Ebola virus VP35 protein and the RIG-I activator PACT determines infection outcome. Cell host & microbe *14*, 74-84. https://doi.org/10.1016/j.chom.2013.06.010.

Macchietto, M.G., Langlois, R.A., and Shen, S.S. (2020). Virus-induced transposable element expression up-regulation in human and mouse host cells. Life science alliance *3*. https://doi.org/10.26508/lsa.201900536.

Mahanty, S., Hutchinson, K., Agarwal, S., McRae, M., Rollin, P.E., and Pulendran, B. (2003). Cutting edge: impairment of dendritic cells and adaptive immunity by Ebola and Lassa viruses. Journal of immunology (Baltimore, Md. : 1950) *170*, 2797-2801. https://doi.org/10.4049/jimmunol.170.6.2797.

Mankan, A.K., Schmidt, T., Chauhan, D., Goldeck, M., Höning, K., Gaidt, M., Kubarenko, A.V., Andreeva, L., Hopfner, K.-P., and Hornung, V. (2014). Cytosolic RNA:DNA hybrids activate the

cGAS-STING axis. The EMBO journal *33*, 2937-2946. https://doi.org/10.15252/embj.201488726.

Mannion, N.M., Greenwood, S.M., Young, R., Cox, S., Brindle, J., Read, D., Nellåker, C., Vesely, C., Ponting, C.P., and McLaughlin, P.J., et al. (2014). The RNA-editing enzyme ADAR1 controls innate immune responses to RNA. Cell reports *9*, 1482-1494. https://doi.org/10.1016/j.celrep.2014.10.041.

Marcus, P.I., and Sekellick, M.J. (1977). Defective interfering particles with covalently linked +/- RNA induce interferon. Nature *266*, 815-819. https://doi.org/10.1038/266815a0.

Marinus, M.G. (1973). Location of DNA methylation genes on the Escherichia coli K-12 genetic map. Molecular & general genetics : MGG *127*, 47-55. https://doi.org/10.1007/BF00267782.

Marq, J.-B., Hausmann, S., Veillard, N., Kolakofsky, D., and Garcin, D. (2011). Short double-stranded RNAs with an overhanging 5' ppp-nucleotide, as found in arenavirus genomes, act as RIG-I decoys. The Journal of biological chemistry *286*, 6108-6116. https://doi.org/10.1074/jbc.M110.186262.

Martini, G.A. (1969). Marburg agent disease: In man. Transactions of the Royal Society of Tropical Medicine and Hygiene *63*, 295-302. https://doi.org/10.1016/0035-9203(69)90001-7.

Marzi, A., Reinheckel, T., and Feldmann, H. (2012). Cathepsin B & L are not required for ebola virus replication. PLoS neglected tropical diseases *6*, e1923. https://doi.org/10.1371/journal.pntd.0001923.

McBride, K.M., and Reich, N.C. (2003). The ins and outs of STAT1 nuclear transport. Science's STKE : signal transduction knowledge environment *2003*, RE13. https://doi.org/10.1126/stke.2003.195.re13.

McElroy, A.K., Erickson, B.R., Flietstra, T.D., Rollin, P.E., Nichol, S.T., Towner, J.S., and Spiropoulou, C.F. (2014). Ebola hemorrhagic Fever: novel biomarker correlates of clinical outcome. The Journal of infectious diseases *210*, 558-566. https://doi.org/10.1093/infdis/jiu088.

Mehedi, M., Falzarano, D., Seebach, J., Hu, X., Carpenter, M.S., Schnittler, H.-J., and Feldmann, H. (2011). A new Ebola virus nonstructural glycoprotein expressed through RNA editing. Journal of virology *85*, 5406-5414. https://doi.org/10.1128/JVI.02190-10.

Morris, R., Kershaw, N.J., and Babon, J.J. (2018). The molecular details of cytokine signaling via the JAK/STAT pathway. Protein science : a publication of the Protein Society *27*, 1984-2009. https://doi.org/10.1002/pro.3519.

Mu, X., Greenwald, E., Ahmad, S., and Hur, S. (2018). An origin of the immunogenicity of in vitro transcribed RNA. Nucleic acids research *46*, 5239-5249. https://doi.org/10.1093/nar/gky177.

Mühlberger, E. (2007). Filovirus replication and transcription. Future virology *2*, 205-215. https://doi.org/10.2217/17460794.2.2.205.

Mühlberger, E., Lötfering, B., Klenk, H.D., and Becker, S. (1998). Three of the four nucleocapsid proteins of Marburg virus, NP, VP35, and L, are sufficient to mediate replication and transcription of Marburg virus-specific monocistronic minigenomes. Journal of virology *72*, 8756-8764. https://doi.org/10.1128/JVI.72.11.8756-8764.1998.

Mühlberger, E., Trommer, S., Funke, C., Volchkov, V., Klenk, H.D., and Becker, S. (1996). Termini of all mRNA species of Marburg virus: sequence and secondary structure. Virology *223*, 376-380. https://doi.org/10.1006/viro.1996.0490.

Mühlberger, E., Weik, M., Volchkov, V.E., Klenk, H.D., and Becker, S. (1999). Comparison of the transcription and replication strategies of marburg virus and Ebola virus by using artificial replication systems. Journal of virology *73*, 2333-2342. https://doi.org/10.1128/JVI.73.3.2333-2342.1999.

Nakaya, T., Sato, M., Hata, N., Asagiri, M., Suemori, H., Noguchi, S., Tanaka, N., and Taniguchi, T. (2001). Gene induction pathways mediated by distinct IRFs during viral infection. Biochemical and biophysical research communications *283*, 1150-1156. https://doi.org/10.1006/bbrc.2001.4913.

Nallagatla, S.R., Hwang, J., Toroney, R., Zheng, X., Cameron, C.E., and Bevilacqua, P.C. (2007). 5'-triphosphate-dependent activation of PKR by RNAs with short stem-loops. Science (New York, N.Y.) *318*, 1455-1458. https://doi.org/10.1126/science.1147347.

Nanbo, A., Imai, M., Watanabe, S., Noda, T., Takahashi, K., Neumann, G., Halfmann, P., and Kawaoka, Y. (2010). Ebolavirus is internalized into host cells via macropinocytosis in a viral glycoprotein-dependent manner. PLoS pathogens *6*, e1001121. https://doi.org/10.1371/journal.ppat.1001121.

Nanduri, S., Carpick, B.W., Yang, Y., Williams, B.R., and Qin, J. (1998). Structure of the double-stranded RNA-binding domain of the protein kinase PKR reveals the molecular basis of its dsRNA-mediated activation. The EMBO journal *17*, 5458-5465. https://doi.org/10.1093/emboj/17.18.5458.

Negredo, A., Palacios, G., Vázquez-Morón, S., González, F., Dopazo, H., Molero, F., Juste, J., Quetglas, J., Savji, N., and La Cruz Martínez, M. de, et al. (2011). Discovery of an ebolavirus-like filovirus in europe. PLoS pathogens *7*, e1002304. https://doi.org/10.1371/journal.ppat.1002304.

Ning, Y.-J., Wang, M., Deng, M., Shen, S., Liu, W., Cao, W.-C., Deng, F., Wang, Y.-Y., Hu, Z., and Wang, H. (2014). Viral suppression of innate immunity via spatial isolation of TBK1/IKKε from mitochondrial antiviral platform. Journal of molecular cell biology *6*, 324-337. https://doi.org/10.1093/jmcb/mju015.

Okonski, K.M., and Samuel, C.E. (2013). Stress granule formation induced by measles virus is protein kinase PKR dependent and impaired by RNA adenosine deaminase ADAR1. Journal of virology *87*, 756-766. https://doi.org/10.1128/JVI.02270-12.

Okumura, A., Pitha, P.M., Yoshimura, A., and Harty, R.N. (2010). Interaction between Ebola virus glycoprotein and host toll-like receptor 4 leads to induction of proinflammatory cytokines and SOCS1. Journal of virology *84*, 27-33. https://doi.org/10.1128/JVI.01462-09.

Olejnik, J., Forero, A., Deflubé, L.R., Hume, A.J., Manhart, W.A., Nishida, A., Marzi, A., Katze, M.G., Ebihara, H., and Rasmussen, A.L., et al. (2017a). Ebolaviruses Associated with Differential Pathogenicity Induce Distinct Host Responses in Human Macrophages. Journal of virology *91*. https://doi.org/10.1128/JVI.00179-17.

Olejnik, J., Hume, A.J., Leung, D.W., Amarasinghe, G.K., Basler, C.F., and Mühlberger, E. (2017b). Filovirus Strategies to Escape Antiviral Responses. Current topics in microbiology and immunology *411*, 293-322. https://doi.org/10.1007/82_2017_13.

Patel, R.C., and Sen, G.C. (1998). PACT, a protein activator of the interferon-induced protein kinase, PKR. The EMBO journal *17*, 4379-4390. https://doi.org/10.1093/emboj/17.15.4379.

Pattabhi, S., Knoll, M.L., Gale, M., and Loo, Y.-M. (2019). DHX15 Is a Coreceptor for RLR Signaling That Promotes Antiviral Defense Against RNA Virus Infection. Journal of interferon & cytokine research : the official journal of the International Society for Interferon and Cytokine Research *39*, 331-346. https://doi.org/10.1089/jir.2018.0163.

Patterson, J.B., and Samuel, C.E. (1995). Expression and regulation by interferon of a double-stranded-RNA-specific adenosine deaminase from human cells: evidence for two forms of the deaminase. Molecular and cellular biology *15*, 5376-5388. https://doi.org/10.1128/MCB.15.10.5376.

Pear, W.S., Nolan, G.P., Scott, M.L., and Baltimore, D. (1993). Production of high-titer helper-free retroviruses by transient transfection. Proceedings of the National Academy of Sciences *90*, 8392-8396. https://doi.org/10.1073/pnas.90.18.8392.

Pestal, K., Funk, C.C., Snyder, J.M., Price, N.D., Treuting, P.M., and Stetson, D.B. (2015). Isoforms of RNA-Editing Enzyme ADAR1 Independently Control Nucleic Acid Sensor MDA5-Driven Autoimmunity and Multi-organ Development. Immunity *43*, 933-944. https://doi.org/10.1016/j.immuni.2015.11.001.

Pfaller, C.K., Donohue, R.C., Nersisyan, S., Brodsky, L., and Cattaneo, R. (2018). Extensive editing of cellular and viral double-stranded RNA structures accounts for innate immunity suppression and the proviral activity of ADAR1p150. PLoS biology *16*, e2006577. https://doi.org/10.1371/journal.pbio.2006577.

Pfaller, C.K., Mastorakos, G.M., Matchett, W.E., Ma, X., Samuel, C.E., and Cattaneo, R. (2015). Measles Virus Defective Interfering RNAs Are Generated Frequently and Early in the Absence of C Protein and Can Be Destabilized by Adenosine Deaminase Acting on RNA-1-Like Hypermutations. Journal of virology *89*, 7735-7747. https://doi.org/10.1128/JVI.01017-15.

Pfaller, C.K., Radeke, M.J., Cattaneo, R., and Samuel, C.E. (2014). Measles virus C protein impairs production of defective copyback double-stranded viral RNA and activation of protein kinase R. Journal of virology *88*, 456-468. https://doi.org/10.1128/JVI.02572-13.

Pichlmair, A., Schulz, O., Tan, C.P., Näslund, T.I., Liljeström, P., Weber, F., and Reis e Sousa, C. (2006). RIG-I-mediated antiviral responses to single-stranded RNA bearing 5'-phosphates. Science (New York, N.Y.) *314*, 997-1001. https://doi.org/10.1126/science.1132998.

Prins, K.C., Binning, J.M., Shabman, R.S., Leung, D.W., Amarasinghe, G.K., and Basler, C.F. (2010a). Basic residues within the ebolavirus VP35 protein are required for its viral polymerase cofactor function. Journal of virology *84*, 10581-10591. https://doi.org/10.1128/JVI.00925-10.

Prins, K.C., Cárdenas, W.B., and Basler, C.F. (2009). Ebola virus protein VP35 impairs the function of interferon regulatory factor-activating kinases IKKepsilon and TBK-1. Journal of virology *83*, 3069-3077. https://doi.org/10.1128/JVI.01875-08.

Prins, K.C., Delpeut, S., Leung, D.W., Reynard, O., Volchkova, V.A., Reid, S.P., Ramanan, P., Cárdenas, W.B., Amarasinghe, G.K., and Volchkov, V.E., et al. (2010b). Mutations abrogating VP35 interaction with double-stranded RNA render Ebola virus avirulent in guinea pigs. Journal of virology *84*, 3004-3015. https://doi.org/10.1128/JVI.02459-09.

Ramanan, P., Shabman, R.S., Brown, C.S., Amarasinghe, G.K., Basler, C.F., and Leung, D.W. (2011). Filoviral immune evasion mechanisms. Viruses *3*, 1634-1649. https://doi.org/10.3390/v3091634.

Ramaswami, G., Lin, W., Piskol, R., Tan, M.H., Davis, C., and Li, J.B. (2012). Accurate identification of human Alu and non-Alu RNA editing sites. Nature methods *9*, 579-581. https://doi.org/10.1038/nmeth.1982.

Reid, S.P., Cárdenas, W.B., and Basler, C.F. (2005). Homo-oligomerization facilitates the interferon-antagonist activity of the ebolavirus VP35 protein. Virology *341*, 179-189. https://doi.org/10.1016/j.virol.2005.06.044.

Reid, S.P., Leung, L.W., Hartman, A.L., Martinez, O., Shaw, M.L., Carbonnelle, C., Volchkov, V.E., Nichol, S.T., and Basler, C.F. (2006). Ebola virus VP24 binds karyopherin alpha1 and blocks STAT1 nuclear accumulation. Journal of virology *80*, 5156-5167. https://doi.org/10.1128/JVI.02349-05.

Reid, S.P., Valmas, C., Martinez, O., Sanchez, F.M., and Basler, C.F. (2007). Ebola virus VP24 proteins inhibit the interaction of NPI-1 subfamily karyopherin alpha proteins with activated STAT1. Journal of virology *81*, 13469-13477. https://doi.org/10.1128/JVI.01097-07.

Rice, G.I., Kasher, P.R., Forte, G.M.A., Mannion, N.M., Greenwood, S.M., Szynkiewicz, M., Dickerson, J.E., Bhaskar, S.S., Zampini, M., and Briggs, T.A., et al. (2012). Mutations in ADAR1 cause Aicardi-Goutières syndrome associated with a type I interferon signature. Nature genetics *44*, 1243-1248. https://doi.org/10.1038/ng.2414.

Riess, M., Fuchs, N.V., Idica, A., Hamdorf, M., Flory, E., Pedersen, I.M., and König, R. (2017). Interferons Induce Expression of SAMHD1 in Monocytes through Down-regulation of miR-181a and miR-30a. The Journal of biological chemistry *292*, 264-277. https://doi.org/10.1074/jbc.M116.752584.

Rookhuizen, D.C., Bonte, P.-E., Ye, M., Hoyler, T., Gentili, M., Burgdorf, N., Durand, S., Aprahamian, F., Kroemer, G., and Manel, N., et al. (2021). Induction of transposable element expression is central to innate sensing.

Runge, S., Sparrer, K.M.J., Lässig, C., Hembach, K., Baum, A., García-Sastre, A., Söding, J., Conzelmann, K.-K., and Hopfner, K.-P. (2014). In vivo ligands of MDA5 and RIG-I in measles virus-infected cells. PLoS pathogens *10*, e1004081. https://doi.org/10.1371/journal.ppat.1004081.

Sabbah, A., Chang, T.H., Harnack, R., Frohlich, V., Tominaga, K., Dube, P.H., Xiang, Y., and Bose, S. (2009). Activation of innate immune antiviral responses by Nod2. Nature immunology *10*, 1073-1080. https://doi.org/10.1038/ni.1782.

Saeed, M.F., Kolokoltsov, A.A., Albrecht, T., and Davey, R.A. (2010). Cellular entry of ebola virus involves uptake by a macropinocytosis-like mechanism and subsequent trafficking through

early and late endosomes. PLoS pathogens *6*, e1001110. https://doi.org/10.1371/journal.ppat.1001110.

Saito, T., and Gale, M. (2007). Principles of intracellular viral recognition. Current opinion in immunology *19*, 17-23. https://doi.org/10.1016/j.coi.2006.11.003.

Sanchez, A. (2007). Analysis of filovirus entry into vero e6 cells, using inhibitors of endocytosis, endosomal acidification, structural integrity, and cathepsin (B and L) activity. The Journal of infectious diseases *196 Suppl 2*, S251-8. https://doi.org/10.1086/520597.

Sanchez, A., Kiley, M.P., Holloway, B.P., and Auperin, D.D. (1993). Sequence analysis of the Ebola virus genome: organization, genetic elements, and comparison with the genome of Marburg virus. Virus Research *29*, 215-240. https://doi.org/10.1016/0168-1702(93)90063-s.

Sanchez, A., Ksiazek, T.G., Rollin, P.E., Miranda, M.E., Trappier, S.G., Khan, A.S., Peters, C.J., and Nichol, S.T. (1999). Detection and molecular characterization of Ebola viruses causing disease in human and nonhuman primates. The Journal of infectious diseases *179 Suppl 1*, S164-9. https://doi.org/10.1086/514282.

Sanchez, A., Trappier, S.G., Mahy, B.W., Peters, C.J., and Nichol, S.T. (1996). The virion glycoproteins of Ebola viruses are encoded in two reading frames and are expressed through transcriptional editing. Proceedings of the National Academy of Sciences *93*, 3602-3607. https://doi.org/10.1073/pnas.93.8.3602.

Schlee, M., and Hartmann, G. (2016). Discriminating self from non-self in nucleic acid sensing. Nature reviews. Immunology *16*, 566-580. https://doi.org/10.1038/nri.2016.78.

Schlee, M., Roth, A., Hornung, V., Hagmann, C.A., Wimmenauer, V., Barchet, W., Coch, C., Janke, M., Mihailovic, A., and Wardle, G., et al. (2009). Recognition of 5' triphosphate by RIG-I helicase requires short blunt double-stranded RNA as contained in panhandle of negative-strand virus. Immunity *31*, 25-34. https://doi.org/10.1016/j.immuni.2009.05.008.

Schmidt, A., Schwerd, T., Hamm, W., Hellmuth, J.C., Cui, S., Wenzel, M., Hoffmann, F.S., Michallet, M.-C., Besch, R., and Hopfner, K.-P., et al. (2009). 5'-triphosphate RNA requires base-paired structures to activate antiviral signaling via RIG-I. Proceedings of the National Academy of Sciences *106*, 12067-12072. https://doi.org/10.1073/pnas.0900971106.

Schmidt, M.L., Tews, B.A., Groseth, A., and Hoenen, T. (2018). Generation and Optimization of a Green Fluorescent Protein-Expressing Transcription and Replication-Competent Virus-Like Particle System for Ebola Virus. The Journal of infectious diseases *218*, S360-S364. https://doi.org/10.1093/infdis/jiy405.

Schneider, W.M., Chevillotte, M.D., and Rice, C.M. (2014). Interferon-stimulated genes: a complex web of host defenses. Annual review of immunology *32*, 513-545. https://doi.org/10.1146/annurev-immunol-032713-120231.

Schornberg, K.L., Shoemaker, C.J., Dube, D., Abshire, M.Y., Delos, S.E., Bouton, A.H., and White, J.M. (2009). Alpha5beta1-integrin controls ebolavirus entry by regulating endosomal cathepsins. Proceedings of the National Academy of Sciences *106*, 8003-8008. https://doi.org/10.1073/pnas.0807578106.

Schuh, A.J., Amman, B.R., and Towner, J.S. (2017). Filoviruses and bats. Microbiology Australia *38*, 12-16. https://doi.org/10.1071/MA17005.

Schümann, M., Gantke, T., and Mühlberger, E. (2009). Ebola virus VP35 antagonizes PKR activity through its C-terminal interferon inhibitory domain. Journal of virology *83*, 8993-8997. https://doi.org/10.1128/JVI.00523-09.

Schwarz, T.M., Edwards, M.R., Diederichs, A., Alinger, J.B., Leung, D.W., Amarasinghe, G.K., and Basler, C.F. (2017). VP24-Karyopherin Alpha Binding Affinities Differ between Ebolavirus Species, Influencing Interferon Inhibition and VP24 Stability. Journal of virology *91*. https://doi.org/10.1128/JVI.01715-16.

Scianimanico, S., Schoehn, G., Timmins, J., Ruigrok, R.H., Klenk, H.D., and Weissenhorn, W. (2000). Membrane association induces a conformational change in the Ebola virus matrix protein. The EMBO journal *19*, 6732-6741. https://doi.org/10.1093/emboj/19.24.6732.

Serra, M.J., Smolter, P.E., and Westhof, E. (2004). Pronounced instability of tandem IU base pairs in RNA. Nucleic acids research *32*, 1824-1828. https://doi.org/10.1093/nar/gkh501.

Seth, R.B., Sun, L., Ea, C.-K., and Chen, Z.J. (2005). Identification and characterization of MAVS, a mitochondrial antiviral signaling protein that activates NF-kappaB and IRF 3. Cell *122*, 669-682. https://doi.org/10.1016/j.cell.2005.08.012.

Shabman, R.S., Jabado, O.J., Mire, C.E., Stockwell, T.B., Edwards, M., Mahajan, M., Geisbert, T.W., and Basler, C.F. (2014). Deep sequencing identifies noncanonical editing of Ebola and Marburg virus RNAs in infected cells. mBio *5*, e02011. https://doi.org/10.1128/mBio.02011-14.

Shi, M., Lin, X.-D., Chen, X., Tian, J.-H., Chen, L.-J., Li, K., Wang, W., Eden, J.-S., Shen, J.-J., and Liu, L., et al. (2018). The evolutionary history of vertebrate RNA viruses. Nature *556*, 197-202. https://doi.org/10.1038/s41586-018-0012-7.

Shimojima, M., Takada, A., Ebihara, H., Neumann, G., Fujioka, K., Irimura, T., Jones, S., Feldmann, H., and Kawaoka, Y. (2006). Tyro3 family-mediated cell entry of Ebola and Marburg viruses. Journal of virology *80*, 10109-10116. https://doi.org/10.1128/JVI.01157-06.

Simmons, G., Reeves, J.D., Grogan, C.C., Vandenberghe, L.H., Baribaud, F., Whitbeck, J.C., Burke, E., Buchmeier, M.J., Soilleux, E.J., and Riley, J.L., et al. (2003). DC-SIGN and DC-SIGNR bind ebola glycoproteins and enhance infection of macrophages and endothelial cells. Virology *305*, 115-123. https://doi.org/10.1006/viro.2002.1730.

Slenczka, W., and Klenk, H.D. (2007). Forty years of marburg virus. The Journal of infectious diseases *196 Suppl 2*, S131-5. https://doi.org/10.1086/520551.

Son, K.-N., Liang, Z., and Lipton, H.L. (2015). Double-Stranded RNA Is Detected by Immunofluorescence Analysis in RNA and DNA Virus Infections, Including Those by Negative-Stranded RNA Viruses. Journal of virology *89*, 9383-9392. https://doi.org/10.1128/JVI.01299-15.

Soonthornvacharin, S., Rodriguez-Frandsen, A., Zhou, Y., Galvez, F., Huffmaster, N.J., Tripathi, S., Balasubramaniam, V.R.M.T., Inoue, A., Castro, E. de, and Moulton, H., et al. (2017). Systems-based analysis of RIG-I-dependent signalling identifies KHSRP as an inhibitor of RIG-I receptor activation. Nature microbiology *2*, 17022. https://doi.org/10.1038/nmicrobiol.2017.22.

Spiropoulou, C.F., Ranjan, P., Pearce, M.B., Sealy, T.K., Albariño, C.G., Gangappa, S., Fujita, T., Rollin, P.E., Nichol, S.T., and Ksiazek, T.G., et al. (2009). RIG-I activation inhibits ebolavirus replication. Virology *392*, 11-15. https://doi.org/10.1016/j.virol.2009.06.032.

Strahle, L., Garcin, D., and Kolakofsky, D. (2006). Sendai virus defective-interfering genomes and the activation of interferon-beta. Virology *351*, 101-111. https://doi.org/10.1016/j.virol.2006.03.022.

Ströher, U., West, E., Bugany, H., Klenk, H.D., Schnittler, H.J., and Feldmann, H. (2001). Infection and activation of monocytes by Marburg and Ebola viruses. Journal of virology *75*, 11025-11033. https://doi.org/10.1128/JVI.75.22.11025-11033.2001.

Sztuba-Solinska, J., Diaz, L., Kumar, M.R., Kolb, G., Wiley, M.R., Jozwick, L., Kuhn, J.H., Palacios, G., Radoshitzky, S.R., and Le J Grice, S.F., et al. (2016). A small stem-loop structure of the Ebola virus trailer is essential for replication and interacts with heat-shock protein A8. Nucleic acids research *44*, 9831-9846. https://doi.org/10.1093/nar/gkw825.

Takamatsu, Y., Kolesnikova, L., and Becker, S. (2018). Ebola virus proteins NP, VP35, and VP24 are essential and sufficient to mediate nucleocapsid transport. Proceedings of the National Academy of Sciences *115*, 1075-1080. https://doi.org/10.1073/pnas.1712263115.

Takamatsu, Y., Kolesnikova, L., Schauflinger, M., Noda, T., and Becker, S. (2020). The Integrity of the YxxL Motif of Ebola Virus VP24 Is Important for the Transport of Nucleocapsid-Like Structures and for the Regulation of Viral RNA Synthesis. Journal of virology *94*. https://doi.org/10.1128/JVI.02170-19.

Takeda, K., and Akira, S. (2015). Toll-like receptors. Current protocols in immunology *109*, 14.12.1-14.12.10. https://doi.org/10.1002/0471142735.im1412s109.

Takeuchi, K., Komatsu, T., Kitagawa, Y., Sada, K., and Gotoh, B. (2008). Sendai virus C protein plays a role in restricting PKR activation by limiting the generation of intracellular double-stranded RNA. Journal of virology *82*, 10102-10110. https://doi.org/10.1128/JVI.00599-08.

Takeuchi, O., and Akira, S. (2009). Innate immunity to virus infection. Immunological reviews *227*, 75-86. https://doi.org/10.1111/j.1600-065X.2008.00737.x.

Tan, M.H., Li, Q., Shanmugam, R., Piskol, R., Kohler, J., Young, A.N., Liu, K.I., Zhang, R., Ramaswami, G., and Ariyoshi, K., et al. (2017). Dynamic landscape and regulation of RNA editing in mammals. Nature *550*, 249-254. https://doi.org/10.1038/nature24041.

Timmins, J., Scianimanico, S., Schoehn, G., and Weissenhorn, W. (2001). Vesicular release of ebola virus matrix protein VP40. Virology *283*, 1-6. https://doi.org/10.1006/viro.2001.0860.

Toth, A.M., Li, Z., Cattaneo, R., and Samuel, C.E. (2009). RNA-specific adenosine deaminase ADAR1 suppresses measles virus-induced apoptosis and activation of protein kinase PKR. The Journal of biological chemistry *284*, 29350-29356. https://doi.org/10.1074/jbc.M109.045146.

Towner, J.S., Sealy, T.K., Khristova, M.L., Albariño, C.G., Conlan, S., Reeder, S.A., Quan, P.-L., Lipkin, W.I., Downing, R., and Tappero, J.W., et al. (2008). Newly discovered ebola virus associated with hemorrhagic fever outbreak in Uganda. PLoS pathogens *4*, e1000212. https://doi.org/10.1371/journal.ppat.1000212.

Trunschke, M., Conrad, D., Enterlein, S., Olejnik, J., Brauburger, K., and Mühlberger, E. (2013). The L-VP35 and L-L interaction domains reside in the amino terminus of the Ebola virus L

protein and are potential targets for antivirals. Virology *441*, 135-145. https://doi.org/10.1016/j.virol.2013.03.013.

Tsuchiya, S., Kobayashi, Y., Goto, Y., Okumura, H., Nakae, S., Konno, T., and Tada, K. (1982). Induction of maturation in cultured human monocytic leukemia cells by a phorbol diester. Cancer research *42*, 1530-1536.

Varkey, J.B., Shantha, J.G., Crozier, I., Kraft, C.S., Lyon, G.M., Mehta, A.K., Kumar, G., Smith, J.R., Kainulainen, M.H., and Whitmer, S., et al. (2015). Persistence of Ebola Virus in Ocular Fluid during Convalescence. The New England journal of medicine *372*, 2423-2427. https://doi.org/10.1056/NEJMoa1500306.

Vetter, P., Fischer, W.A., Schibler, M., Jacobs, M., Bausch, D.G., and Kaiser, L. (2016). Ebola Virus Shedding and Transmission: Review of Current Evidence. The Journal of infectious diseases *214*, S177-S184. https://doi.org/10.1093/infdis/jiw254.

Vignuzzi, M., and López, C.B. (2019). Defective viral genomes are key drivers of the virus-host interaction. Nature microbiology *4*, 1075-1087. https://doi.org/10.1038/s41564-019-0465-y.

Vogel, O.A., Han, J., Liang, C.-Y., Manicassamy, S., Perez, J.T., and Manicassamy, B. (2020). The p150 Isoform of ADAR1 Blocks Sustained RLR signaling and Apoptosis during Influenza Virus Infection. PLoS pathogens *16*, e1008842. https://doi.org/10.1371/journal.ppat.1008842.

Wagner, R.W., Smith, J.E., Cooperman, B.S., and Nishikura, K. (1989). A double-stranded RNA unwinding activity introduces structural alterations by means of adenosine to inosine conversions in mammalian cells and Xenopus eggs. Proceedings of the National Academy of Sciences *86*, 2647-2651. https://doi.org/10.1073/pnas.86.8.2647.

Wang, L., Sun, Y., Song, X., Wang, Z., Zhang, Y., Zhao, Y., Peng, X., Zhang, X., Li, C., and Gao, C., et al. (2021). Hepatitis B virus evades immune recognition via RNA adenosine deaminase ADAR1-mediated viral RNA editing in hepatocytes. Cellular & molecular immunology *18*, 1871-1882. https://doi.org/10.1038/s41423-021-00729-1.

Wang, Y., Yuan, S., Jia, X., Ge, Y., Ling, T., Nie, M., Lan, X., Chen, S., and Xu, A. (2019). Mitochondria-localised ZNFX1 functions as a dsRNA sensor to initiate antiviral responses through MAVS. Nature cell biology *21*, 1346-1356. https://doi.org/10.1038/s41556-019-0416-0.

Watanabe, S., Watanabe, T., Noda, T., Takada, A., Feldmann, H., Jasenosky, L.D., and Kawaoka, Y. (2004). Production of novel ebola virus-like particles from cDNAs: an alternative to ebola virus generation by reverse genetics. Journal of virology *78*, 999-1005. https://doi.org/10.1128/jvi.78.2.999-1005.2004.

Watt, A., Moukambi, F., Banadyga, L., Groseth, A., Callison, J., Herwig, A., Ebihara, H., Feldmann, H., and Hoenen, T. (2014). A novel life cycle modeling system for Ebola virus shows a genome length-dependent role of VP24 in virus infectivity. Journal of virology *88*, 10511-10524. https://doi.org/10.1128/JVI.01272-14.

Weber, F., Wagner, V., Rasmussen, S.B., Hartmann, R., and Paludan, S.R. (2006). Double-stranded RNA is produced by positive-strand RNA viruses and DNA viruses but not in detectable amounts by negative-strand RNA viruses. Journal of virology *80*, 5059-5064. https://doi.org/10.1128/JVI.80.10.5059-5064.2006.

Weber, M., Gawanbacht, A., Habjan, M., Rang, A., Borner, C., Schmidt, A.M., Veitinger, S., Jacob, R., Devignot, S., and Kochs, G., et al. (2013). Incoming RNA virus nucleocapsids containing a 5'-triphosphorylated genome activate RIG-I and antiviral signaling. Cell host & microbe *13*, 336-346. https://doi.org/10.1016/j.chom.2013.01.012.

Weik, M., Modrof, J., Klenk, H.-D., Becker, S., and Mühlberger, E. (2002). Ebola virus VP30-mediated transcription is regulated by RNA secondary structure formation. Journal of virology *76*, 8532-8539. https://doi.org/10.1128/jvi.76.17.8532-8539.2002.

Weingartl, H.M., Nfon, C., and Kobinger, G. (2013). Review of Ebola virus infections in domestic animals. Developments in biologicals *135*, 211-218. https://doi.org/10.1159/000178495.

Whitfield, Z.J., Prasad, A.N., Ronk, A.J., Kuzmin, I.V., Ilinykh, P.A., Andino, R., and Bukreyev, A. (2020). Species-Specific Evolution of Ebola Virus during Replication in Human and Bat Cells. Cell reports *32*, 108028. https://doi.org/10.1016/j.celrep.2020.108028.

Whitmer, S.L.M., Ladner, J.T., Wiley, M.R., Patel, K., Dudas, G., Rambaut, A., Sahr, F., Prieto, K., Shepard, S.S., and Carmody, E., et al. (2018). Active Ebola Virus Replication and Heterogeneous Evolutionary Rates in EVD Survivors. Cell reports *22*, 1159-1168. https://doi.org/10.1016/j.celrep.2018.01.008.

WHO (2022a). Ebola virus disease. https://www.who.int/news-room/fact-sheets/detail/ebola-virus-disease. 22.03.2022.

WHO (2022b). Marburg virus disease. https://www.who.int/news-room/fact-sheets/detail/marburg-virus-disease. 22.03.2022.

WHO/International Study Team (1978a). Ebola haemorrhagic fever in Sudan, 1976. Bulletin of the World Health Organization *56*, 247-270.

WHO/International Study Team (1978b). Ebola haemorrhagic fever in Zaire, 1976. Bulletin of the World Health Organization *56*, 271-293.

Wilkins, C., and Gale, M. (2010). Recognition of viruses by cytoplasmic sensors. Current opinion in immunology *22*, 41-47. https://doi.org/10.1016/j.coi.2009.12.003.

Woolsey, C., and Geisbert, T.W. (2021). Current state of Ebola virus vaccines: A snapshot. PLoS pathogens *17*, e1010078. https://doi.org/10.1371/journal.ppat.1010078.

Woolsey, C., Menicucci, A.R., Cross, R.W., Luthra, P., Agans, K.N., Borisevich, V., Geisbert, J.B., Mire, C.E., Fenton, K.A., and Jankeel, A., et al. (2019). A VP35 Mutant Ebola Virus Lacks Virulence but Can Elicit Protective Immunity to Wild-Type Virus Challenge. Cell reports *28*, 3032-3046.e6. https://doi.org/10.1016/j.celrep.2019.08.047.

Wu, X., Qi, X., Qu, B., Zhang, Z., Liang, M., Li, C., Cardona, C.J., Li, D., and Xing, Z. (2014). Evasion of antiviral immunity through sequestering of TBK1/IKKε/IRF3 into viral inclusion bodies. Journal of virology *88*, 3067-3076. https://doi.org/10.1128/JVI.03510-13.

Xu, L.-G., Wang, Y.-Y., Han, K.-J., Li, L.-Y., Zhai, Z., and Shu, H.-B. (2005). VISA is an adapter protein required for virus-triggered IFN-beta signaling. Molecular cell *19*, 727-740. https://doi.org/10.1016/j.molcel.2005.08.014.

Xu, W., Edwards, M.R., Borek, D.M., Feagins, A.R., Mittal, A., Alinger, J.B., Berry, K.N., Yen, B., Hamilton, J., and Brett, T.J., et al. (2014). Ebola virus VP24 targets a unique NLS binding site on

karyopherin alpha 5 to selectively compete with nuclear import of phosphorylated STAT1. Cell host & microbe *16*, 187-200. https://doi.org/10.1016/j.chom.2014.07.008.

Yang, S., Deng, P., Zhu, Z., Zhu, J., Wang, G., Zhang, L., Chen, A.F., Wang, T., Sarkar, S.N., and Billiar, T.R., et al. (2014). Adenosine deaminase acting on RNA 1 limits RIG-I RNA detection and suppresses IFN production responding to viral and endogenous RNAs. Journal of immunology (Baltimore, Md. : 1950) *193*, 3436-3445. https://doi.org/10.4049/jimmunol.1401136.

Yang, X.-L., Tan, C.W., Anderson, D.E., Jiang, R.-D., Li, B., Zhang, W., Zhu, Y., Lim, X.F., Zhou, P., and Liu, X.-L., et al. (2019). Characterization of a filovirus (Měnglà virus) from Rousettus bats in China. Nature microbiology *4*, 390-395. https://doi.org/10.1038/s41564-018-0328-y.

Yen, B., Mulder, L.C.F., Martinez, O., and Basler, C.F. (2014). Molecular basis for ebolavirus VP35 suppression of human dendritic cell maturation. Journal of virology *88*, 12500-12510. https://doi.org/10.1128/JVI.02163-14.

Yoh, S.M., Schneider, M., Seifried, J., Soonthornvacharin, S., Akleh, R.E., Olivieri, K.C., Jesus, P.D. de, Ruan, C., Castro, E. de, and Ruiz, P.A., et al. (2015). PQBP1 Is a Proximal Sensor of the cGAS-Dependent Innate Response to HIV-1. Cell *161*, 1293-1305. https://doi.org/10.1016/j.cell.2015.04.050.

Zhang, Y.-J., Ding, J.-N., Zhong, H., and Han, J.-G. (2017). Exploration micromechanism of VP35 IID interaction and recognition dsRNA: A molecular dynamics simulation. Proteins *85*, 1008-1023. https://doi.org/10.1002/prot.25269.

Zhang, Z., Kim, T., Bao, M., Facchinetti, V., Jung, S.Y., Ghaffari, A.A., Qin, J., Cheng, G., and Liu, Y.-J. (2011). DDX1, DDX21, and DHX36 helicases form a complex with the adaptor molecule TRIF to sense dsRNA in dendritic cells. Immunity *34*, 866-878. https://doi.org/10.1016/j.immuni.2011.03.027.

Zhao, Y., Ye, X., Dunker, W., Song, Y., and Karijolich, J. (2018). RIG-I like receptor sensing of host RNAs facilitates the cell-intrinsic immune response to KSHV infection. Nature communications *9*, 4841. https://doi.org/10.1038/s41467-018-07314-7.

Zhu, W., Banadyga, L., Emeterio, K., Wong, G., and Qiu, X. (2019). The Roles of Ebola Virus Soluble Glycoprotein in Replication, Pathogenesis, and Countermeasure Development. Viruses *11*. https://doi.org/10.3390/v11110999.

Zinzula, L., Nagy, I., Orsini, M., Weyher-Stingl, E., Bracher, A., and Baumeister, W. (2019). Structures of Ebola and Reston Virus VP35 Oligomerization Domains and Comparative Biophysical Characterization in All Ebolavirus Species. Structure (London, England : 1993) *27*, 39-54.e6. https://doi.org/10.1016/j.str.2018.09.009.

8 Appendix

8.1 Publications and presentations

8.1.1 Publications

Innate immunity to Filoviruses. (2022) J. Wildemann, T. Hoenen, R. König. (Review article in preparation).

ADAR1^{p150} is a negative regulator of EBOV RNA innate sensing. (2022) J. Wildemann, C. Helmer, S. Mönch, L. Lauterbach-Rivière, N. Hein-Fuchs, O. Siering, C. Pfaller, T. Hoenen, R. König. (Article in preparation).

8.1.2 Presentations

Identification of innate sensors to Ebola virus. J. Wildemann, L. Rivière, S. Chanda, T. Hoenen, R. König – Paul-Ehrlich-Institut Retreat – Poster – 31.01.2018

Identification of cellular sensors and RNA signatures of Ebola virus. J.Wildemann, L. Rivière, T. Hoenen, R. König – German One Health Initiative (GOHI) Meeting – Robert Koch Institut Berlin – Presentation – 31.05.-01.06.2018

Innate immune response to Ebola virus. J. Wildemann, L. Rivière, T. Hoenen, R. König – Paul-Ehrlich-Institut Retreat – Presentation – 31.01.2019

Innate immune response to Ebola virus. J. Wildemann, L. Rivière, T. Hoenen, R. König – Annual meeting of the Society for Virology (GfV) – Düsseldorf – Poster – 20.-23.03.2019

Innate immune response to Ebola virus. J. Wildemann, L. Rivière, T. Hoenen, R. König – Workshop on Cell Biology of Viral Infections of the German Research Platform for Zoonoses and the Society for Virology (GfV) – Kloster Schöntal – Presentation - 23.-25.10.2019

Innate immune response to Ebola virus. J. Wildemann, L. Rivière, C. Helmer, T. Hoenen, R. König – Paul-Ehrlich-Institut Retreat – Poster – 31.01.2020

ADAR1 is a negative regulator of EBOV RNA innate sensing. - J. Wildemann, L. Rivière, C. Helmer, T. Hoenen, C. Pfaller, R. König – Congress for infectious diseases and tropical medicine (KIT) – virtual – Poster – 16.-19.06.2021

ADAR1 is a negative regulator of EBOV RNA innate sensing. - J. Wildemann, L. Rivière, C. Helmer, T. Hoenen, C. Pfaller, R. König – Robert Koch Institut – virtual – Poster – 28.-29.10.2021

8.2 Curriculum Vitae

8.3 Akademische Lehrer

Meine akademischen Lehrer/innen an der Universität Utrecht, Niederlande:

Andino (UCSF), Bloem, Bosch, Coffer, de Groot, Denzer, Egberink, Fischer, Hack, Hall, Kersten, Kesmir, Knol, Kortekaas, Nijhuis, Pinelli, Rimmelzwaan, Rooijakkers, Spaargaren, Thomas, van Els, van Kuppeveld

Meine akademischen Lehrer/innen an der Universität Lund, Schweden:

Arevalo, Berglund, Ivars, Prykhodko, Weström

Meine akademischen Lehrer/innen an der Universität zu Köln:

Arndt, Baumann, Becks, Berger, Bonkowski, Borcherding, Braden, Breitenkamp, Bucher, Büschges, Falk, Fischer, Fleck, Flügge, Frerigmann, Gründemann, Güttler, Häusler, Herrmann, Hoecker, Hoef-Emden, Horstmann, Hülskamp, Kemper, Knittler, Korsching, Krämer, Kretschmar, Kroiher, Krüger, Langer, Lichtenberg, Ludewig, Marin, Melkonian, Neundorf, Pietsch, Plickert, Predel, Queckenberg, Roth, Schäfer, Schierenberg, Schnetz, Schreier, Schulz, Schwarz, Stucky, Thomopoulou, Tilmann, von Berg, von Elert, Waffenschmidt, Walkowiak, Werr, Wester, Wiehe, Wipking, Zapilko

8.4 Danksagung

An erster Stelle möchte ich meinen Dank an Dr. Renate König richten, die mich stets sehr gut betreut und unterstützt hat und mich durchweg motiviert hat mit ihrer Begeisterung für die Forschung im Bereich „host-pathogen interactions“.
Außerdem möchte ich gerne Prof. Dr. Klaus Cichutek meinen Dank aussprechen für die Möglichkeit diese Promotion am Paul-Ehrlich-Institut durchzuführen.
Prof. Dr. Stephan Becker möchte ich ebenfalls danken für die Betreuung seitens der Universität Marburg.
Weiterhin gebührt mein Dank Dr. Thomas Hoenen vom Friedrich-Loeffler-Institut, in dessen Arbeitsgruppe ich zu Beginn dieser Promotion einige relevante Methoden lernen durfte. Auch Dr. Lisa Wendt und Dr. Alison Groseth sowie alle weiteren Gruppenmitglieder der Gruppe Hoenen und Gruppe Groseth hatten stets ein offenes Ohr für meine Fragen.
Vielen Dank auch an Prof. Dr. Veronika von Messling, Prof. Dr. Ute Modlich und Dr. Christian Pfaller, die mir während der Promotion ebenfalls mit Rat und Tat zur Seite standen.
Zudem möchte ich mich bei allen weiteren Kooperationspartnern und Kooperationspartnerinnen sowie Co-Autoren und -Autorinnen von aus dieser Arbeit resultierenden Publikationen bedanken.
Ein sehr großes Dankeschön gebührt auch der gesamten NG3 für die Unterstützung. Besonders meine Kollegen und Kolleginnen und mittlerweile Freunde und Freundinnen haben mir sehr geholfen und ohne euch wäre meine Doktorarbeit wohl kaum möglich gewesen: Lise, Kerstin, Nina, Manja, Christiane, Heike, Saskia, Maïwenn, Max, Catharina, Moritz und Carl.
Durch viele anregende Gespräche und das ein oder andere nicht auf die Arbeit bezogene Treffen haben mich meine neuen Freunde, die ich während der Promotion gefunden habe ebenfalls sehr unterstützt, vor allem Arne, Kevin, Marcel, Max und Matthias.
Zuletzt möchte ich meiner Familie und meinen Freunden und Freundinnen für ihr stets offenes Ohr danken und dafür, dass sie nicht müde wurden mich über meine Promotion

auszufragen und mich extrem motiviert haben, aber auch abgelenkt haben, wenn es mal notwendig war. Ein dickes Dankeschön an Ricarda und an meine wunderbare WG aus Darmstadt, die mich von der ersten Sekunde an als Familienmitglied aufgenommen hat, Marina, Sebastian und David. Meiner Familie möchte ich von Herzen danken für ihre bedingungslose Unterstützung und Motivation und weil sie stets stolz auf mich waren, obwohl ich oft selbst nicht zufrieden mit mir war. Zuletzt gebührt mein Dank Simon, der vor allem in den letzten Monaten alle meine Stimmungen ausgehalten hat und mir stets so viel Liebe und Unterstützung gegeben hat.
Ohne euch hätte ich es nie soweit geschafft!

8.5 Ehrenwörtliche Erklärung

Ich erkläre ehrenwörtlich, dass ich die dem Fachbereich Medizin Marburg zur Promotionsprüfung eingereichte Arbeit mit dem Titel ‚Innate Immunity to Ebola Virus' am Institut für Virologie unter der Leitung von Herrn Prof. Dr. Stephan Becker in Zusammenarbeit mit dem Paul-Ehrlich-Institut unter der Leitung von Frau Dr. Renate König, ohne sonstige Hilfe selbst durchgeführt und bei der Abfassung der Arbeit keine anderen als die in der Dissertation aufgeführten Hilfsmittel benutzt habe. Ich habe bisher an keinem in- oder ausländischen Medizinischen Fachbereich ein Gesuch um Zulassung zur Promotion eingereicht, noch die vorliegende oder eine andere Arbeit als Dissertation vorgelegt.

Ich versichere, dass ich sämtliche wörtlichen oder sinngemäßen Übernahmen und Zitate kenntlich gemacht habe.

Mit dem Einsatz von Software zur Erkennung von Plagiaten bin ich einverstanden.

Ort, Datum, Unterschrift Doktorandin

Die Hinweise zur Erkennung von Plagiaten habe ich zur Kenntnis genommen.

Ort, Datum, Unterschrift Referent
